

République Algérienne Démocratique et Populaire  
Ministère de l'Enseignement Supérieur et de la Recherche Scientifique  
Université 8 Mai 1945 Guelma



Faculté des Sciences et de la Technologie  
Département de Génie des Procédés  
Laboratoire d'Analyses Industrielles et Génie des Matériaux (LAIGM)

**THÈSE**  
**EN VUE DE L'OBTENTION DU DIPLOME DE**  
**DOCTORAT EN 3<sup>ème</sup> CYCLE**

Domaine : Sciences et Techniques      Filière : Génie des Procédés  
Spécialité : Génie des Procédés

**Présentée par**

**Atek Imene**

*Intitulée*

**Etude des mécanismes des réactions électrochimiques par simulation  
de voltampérométrie cyclique. Application aux réactions  
d'électrodéposition.**

**(Study of the mechanisms of electrochemical reactions by simulation  
of cyclic voltammetry. Application to electrodeposition reactions)**

Soutenue le : 06/12/2021

Devant le Jury composé de:

<b>M. BORDJIBA Tarik</b>	Pr.	Univ. de 8 Mai 1945 Guelma	Président
<b>M. AFFOUNE Abed Mohamed</b>	Pr.	Univ. de 8 Mai 1945 Guelma	Encadreur
<b>M. REHAMNIA Rabah</b>	Pr	Univ. de Badji Mokhtar Annaba	Examinateur
<b>Melle NIGRI Soraya</b>	Pr.	Univ. de 8 Mai 1945 Guelma	Examinatrice
<b>Mme Djaghout Ilhem</b>	MCB	Univ. de Mohamed Chérif Messaadia de Souk-Ahras	Invitée

**Année Universitaire : 2020-2021.**

## **ACKNOWLEDGEMENTS**

It's difficult to find the right words to express my gratitude to everyone who has helped me, directly or indirectly, during these years of doctoral work.

First and foremost, I am grateful to Allah (GOD) for providing me with the knowledge and strength to complete this PhD thesis. Without Allah's blessings, I would have never accomplished anything in my life.

I am also forever grateful to my mother, for being the first person to encourage me when I decided to pursue my doctorate.

Particularly, I acknowledge and thank my supervisor Prof. Abed Mohamed AFFOUNE from the University of 8 Mai 1945 Guelma for his excellent guidance, unwavering support, and valuable suggestion to carry out this research work. His belief in my abilities pushed me forward even when finishing a PhD seemed impossible. Additionally, I thank Prof. Hubert Girault, the director of LEPA Laboratory at EPFL University, for giving me the opportunity to perform part of my PhD thesis at his lab. Special thanks I want to say to Dr. Pekka Peljo for his comments, suggestion and follow up. It was a real pleasure to work with him on a LEPA team! He was always willing to assist me with both ideas and experimental work.

I would like to thank the Laboratory of LAIGM of the University of 8 May 1945 Guelma for the help received in each step of my thesis.

I would like to grateful the financial support from Ministère de l'Enseignement Supérieur et de la Recherche Scientifique, République Algérienne Démocratique et Populaire, Programme National Exceptionnel, Algeria, and acknowledge the financial support from the Swiss National Science Foundation under Grant Ambizione Energy.

I would like to acknowledge Prof. BORDJIBA Tarik from the University of 8 Mai 1945 Guelma for his accepting to be the jury president for my PhD thesis.

I wish also to express my gratitude to all the members of the jury, for accepting the task of examining my work and for the time they spent in it, namely Prof. REHAMNIA Rabah from the University of Badji Mokhtar Annaba, Prof. NIGRI Soraya and Dr. Djaghout Ilhem from the University of 8 Mai 1945 Guelma.

Lastly, no acknowledgement list would be complete without mentioning my member family: my brothers, sisters, and my husband. Without them, I wouldn't be writing this today.

\*Thanks to all\*

## **Abstract**

The absence of general theoretical models describing linear sweep voltammetry (LSV) or cyclic voltammetry (CV) responses for soluble-insoluble systems such as one-step electrodeposition reactions under quasi-reversible condition makes it difficult to extract quantitative kinetic information from experimental voltammograms. In this work, the semi-analytical method and the finite-element method included in COMSOL Multiphysics software for simulating LSV and CV responses for one-step electrodeposition process are described, for a case where instantaneous nucleation takes place, such as metal deposition on same metal. Voltammetric peaks were analyzed following variation of both dimensionless rate constants and charge transfer coefficients in a broad range. Therefore, kinetic curves for electron transfer processes were established and fitted perfectly by sigmoidal Boltzmann function and linear models. With these models, LSV or CV experimental data can be used to measure electrodeposition reactions kinetics whatever the degree of reversibility. The Cu(I)/Cu(0) couple in acetonitrile was selected as an experimental example. The model developed in this work predicts accurately the current response for Cu electrodeposition reaction and an excellent experiment-theory agreement was found. Furthermore, the LSV and CV models developed in this work, allow the theoretical concentration profiles for soluble-insoluble redox couples to be established for either reversible, quasi-reversible and irreversible cases.

**Keywords:** Simulation, Metal deposition, Soluble-insoluble system, Linear sweep voltammetry, Cyclic voltammetry.

## Résumé

L'absence de modèles théoriques généraux décrivant les réponses de la voltampérométrie à balayage linéaire (LSV) ou de la voltampérométrie cyclique (CV) pour les systèmes solubles-insolubles tels que les réactions d'électrodéposition en une seule étape dans des conditions quasi-réversibles rend difficile l'extraction d'informations cinétiques quantitatives à partir des voltampérogrammes expérimentaux. Dans ce travail, la méthode semi-analytique et la méthode des éléments finis sous le logiciel COMSOL Multiphysics sont décrites pour simuler les réponses LSV et CV pour le processus d'électrodéposition en une seule étape, dans le cas où la nucléation instantanée a lieu, comme le dépôt de métal sur le même métal. Les réponses voltampérométriques ont été analysées suite à la variation à la fois de la constante de vitesse adimensionnelle et de la coefficient de transfert de charge dans une large intervalle. Par conséquent, des courbes cinétiques des processus de transfert d'électrons ont été établies et parfaitement ajustées par une fonction sigmoïde de Boltzmann et des modèles linéaires. Avec ces modèles, les données expérimentales LSV ou CV permettent de mesurer la cinétique des réactions d'électrodéposition quel que soit le degré de réversibilité. Le couple Cu(I)/Cu(0) dans l'acétonitrile a été choisi comme exemple expérimental. Le modèle développé dans ce travail prédit avec précision les réponses en courant pour la réaction d'électrodéposition de Cu. Un bon accord entre la théorie et l'expérimental a été trouvé. De plus, les modèles LSV et CV développés dans ce travail, permettent d'établir les profils de concentration théoriques des couples redox solubles-insolubles pour les cas réversibles, quasi-réversibles et irréversibles.

**Mots clés:** Simulation, Déposition du métal, Système soluble-insoluble, Voltampérométrie à balayage linéaire (LSV), Voltampérométrie cyclique.

## ملخص

عدم وجود نماذج نظرية تستعمل لوصف استجابات النظام الذي تكون فيه التفاعل من نوع قابل للذوبان-غير قابل للذوبان مثل في حالة تفاعلات ترسب المعادن باستعمال الطريقة الفولتميترية الخطية أو الدورية لاسيما التي تخضع لشروط شبه العكوسة، ادى الى عجز المجرى في حساب واستخراج معلومات كمية تصف الخصائص الحركية لهذا النظام. في هذا العمل تم استعمال طريقتين: الطريقة الشبه التحليلية وطريقة العناصر المحدودة المندرجة في برنامج COMSOL MULTIPHYSIC. بهدف محاكاة عملية الترسيب الكهربائي التي تحدث في خطوة واحدة، في حالة حدوث التنوي الفوري مثل ترسب المعادن على نفس المعدن. تم تحليل القمم الفولتميترية بعد دراسة اثر تغيير كل من ثابت السرعة و معامل نقل الشحنات في مجال واسع. بناء على ذلك تم إنشاء منحنيات حركية لعملية نقل الإلكترونات وتم نمذجتها باستعمال نموذج بولتزمان السيني وكذا نمودجا خطيا مع هذه النماذج يمكن استخدام البيانات الفولتميترية الخطية أو الدورية التجريبية لقياس حركية تفاعل الترسيب الكهربائي مهما كانت درجة العكوس. تم اختيار الثنائية  $Cu(I)/Cu(0)$  للنظرية التي تم تطويرها. علاوة على ذلك، فان النماذج الفولتميترية الخطية أو الدورية التي تم تطويرها في هذا العمل تسمح بانشاء مخططات تغير التراكيز النظرية للنظام الأوكسدة والارجاع القابلة للذوبان-والغير قابلة للذوبان في الحالات العكوسة، الشبه العكوسة، والغير العكوسة.

**الكلمات المفتاحية:** المحاكاة ، الترسيب المعدني، النظام القابل للذوبان-الغير قابل للذوبان ، الطريقة الفولتميترية الخطية،

الطريقة الفولتميترية الدورية.

# TABLE OF CONTENTS

LIST OF ABBREVIATIONS AND SYMBOLS	i
LIST OF TABLES	ii
LIST OF FIGURES	iii
INTRODUCTION	1

## CHAPTER I

### *Background and literature review*

<b>I.1. Description of electrochemical systems</b>	5
I.1. 1. Helmholtz EDL model	5
I.1. 2. Gouy-Chapman EDL model	6
I.1. 3. Stern EDL Model	6
I.1. 4. Grahame EDL Model	7
<b>I.2. Electrochemical thermodynamic and kinetics</b>	8
I.2.1. Steps of electrode process	8
I.2.2. Nernst equation	9
I.2.3. Butler-Volmer equation	10
<b>I.3. Mass transport phenomena</b>	11
I.3.1. Diffusion	11
I.3.2. Migration	12
I.3.3. Convection	12
<b>I.4. Voltammetry-sweep techniques to study electrochemical systems</b>	13
I.4.1. Linear scan voltammetry (LSV)	13
I.4.2. Cyclic voltammetry (CV)	14
I.4.3. Electrochemical voltammetry measurement system	14
I.4.4. Common causes of distortion in voltammetric curves	16
<b>I.5. General overview on the LSV and CV theories in the case of one step electrode process</b>	17
I.5.1. Survey of existing simulation approaches	17
I.5.1.1. analytical method	18
I.5.1.2. Numerical method	19
I.5.1.3. Semi-analytical method	19

I.5.2. Chronology of some important events in history of LSV and CV theories	19
I.5.3. Calculation of voltammograms for soluble-soluble redox reactions	21
<i>I.5.3.1. Reversible system</i>	22
<i>I.5.3.1.1. Theory and mathematical models</i>	22
<i>I.5.3.1.2. Potential and current peaks in LSV and CV for reversible soluble—soluble redox reaction</i>	23
<i>I.5.3.2. Quasi-reversible system</i>	24
<i>I.5.3.2.1. Theory and mathematical models</i>	24
<i>I.5.3.2.2. Potential and current peaks in LSV and CV for quasi-reversible soluble-soluble redox reaction</i>	26
<i>I.5.3.3. Totally irreversible system</i>	27
<i>I.5.3.3.1. Theory and mathematical models</i>	27
<i>I.5.3.3.2. Potential and current peaks for irreversible soluble-soluble redox reaction</i>	28
I.5.4. Calculation of voltammograms for soluble-insoluble redox reactions	28
<i>I.5.4.1. Reversible system</i>	29
<i>I.5.4.1.1. Theory and mathematical models</i>	29
<i>I.5.4.1.2. Potential and current peaks in LSV and CV for reversible soluble-insoluble redox reaction</i>	30
<i>I.5.4.2. quasi-reversible system</i>	30
<i>I.5.4.3. Totally irreversible system</i>	30
<i>I.5.4.3.1. Theory and mathematical models</i>	30
<i>I.5.4.3.2. Potential and current peaks for irreversible soluble-insoluble redox reaction</i>	30
<b>I.6. Scope of the present thesis</b>	31
<b>I.7. References</b>	32

## CHAPTER II

### *Experiment and simulations details*

II.1. Chemicals and supplies	37
II.2. Apparatus and accessories	37
II.3. Procedure	37
II.4. Choice of Working Electrode material	38
II.5. Simulation and Analysis tools	38
II.5.1. Semi-analytical method	38
II.5. 2. Finite element method software using COMSOL multiphysics	39
<i>II.5. 2.1. Finite elements solution procedure</i>	40
<i>II.5. 2.2. COMSOL Multiphysics calculation process</i>	40
II.5.3. Semi-integral method	41

II.5.4. Fortran	42
II.5.5. Origin software	42
II.6. References	43

## CHAPTER III

### *Simulation of linear sweep voltammetric behaviour for soluble-insoluble redox reaction*

<b>III.1. Mathematical formulation of the problem</b>	44
III.1.1. Hypotheses to metal/metal-ion system	44
III.1.2. Governing equations of mass transport process	44
<b>III.2. Solution methodology via use of semi analytical techniques</b>	45
IV.2.1. Stage I: Analytical solution	45
IV.2.1.1 <i>Application of the Laplace transform and numerical inversion to diffusion equation.</i>	45
IV.2.1.2 <i>Derivation of the voltammetry integral equation</i>	47
IV.2.2. Stage II: Numerical resolution	48
IV.2.3. Implementation of developed models in Fortran	51
<b>III.3. Solution methodology via use of the finite element COMSOL Multiphysics software</b>	53
III.3.1. Stage I: Pre-processing Stage	54
III.3.1.1. <i>Definition of governing equations</i>	54
III.3.1.1.1. <i>Mass transport and mass conservation equations</i>	54
III.3.1.1.2. <i>Potential sweep equation</i>	54
III.3.1.1.3. <i>Electrochemical reaction kinetics</i>	54
III.3.1.2. <i>Drawing the Geometry domain</i>	54
III.3.1.3. <i>Setting of initial and boundary conditions</i>	55
III.3.1.4. <i>Meshing</i>	56
III.3.2. Stage II: Processing stage	56
III.3.3. Stage III: Post-processing stage	56

<b>III.4. Results and discussion</b>	56
III.4.1. Theoretical results	56
<i>III.4.1.1. Calculation of linear scan voltammograms using semi analytical method and finite element method (COMSOL Multiphysics)</i>	56
<i>III.4.1.2. Effect of the kinetic rate</i>	57
<i>III.4.1.3. Effect of the charge transfer coefficient</i>	59
<i>III.4.1.4. Kinetics curves: coupling effects of kinetic rate and charge transfer coefficient</i>	60
III.4.2. Experiment–theory comparison	65
<i>III.4.2.1. Utilization of working curves</i>	66
<i>III.4.2.2. Fit and simulation</i>	67
<b>III.5. Conclusion</b>	70
<b>III.6. References</b>	71

## **CHAPTER IV**

### *Simulation of cyclic voltammograms for soluble-insoluble redox reaction*

<b>IV.1. Modelling cyclic voltammetry profile for metal/metal-ion system</b>	72
<b>IV.2. Resolution</b>	72
III.2.1. Semi-analytical approach	72
III.2.2. Finite element approach (COMSOL Multiphysics)	75
<b>IV.4. Results and discussion</b>	76
IV.4.1. Calculation of theoretical cyclic voltammograms using semi analytical method and finite element method (COMSOL Multiphysics)	76
IV.4.2. Effect of the kinetic rate	76
IV.4.3. Effect of the charge transfer coefficient	78
IV.4.4. Effect of the switching potential	79
IV.4.5. Theoretical visualization of concentration profiles	80
<b>IV.5. Conclusion</b>	80
<b>IV.6. References</b>	82
<b>General conclusion</b>	83

## LIST OF ABBREVIATIONS AND SYMBOLS

$C_M$	Concentration of the metal M
$C_{M^{n+}}$	Concentration of the metallic ions $M^{n+}$
$C_{M^{n+}}^*$	Bulk concentration of the metallic ions $M^{n+}$
$C^0$	Standard concentration
$D_{M^{n+}}$	Diffusion coefficient of metallic ions $M^{n+}$
$A$	Electroactive surface area
$n$	Number of electrons
$F$	Faraday's constant
$R$	Universal gas constant
$T$	Absolute temperature
$k^0$	Standard rate constant
$I$	Current
$E(t)$	Electrode potential
$E_i$	Initial potential
$E^0$	Standard potential
$E_{eq}$	Equilibrium potential
$v$	Potential scan rate
$t$	Time
$\alpha$	Charge transfer coefficient
$1-\alpha$	Anodic charge transfer coefficient
$\omega$	Dimensionless kinetic rate parameter
$\Psi$	Dimensionless current
$\eta$	Dimensionless overvoltage ( $\eta = nF / RT (E - E_{eq})$ )
$\sigma$	Dimensionless scan rate
$\gamma_{M^{n+}}$	Activity coefficient of the metallic ions $M^{n+}$
$\delta_k$	Small time interval

## LIST OF FIGURES

- Figure I.1.** *Simple structure of solid-liquid electrochemical systems. Electrode materials can either be metals, semimetals, or semiconductors, which choice should depend on the application. The electrolytic ions perform the role of enabling electric current to flow through an electrochemical cell from one electrode to the other.* 5
- Figure I.2.** *Electric charge and potential distribution in EDL. (a) Helmholtz, (b) Gouy -Chapman and (c) Stern models* 7
- Figure I.3.** *Schematic representation of the Grahame model of the double layer* 8
- Figure I.4.** *Essential steps of electrochemical reactions* 8
- Figure I.5.** *Free- energy reaction coordinate diagram for a simple redox reaction. Full lines: zero applied potential  $E = 0$ , dashed line: with applied potential  $E=E$*  10
- Figure I.6.** *a) Potential function applied at the electrode to oxidize the reduced species in the solution Redox couple. b) linear potential sweep voltammogram* 14
- Figure I.7.** *a) Potential function applied in cyclic voltammetry to oxidize the reduced species in the solution Redox couple. b) cyclic voltammogram* 15
- Figure I.8.** *Schematic sketch of the three-electrode voltammetry measurement system* 16
- Figure I.9.** *Diagrammatic representation of the most important steps to predict voltammetric responses.* 18
- Figure I.10.** *Adimensional CV responses for reversible soluble-soluble system, for  $A=10^3$ . the cathodic portion of CV curve is the same for the LSV. Insert is a potential cycling profile.* 24
- Figure I.11.** *Different CV responses for different  $A$  values in quasi-reversible region* 25

<b>Figure I.12.</b>	<i>Adimensional CV responses for irreversible soluble-soluble system, for <math>\alpha=0.5</math> and <math>\Lambda=0.0001</math></i>	27
<b>Figure II.1.</b>	<i>Flowchart of semi-analytical simulation of LSV</i>	39
<b>Figure II.2.</b>	<i>Flow chart of COMSOL Multiphysics model to simulate voltammetric responses.</i>	41
<b>Figure III.1.</b>	<i>Flowchart of the implemented LSV models</i>	53
<b>Figure III.2.</b>	<i>1D geometry model used for simulating the diffusion of metal ion.</i>	55
<b>Figure III.3.</b>	<i>Simulated LSV with the Butler-Volmer equation through use of the derived semi-analytical solutions (solid curve) and by the finite element method. <math>\alpha=0,5</math>, <math>INIT=0</math>, <math>LIMIT=-30</math> and <math>\omega=10^3</math> <math>LIMIT=-30</math>, a) <math>\omega=10^3</math> and b) <math>\omega=10^{-1}</math></i>	57
<b>Figure III.4.</b>	<i>Calculated linear sweep voltammograms for various value of <math>\omega</math> with <math>\alpha=0.5</math>; <b>a:</b> <math>\omega=10^5</math>, <b>b:</b> <math>\omega=10^4</math>, <b>c:</b> <math>\omega=10^3</math>, <b>d:</b> <math>\omega=10^2</math>, <b>e:</b> <math>\omega=10^1</math>, <b>f:</b> <math>\omega=1</math>, <b>g:</b> <math>\omega=10^{-1}</math>, <b>h:</b> <math>\omega=10^{-2}</math>, <b>i:</b> <math>\omega=10^{-3}</math>, <b>j:</b> <math>\omega=10^{-4}</math>, <b>k:</b> <math>\omega=10^{-5}</math></i>	59
<b>Figure III.5.</b>	<i>The effect of transfer coefficient <math>\alpha</math> on theoretical voltammograms</i>	60
<b>Figure III.6.</b>	<i>Variation of the peak current ratio, <math>\Psi_p / (\Psi_p)_{rev}</math>, as the function of the dimensionless rate constant for several values of <math>\alpha</math>. Solid lines are best fits to the sigmoidal Boltzmann functions with a correlation coefficient of 0.99. Zones A, B, C denote the reversible, quasi-reversible and totally irreversible zones, respectively.</i>	62
<b>Figure III.7.</b>	<i>Dependence of the half peak width of linear sweep voltammograms (<math>\Phi_{p/2}</math>) on the logarithm of the kinetic parameter <math>\omega</math> for various <math>\alpha</math> values. Solid lines are best fits to the sigmoidal Boltzmann functions with a correlation coefficient of 0.98</i>	62
<b>Figure III.8.</b>	<i>Plots of the reduction peak position (<math>\eta_p</math>) against <math>\log(\omega)</math> for various <math>\alpha</math> values</i>	63
<b>Figure III.9.</b>	<i>(a) LSV curves of electrodeposition of Cu(I) on Cu disc electrode from 10.25 mM of tetrakis(acetonitrile)copper(I) tetrafluoroborate in acetonitrile at various scan rates. (b) LSV curve of reduction reaction of Cu(I) recorded scan rate of 100 mV/s. The dotted line indicates semi-integrated current for forward scan (c) Tafel curve derived from</i>	66

the rising part of the LSV curve at scan rate of 100 mV/s. The inset shows the LSV data used for drawing the Tafel curve. The potential is expressed vs. the Cu reference in equilibrium with 10.25 mM Cu<sup>+</sup> in solution, i.e. -0.118 V vs. standard copper electrode in acetonitrile.

**Figure III.10.** (a) Comparison between theoretical linear scan voltammogram and experimental voltammogram obtained and recorded at 100mV s<sup>-1</sup> scan rate. The parameters used for theoretical prediction are:

$$D_{\text{Cu}(t)} = 1.70 \times 10^{-9} \text{ m}^2 \text{ s}^{-1}, \alpha = 0.8 \text{ and } k^0 = 5.12 \times 10^{-5} \text{ cm s}^{-1} \text{ (b)}$$

Comparison of theoretical LSV responses with experimental data using Fit models presented by Eq (53), Eq (54) and Eq (60).

Parameters used for LSV modelling:  $D_{\text{Cu}(t)} = 1.75 \times 10^{-9} \text{ m}^2 \text{ s}^{-1}$   $\alpha = 0.82$

and  $k^0 = 3.83 \times 10^{-5} \text{ cm s}^{-1}$  calculated from Eq (53),

$k^0 = 3.83 \times 10^{-5} \text{ cm s}^{-1}$  calculated from Eq (54) and

$k^0 = 5.88 \times 10^{-5} \text{ cm s}^{-1}$  calculated from Eq (60) The potential is

expressed vs. the Cu reference in equilibrium with 10.25 mM Cu<sup>+</sup> in solution, i.e. -0.118 V vs. standard copper electrode in acetonitrile.

**Figure IV.1.** Flowchart of the implemented CV models 75

**Figure IV.2.** Simulated cyclic voltammograms obtained with the Butler-Volmer equation through use of the derived semi-analytical solutions (black curve) and by the finite element method (red-curve).  $\alpha=0.5$ ,  $INIT=0$ ,  $LIMIT=-5$  and  $\omega=10^3$  76

**Figure IV.3.** Calculated cyclic voltammograms for various value of  $\omega$  with  $\alpha=0.5$ ,  $INIT=0$ ,  $LIMIT=-30$ . (a) reversible case ( $\omega=10^3$ ), (b) quasi-reversible case ( $\omega=10^1$ ), (c) irreversible case ( $\omega=10^{-3}$ ). 77

**Figure IV.4.** Effect of the transfer charge coefficient on the cyclic voltammetry responses for soluble-insoluble system. (a) quasi-reversible case ( $\omega=10^1$ ), (b) irreversible case ( $\omega=10^{-3}$ ). 78

**Figure IV.5.** The effect of switching potential on theoretical CVs. (a) reversible case ( $\omega=10^3$ ), (b) quasi-reversible case ( $\omega=10^1$ ), (c) irreversible case ( $\omega=10^{-3}$ ). 79

**Figure IV.6.** *Simulated CVs (a1, a2 and a3) and theoretical concentration profiles (b1, b2 and b3) of the soluble-insoluble redox system. a1-b1: reversible case ( $\omega=10^3$ ), a2-b2: quasi-reversible case ( $\omega=10^1$ ) and a3-b3: irreversible case ( $\omega=10^{-3}$ ).*

## LIST OF TABLES

<b>Table I.1.</b>	<i>Chronology of some important events in history of LSV and CV theories to study soluble-soluble and soluble-insoluble redox couples.</i>	20
<b>Table I.2.</b>	<i>Variation of the peak potential separation with dimensionless kinetic parameter at 25 °C for a One-Step Reaction, and for <math>\alpha=0.5</math>.</i>	26
<b>Table III.1.</b>	<i>Mesh properties</i>	56
<b>Table III.2.</b>	<i>Kinetic-mass transport parameters for Cu(I)/Cu(0) redox couple</i>	67

# ***Introduction***

## Introduction

Our thesis research concerns the visualization and the electrochemical evaluation by means of the potential scanning methods of voltammetry, the behavior of a metal electrodeposition reaction. Electrochemical electrodeposition is one-of-a-kind methods that aimed on depositing metal or alloy coatings on conductive substrates in the presence of an electrolyte using an electric field [1]. Owing to its possible applications in advanced technologies such as. microelectronics and, most recently, to energy conversion, it has attracted increasing attention in the research community [2].

Voltammetry techniques are a group of electroanalytical techniques which imposes a controlled variable voltage power source on the solution to be analyzed, to force an electrochemical reaction to proceed [3], and then monitors the corresponding current behaviors. Information on the redox reaction process is represented by a peak or trough in the current signal. Because there are so many ways to vary a potential, there are also many different types of voltammetric techniques, including polarography (DC Voltage), linear or cyclic sweep, differential staircase, normal pulse, reverse pulse, differential pulse, and others [3]. In this study, we focus solely on Linear Sweep Voltammetry (LSV) and Cyclic Voltammetry (CV), which may be the most selective techniques for the rapid quantitative determination of the kinetic and thermodynamic characteristics of an electrode reaction in electrochemistry.

On another note, an analysis of typical voltammetric behavior, such the position and shape of peak can be helpful, but it is often not enough to probe kinetic and thermodynamic properties of redox process, and a computer simulation, becomes indispensable then. When introducing simulation in LSV or CV techniques, naturally the well-known simple one-step redox system is usually discussed, which allows researchers working on electrochemistry to become acquainted with the main processes involved in a voltammetry experiment. An analysis of the literature allows distinguishing various redox system types. Firstly, by describing the nature of the redox couples which are involved in an electrochemical system, we can cite soluble-soluble, insoluble soluble and soluble-insoluble redox systems. And secondly by examining the rate of the reaction, we cite reversible, quasi-reversible and irreversible systems [4].

For the case of soluble-soluble redox system, diverse theoretical studies have simulated the current responses and many models are available that can be used in the estimation of kinetic parameters [5], pointing that the first LSV responses were first theorized in 1948 by Randles for reversible processes [6], and over the years subsequently expanded and developed for additional aspects, irreversible or quasi-reversible electron transfers, coupled chemical or adsorption-desorption processes and multiple charge transfer process, etc.

Likewise, to predict mathematically how does an insoluble-soluble system respond under LSV or CV conditions, several studies were done [4]. While there has been comparatively little effort to theoretically model voltammetry experiments involving soluble-insoluble couples [7]. and until this study, the full CV theory for reversible and irreversible cases has not yet completely understood and the quasi-reversible electron transfer has never been addressed before. That is why, many researchers incorrectly use general models developed for soluble-soluble systems also for soluble-insoluble systems, leading to misinterpretation of the experimental data, so there is clearly a need for LSV and CV models and characteristic diagnostic criteria also for soluble-insoluble system.

In light of this, the objective of this thesis is to:

- Study, understand and model the theoretical LSV and CV behaviour for reversible, quasi reversible and irreversible soluble-insoluble redox reactions. for this purpose, the semi-analytical method and the finite element method have been chosen to build a theoretical model based on Butler-Volmer type equation to produce theoretical LSV and CV curves.
- Developing algorithm, by matching the theoretical and experimental LSV or CV responses, it should be possible to extract useful mass transport and kinetic information whatever the degree of the reversibility.
- Propose mathematical models for use in direct determination of kinetic electrochemical parameters from experimental LSV or CV curves of metal deposition process.

To verify the theoretical conclusions and demonstrate the accuracy and the effectiveness of our numerical models, experimental tests with the system Cu(I)/Cu(0) are performed. The accurate estimation of the electrochemical kinetics of this process is required to understand better the limitations for the nonaqueous batteries utilizing Cu(I)/Cu(0) couple as the negative redox couple.

This thesis is divided into four chapters. The first chapter is background, literature review of previous fundamental studies on simulation of voltammetry responses, and it also contains the problematic and detailed scope of this work. The second describe the experimental devices and simulation tools employed in this study. The subsequent two chapters describe in detail the mathematical approaches to the solution used for the simulation of LSV and CV responses.

## References

- [1] M. K. Kolle, S. Shajahan, A. Basu, *Effect of Electrodeposition Current and Pulse Parameter on Surface Mechanical and Electrochemical Behavior of Ni–W Alloy Coatings*, *Metall Mater Trans A*, 51, 3721-3731, 2020.
- [2] G. Zangari, *Electrodeposition of alloys and compounds in the era of microelectronics and energy conversion technology*. *Coatings*, 5(2), 195-218, 2015.
- [3] B. Rezaei, N. Irannejad, *Electrochemical detection techniques in biosensor applications*, In *Electrochemical Biosensors*; Elsevier, Amsterdam, 2019.
- [4] A. Saila, *Etude des systèmes électrochimiques quasi-réversibles par voltamperométrie à balayage linéaire et semi-intégration, Applications aux comportements de rhenium et dysprosium en milieux de sels fondus*, Thèse de doctorat, Université de Badji Mokhtar, Annaba, 2010.
- [5] R. G. Compton, E. Laborda, K. R. Ward, *Understanding voltammetry: simulation of electrode processes*, Imperial College Press, London, 2013.
- [6] J. E. B. Randles, *A cathode ray polarograph. Part II. —the current-voltage curves*, *Trans. Faraday Soc*, 44, 327–338, 1948.
- [7] D. Krulic, N. Fatouros, D. Liu, *A complementary survey of staircase voltammetry with metal ion deposition on macroelectrodes*, *J. Electroanal. Chem.* 754, 30–39, 2015

# **CHAPTER I**

## *Background and literature review*

---

In this chapter, we provide a full description of solid-liquid electrochemical system with fundamental thermodynamic, kinetic, and mass transfer laws that may govern such systems.

Next, we summarize main progresses made to predict the behavior of the system involving soluble-soluble and soluble-insoluble redox couples, by Linear potential scan voltammetry and cyclic voltammetry, we then outline the most common mathematical models.

At the end of this chapter, goals of the present thesis are defined.

---

## I.1. Description of electrochemical systems

Electrochemistry is the study of different electrochemical systems in which charged particles (ions or/and electrons) cross the interface when two phases are brought into contact, can be either: solid/liquid, liquid/liquid or of solid/solid type [1]. This thesis is concerned with phenomena occurring in solid-liquid electrochemical systems.

A solid-liquid electrochemical system (Fig.I.1) can be described as having two electrically conducting media which can be classified as electrodes connected to an external circuit, two electrodes at least, and an electrolyte in between [1,2].

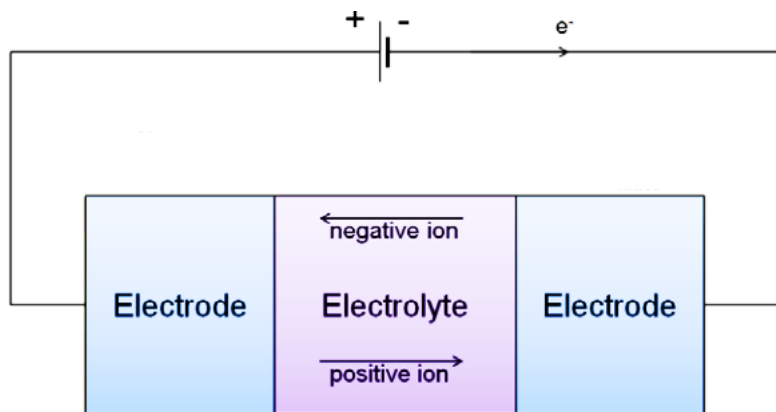


**Figure I.1.** Simple structure of solid-liquid electrochemical systems. Electrode materials can either be metals, semimetals, or semiconductors, which choice should depend on the application. The electrolytic ions perform the role of enabling electric current to flow through an electrochemical cell from one electrode to the other [3].

At solid-liquid phase boundaries, an arrangement of two opposite charges carriers occurs and the interface becomes electrified. Thus, local electric fields and potential differences are produced in the interfacial region. This arrangement area is called the Electrical Double Layer (EDL) [4].

In the context of understanding the structure and proprieties of the EDL, we will briefly review the current EDL models such us those given by Helmholtz, Gouy-Chapman, Stern and Garahme.

### I.1. 1. Helmholtz EDL model

The concept that when the charged electronic conductors is brought into contact with a liquid ionic conductor can repel the co-ions of the charge while attract countersigns ions to their

surfaces was firstly studied in 1853 by the physicist Helmholtz as exemplified in Fig I.2 (a) [5,6]. The gist of this model is that the structure of the interfacial region is treated as two-plate conventional capacitors and the potential falls linearly. The Electrical Double Layer Capacitance (EDLC) can be described as [5]:

$$EDLC_H = \frac{A\varepsilon}{4\pi d} \quad (1)$$

where  $\varepsilon$  is the dielectric constant of the electrolyte,  $A$  is the area of electrode exposed to the electrolyte and  $d$  is the thickness of electric double layer.

This model ignores the capacitance dependence on the temperature and voltage, and hence is inadequate for accurate EDLC estimation [5].

### I.1. 2. Gouy-Chapman EDL model

The Helmholtz simple model was farther extended to the diffuse model of EDL by Gouy and Chapman to include the influence of the thermal motion near the surface, so that the ions would not remain static but would be subject to thermal fluctuation and have a tendency to spread out into solution, forming what is called a diffuse double layer [5-7]. Moreover, the theory of Gouy-Chapman described the dependence of the Electrical Double Layer Capacitance (EDLC) on surface potentials  $E_s$  at temperature  $T$  as follows [5]:

$$EDLC_G = z\sqrt{\frac{2q^2N\varepsilon}{kT}} \cosh\left(\frac{zqE_s}{2kT}\right) \quad (2)$$

where  $z$  is the valence of the ions,  $q$  is the elementary charge,  $N$  is the number of ions per centimeter,  $\varepsilon$  is the dielectric constant of the electrolyte, and  $k$  is the Boltzmann constant.

In such situation, the surface charge potential profile exponentially decreases with distance as shown in Fig I.2 (b) [7].

### I.1. 3. Stern EDL Model

Stern combined the Helmholtz and Gouy-Chapman models and suggested then the existence of two regions of ion distribution namely, (i) the inner compact region also known as the Stern layer, constituted by a layer of strongly adsorbed ions at the electrode surface, and the other (ii) is referred to the diffuse layer region, as exactly what the Gouy-Chapman model defines [8-10]. So that, the total EDLC can be treated as a combination of the capacitances from two regions as [5]:

$$\frac{1}{EDLC} = \frac{1}{EDLC_H} + \frac{1}{EDLC_G}$$

(3)

As shown in Fig I.2 (c), the potential decays linearly in the Stern layer and then exponentially in diffuse layer [11].

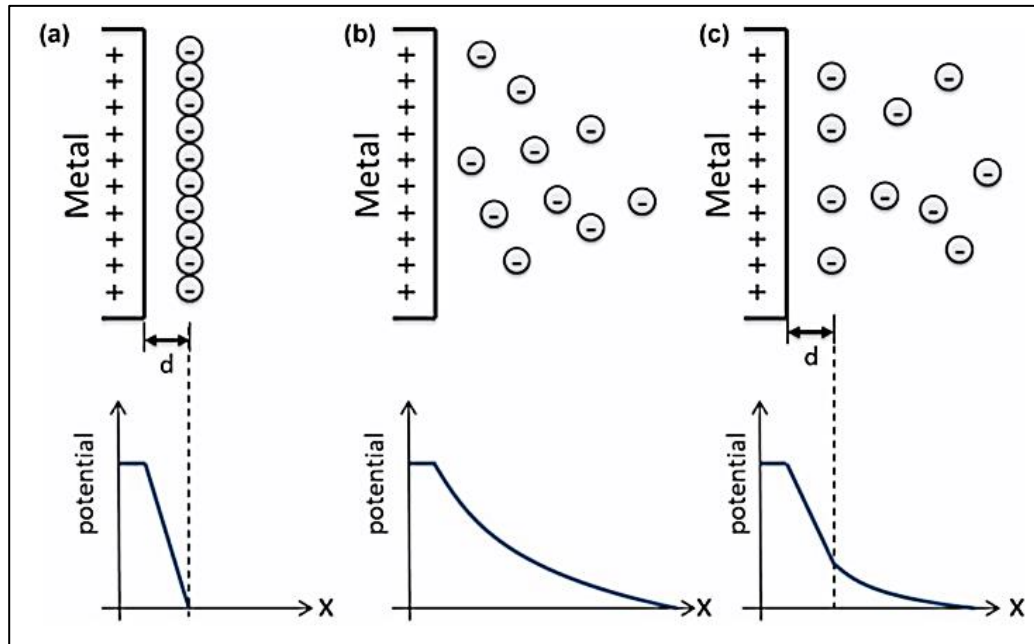


**Figure I.2.** Electric charge and potential distribution in EDL. (a) Helmholtz, (b) Gouy - Chapman and (c) Stern models [7].

#### I.1. 4. Grahame EDL Model

Based on assumptions from earlier models, Grahame suggested further refinement by dividing the compact layer into two parts with the introduction of two planes: (i) an inner Helmholtz plane (IHP) consisting of non-hydrated coions and counterions that are specifically adsorbed on the surface of the electrode and (ii) an outer Helmholtz plane (OHP) consists of solvated ions of opposed charge compared to the electrode, that are non-specifically adsorbed and attracted by the columbic force [8]. Therefore, the Grahame model proposed the existence of three regions: IHP, OHP, and “diffuse layer” (see Fig I.3). the potential drop and the capacitance are similar to what stern described [8].

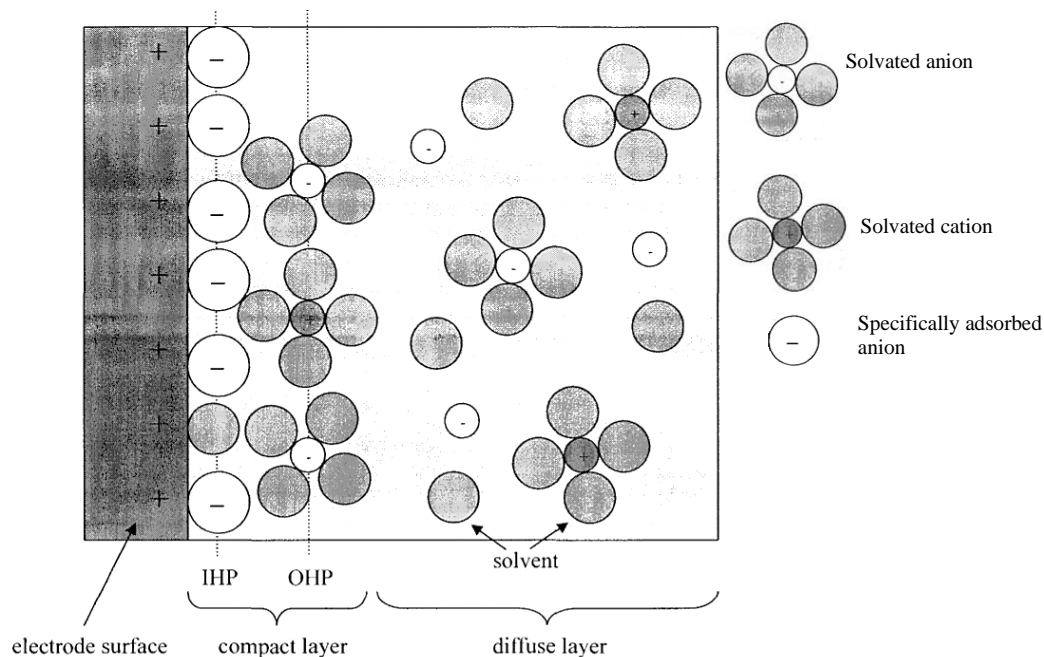


Figure I.3. Schematic representation of the Grahame model of the double layer [8].

## I.2. Electrochemical thermodynamic and kinetics

### I.2.1. Steps of electrode process

An electrochemical reaction occurring in an electrochemical system involves transfer of charges across electrode/electrolyte interface. A simplified mechanism for an electrochemical reaction consists of a sequence of steps (Fig I.4) involving electron transfer, mass transport, adsorption/desorption and chemical reactions [12-13].

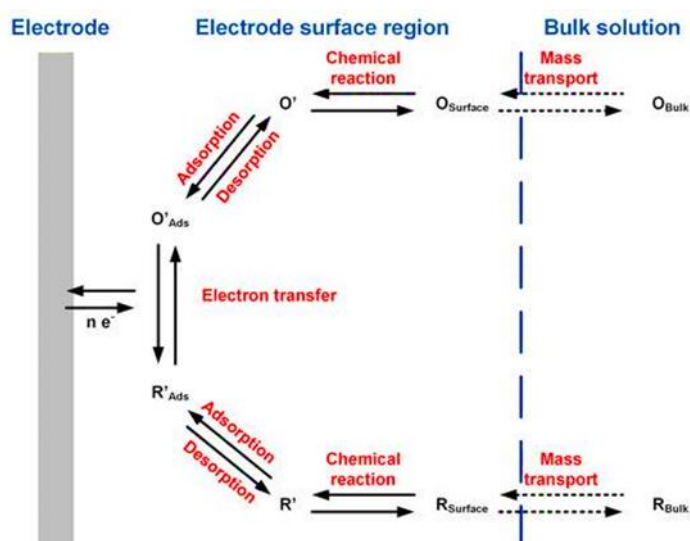


Figure I.4. Essential steps of electrochemical reactions [12].

**I.2.2. Nernst equation**

Consider a generalized process involving the transfer of  $n$  electrons:



Where:

- O: Oxidized species
- n: Number of electrons,  $e^-$ , involved
- R: Reduced species of the redox couple
- $k_o, k_R$ : Electron kinetic transfer constants for the oxidation and for the reduction, respectively-

Thermodynamically speaking, when the system is in a state of zero applied potential, the standard free energies for the reduction reaction (cathodic) and oxidation reaction (anodic) are respectively  $\Delta G_{0c}^\ddagger$  and  $\Delta G_{0a}^\ddagger$  (see solid curve in Fig I.5). By changing the potential to the new value  $E$ , the energy of an electron on the electrode changes by  $nFE$ , consequently the dashed curve for the reduction  $O+ne^- \rightarrow R$  move up or down by that amount [14].

According to the law of conservation of energy, the change in chemical energy should be equal to the electrical energy produced by the system [14-15]. Hence, the Gibbs free energy change is given by:

$$\Delta G = -nFE \quad (5)$$

Under standard conditions (atmospheric pressure and a temperature of 298K), the above equation can be given as [15]:

$$\Delta G^0 = -nFE^0 \quad (6)$$

According to the thermodynamic theory, the Gibbs free energy under given conditions can be related to Gibbs free energy under the standard condition and the reaction quotient  $Q$  as [15]:

$$\Delta G = \Delta G^0 + RT \ln Q \quad (7)$$

By combining the above three equations eqs (5-7), the following Nernst type equation is obtained:

$$E = E^0 - \frac{RT}{nF} \ln Q \quad (8)$$

Which can be simplified to:

$$E = E^0 + \frac{RT}{nF} \ln \frac{[C_o]}{[C_R]} \quad (9)$$

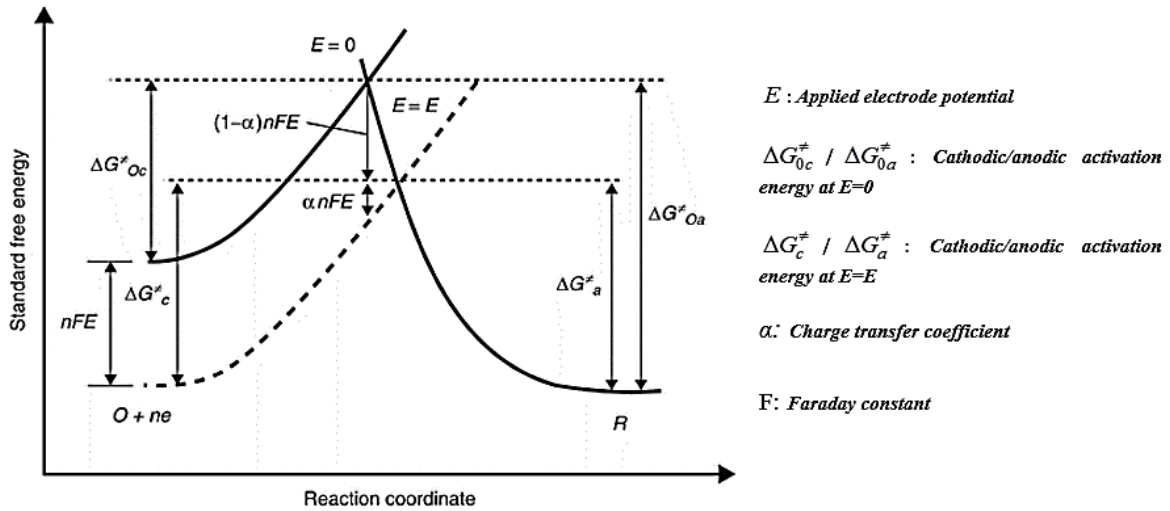


**Figure I.5.** Free- energy reaction coordinate diagram for a simple redox reaction. Full lines: zero applied potential  $E = 0$ , dashed line: with applied potential  $E=E$  [16].

### I.2.3. Butler-Volmer equation

As a result of shift in potential from 0 to a value  $E$ , the system gains the enough energy for the forward reaction to become dominant over the reverse (see Fig I.5). in such situation, we should define the amount of energy necessary for each reaction to occur, which mainly depend on the transfer coefficient  $\alpha$  [17].

For the forward reaction, the new activation barrier is higher than  $\Delta G_{0c}^{\ddagger}$  by an amount  $\alpha nFE$  [14]:

$$\Delta G_c^{\ddagger} = \Delta G_{0c}^{\ddagger} + \alpha nFE \tag{10}$$

For the reverse reaction, the activation barrier is less than  $\Delta G_{0a}^{\ddagger}$  by an amount  $(1-\alpha)nFE$  [14]:

$$\Delta G_a^{\ddagger} = \Delta G_{0a}^{\ddagger} - (1-\alpha)nFE \tag{11}$$

The rate constants,  $k_O$  and  $k_R$  defined previously in eq (4), obeys to Arrhenius equation, and can be expressed as a function of the applied voltage  $E$  by the following generalized equations:

$$k_R = A_R e^{-\frac{\Delta G_c^{\ddagger}}{RT}} = A_R e^{-\frac{\Delta G_{0c}^{\ddagger}}{RT}} e^{-\frac{\alpha nFE}{RT}} \tag{12}$$

And

$$k_O = A_O e^{-\frac{\Delta G_a^{\ddagger}}{RT}} = A_O e^{-\frac{\Delta G_{0a}^{\ddagger}}{RT}} e^{\frac{(1-\alpha)nFE}{RT}} \tag{13}$$

Here,  $A_R$  and  $A_O$  were used to denote the pre-exponential factors of the reduction and the oxidation reaction, respectively.

At equilibrium, the rate of the forward reaction is equal to the rate of the reverse, then we can write [14]:

$$C_O k_O = C_R k_R \quad (14)$$

For equal concentrations of 'O' and 'R', it follows:

$$k_O = k_R = k^0 \quad (15)$$

where  $k^0$  is standard rate constant of the redox reaction, eq (4). The rate constants can be expressed in terms of the standard rate constant by rewriting equations (12) and (13):

$$k_R = k^0 e^{-\frac{\alpha n F (E - E^0)}{RT}} \quad (16)$$

$$k_O = k^0 e^{\frac{(1-\alpha) n F (E - E^0)}{RT}} \quad (17)$$

The expression relating the overall current to the electrode potential, for an electrode of surface area,  $A$ , is formulated in term of the sum of the partial anodic  $I_a$ , and partial cathodic  $I_c$ , currents [18]:

$$I = I_a + I_c = nFAk_O C_R - nFAk_R C_O \quad (18)$$

Substituting for  $k_O$  and  $k_R$  from equations (16) and (17):

$$I = nFAk^0 \left[ C_R \exp\left(\frac{(1-\alpha)nF(E-E^0)}{RT}\right) - C_O \exp\left(\frac{-\alpha nF(E-E^0)}{RT}\right) \right] \quad (19)$$

Which is known as the Butler-Volmer equation.

### I.3. Mass transport phenomena

Regarding to Fig I.4, we can say that the electroactive species should come from the bulk solution to reach the electrode surface or to transfer into the solution from the electrode to allow the electron transfer to occur. Therefore, besides the knowledge of the fundamental concepts and laws of thermodynamics and kinetics, transport processes are as well decisive for performing efficient electrochemical processes. There are three modes of mass transport: Diffusion, Migration and Convection, each with its own effect on the observed current characteristics of the system [19].

#### I.3.1. Diffusion

The movement of electroactive species under concentration gradient is called diffusion. This

is mainly described by Fick's first and second laws [19].

Fick's first law describes the diffusive mass flux as a function of diffusion coefficient and spatial concentration gradient. For the one-dimensional case, it is expressed as [20]:

$$J_d = -D \frac{\partial C}{\partial x} \quad (20)$$

Where,  $J_d$  is the diffusion flux,  $D$  is the ion diffusion coefficient,  $C$  is the ion concentration,  $x$  is the diffusion distance and  $\frac{\partial C}{\partial x}$  is the ion concentration gradient.

While the Fick's second law of diffusion describes how the concentration of a species changes with respect to time and position. For one spatial dimension, it can be expressed as [20]:

$$\frac{\partial C(x,t)}{\partial t} = D \frac{\partial^2 C(x,t)}{\partial x^2} \quad (21)$$

### I.3.2. Migration

Migration is the mechanism of moving of species,  $i$ , with charge  $z_i$  under potential gradient [17]:

$$J_m = \frac{z_i F}{RT} DC \Delta \phi \quad (22)$$

Where  $J_m$  is the migration flux, and  $\Delta \phi$ , is the electrical field gradient.

Due to the mathematical complexity in the treatment of electrochemical systems, the migration contribution can be neglected. This can be achieved, if a sufficiently large concentration of supporting electrolyte is added, that effectively cancels the potential gradient around the electrode surface [20].

### I.3.3. Convection

Convection is the movement of particles resulting from an imbalance of force, either forced or natural. Forced convection occurs when the solution is forced to flow by an external source (e.g., due to stirring, such as generated by the rotating disc electrode). While, natural convection is often due to temperature and solution density gradients and is random in nature, which make it difficult to model. However, it can be considered insignificant for short time periods [22].

## I.4. Voltammetry-sweep techniques to study electrochemical systems

In electrochemical systems, understanding and controlling electron transfer process is of critical importance. However, the topic of interest of this chapter is how an experimenter can visualize and assess the behavior of such system using voltammetry techniques. The term of voltammetry covers a range of electroanalytical methods, based on the measurement of current responses due to a voltage excitation. The obtained data is usually presented as a plot of current versus potential, known as a voltammogram [23].

Depending on the type of potential signal applied to the system, one can distinguish different electrochemical voltammetries that have been reviewed in several literature books [21,22]. In the work described in this thesis, we concentrate only on Linear Sweep Voltammetry (LSV) and Cyclic Voltammetry (CV) under diffusion mass transport control. CV or LSV is capable of yielding a fast and clear view about kinetics, thermodynamics, and mechanisms of electrode reactions, from the inspection of the shape and position of the experimental current-potential curves.

### I.4.1. Linear Sweep Voltammetry (LSV)

In LSV, the current is measured at the electrode while the potential sweeps linearly in time from a lower potential  $E_i$  to a higher upper potential  $E_f$ , or vice versa. The potential-time profile can be expressed as [24,25]:

$$E = E_i \pm vt \quad (23)$$

The characteristics of the LSV recorded depend crucially on the following factors: the rate of the electron transfer reaction, the chemical reactivity of the electroactive species and the potential scan rate.

The results of LSV are presented as one of oxidation or reduction peak.

A linear sweep anodic potential ramp applied to an electrode is shown in Fig I.6.a, and the corresponding voltammogram is shown in Fig I.6.b.

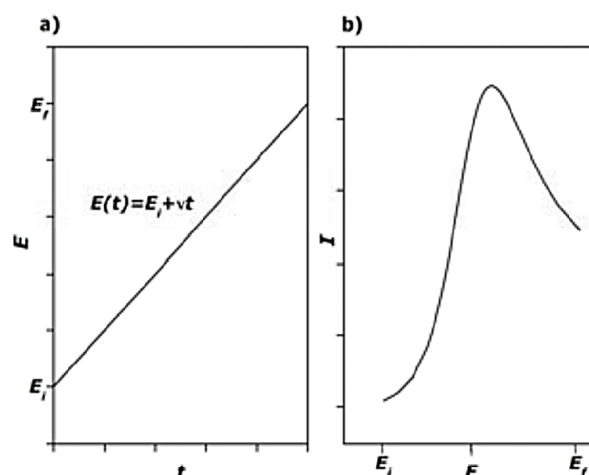


**Figure I.6.** a) Potential function applied at the electrode to oxidize the reduced species in the solution Redox couple. b) linear potential sweep voltammogram [26].

#### I.4.2. Cyclic Voltammetry (CV)

Same as linear sweep voltammetry except that the applied potential goes one step further and does not finish with a single sweep (see Fig I.7). So that, it is ramped up or down linearly from a starting potential  $E_i$  to a defined potential value and then, at switching time  $t_\lambda$ , turned back in a cyclic manner. The following equation is obeyed [27]:

$$E = \begin{cases} E_i \pm vt, & t \leq t_\lambda \\ E_i \pm 2vt_\lambda \pm vt, & t > t_\lambda \end{cases} \quad (24)$$

Where upper signs refer to forward anodic sweeps and lower signs refer to forward cathodic sweeps.

Figure 1.7a shows the triangular wave potential applied to the working electrode and Figure I.7b shows the resulting voltammogram.

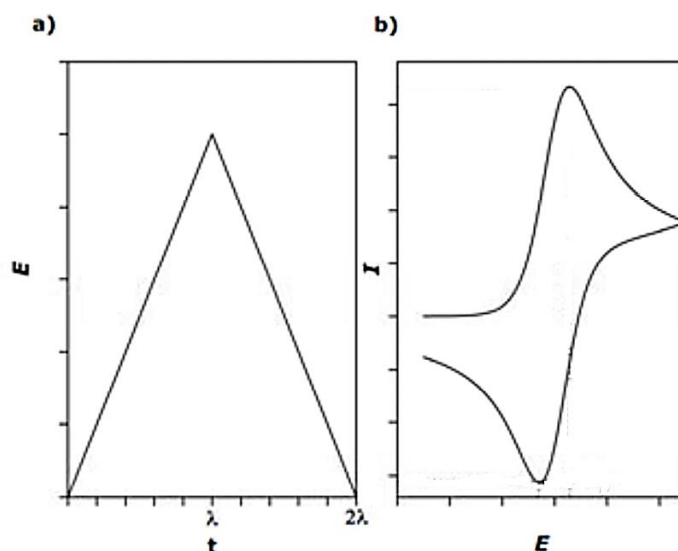


**Figure I.7.** a) Potential function applied in cyclic voltammetry to oxidize the reduced species in the solution Redox couple. b) cyclic voltammogram [26].

From the analytical point of view, parameters that are most useful of CV are [26]:

- Peak potential is the potential at which almost the analyte species on electrode surface is oxidized or reduced.
- Peak current is the maximum (or minimum) intensity of the current attained by an oxidation or reduction peak during an applied potential scan.
- Half wave potential is defined as the potential at half height of the peak current.
- Peak to peak current ratio is the ratio of the forward peak current density to the reverse peak current density which generally used as an indicator of the reversibility of the redox reaction.
- Peak separation is defined as a quantitative measure for how well two peak potentials (anodic and cathodic) are separated.

### I.4.3. Electrochemical voltammetry Measurement System

Electrochemical voltammetry measurement systems typically consist of three electrodes [28]: auxiliary, working and reference electrode, immersed in cell medium and connected to a potentiostat circuit (see Fig I.8).

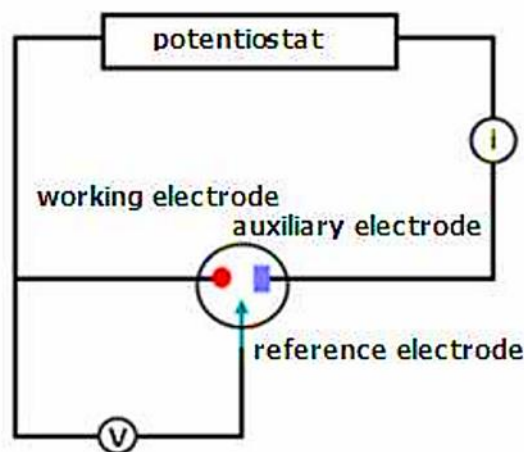


**Figure I.8.** Schematic sketch of the three-electrode voltammetry measurement system [29].

The potentiostat sets the desired control potential of the experiment and monitors the corresponding current. The working electrode is where the reactions of interest take place. The role of the auxiliary electrode is to balance the reactions occurring at the working electrode by acting as a source/sink for electrons to complete the electrical circuit [27-29]. The role of the reference electrode is to provide a stable potential for measurement in the voltammetry measuring systems [30].

#### **I.4.4. Common causes of Distortion in voltammetric curves**

As the assessment of the behavior of an electrochemical system depend strongly on the shape and position of voltammograms, so that, a considerable care should be taken when interpreting the voltametric responses. However, a knowledge of the causes of errors in data obtained from voltammetry techniques, are indispensable. Among these, the uncompensated resistance, and the charging double layer current [31].

The uncompensated resistance in an electrochemical system is defined as the sum of resistances in all current path to the working electrode. The origin of these resistances can be divided into three groups. Group 1: ion migration in the electrolyte, Group 2: electron transport, Group 3: contact resistances [32], with the possible presence of the dominance of one resistance, depend on the type of the system. In the case of voltammetry Measurement System, the uncompensated resistance is often dominated by the resistance of electrolyte solution which in combination with the flowing current yields to the voltage ohmic drop [32]. The effect of the ohmic drop on LSV and CV include: A shift of the current-voltage curve

along the x-axis, which lead to a displacement of the peak potential, broadening of the peak width and a decrease in the peak current [22]

On the other hand, due to the capacitive nature of the electrode-electrolyte interface, an EDL charging current is induced as a result of the applied potential [34]. This current can distort the accuracy of the measurement via a displacement of the voltammogram along the current axis, and this interference can be eliminated either by working with microelectrodes or by separating faradaic current from charging current [34-35].

## **I.5. General Overview on the LSV and CV theories in the case of one-step electrode process**

### **I.5.1. Survey of existing simulation approaches**

The days when the analysis of LSV or CV curves based only on the position and shape of their peaks are almost past. Mostly, nowadays, the simulation methods allow an entire voltammogram to be analyzed.

Indeed, the simulation may be used in a predictive way to identify a phenomenon that has not (yet) been or cannot be experimentally studied or as an ideal tool for getting qualitative (e.g. to determine elementary reaction steps) or quantitative information (e.g. to determine the heterogeneous rate constant of electron transfer reaction) by concordance between the experimental curve and simulated one. It is worthwhile to note that “Computer modelling” and “Simulation” are often used as synonyms [16].

Generally, as illustrated in Fig I.9, to simulate controlled current experiments, the following steps should be considered [16]:

- Kinetics of the electron transfer reaction, most often modelled by a Butler-Volmer type equation.
- Transport properties of the involved molecules: only diffusion is considered as means of mass transport of the analytes to the electrode, so that, a no stirred solution with a sufficiently high concentration of supporting electrolyte is assumed.
- Reaction scheme: reaction scheme may include: the adsorption reaction of electroactive species which can be described by isotherms, heterogeneous/homogeneous chemical reactions with their appropriate kinetics, and thermodynamics, etc.

- The electrical perturbation applied: e.g. triangular potential-excitation signal for CV measurements.

These steps should be combined to formulating theoretical models of voltammetry experiments usually results in partial differential equations (PDE), and subsequently solved using either: analytical, numerical, or semi-analytical methods. The solution to the problem is the concentration profiles of electroactive species, and the system's current-potential-time response for a given electrical excitation can be determined from them [21].

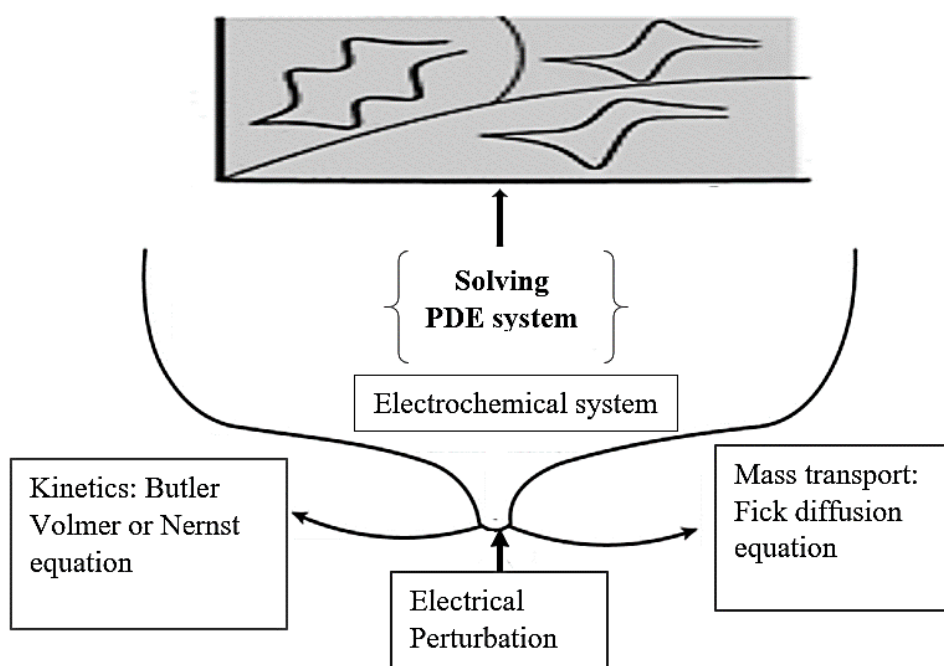


**Figure I.9.** Diagrammatic representation of the most important steps to predict voltammetric responses.

### I.5.1.1. Analytical method

Analytical method is a method which gets exact relationship between current and voltage to establish theoretical voltammograms. It is the output of a mathematical analysis of all steps cited below [21]. Besides, analytical method does not require to waste too much time and money on experiments [36]. In a recent example, redox-electrode reactions with fast electron transfer were investigated analytically by A. Samin *et al.* In this paper, the series solution to predict cyclic voltammetry responses are derived [37].

Nevertheless, a significant deficiency in employing this method for more complex voltammetry problems can be appeared. In such case, numerical methods are more effective and desired than analytical ones [21].

### **I.5.1.2. Numerical method**

It uses numerical step-by-step methods, which are based on the time-space discretization of PDEs, to obtain an approximate expression for the current vs. voltage. Of the several methods available, the most common are: Finite Difference Method, Finite Element Method, and orthogonal collection method. It processes data and solves problems by means of computer or computational model [36]. For example, in the recent work of G. Jia-yao *et al* [38], finite element method was used to simulate the cyclic voltammetric behaviors of heterogeneous electron transfer coupled with Faradic adsorption/desorption processes.

There are different and distinct kinds of software based on numerical methods, which can be used to solve voltammetry problems faster and more accurately.

### **I.5.1.3. Semi analytical method**

It is a method based on combined of two above methods: it solves first analytically the spatial aspects of the voltammetry problem to turn PDEs equations into an integral equation and then solved it numerically by discretizing the time variable [39].

## **I.5.2. Chronology of some important events in history of LSV and CV theories**

In this portion of this chapter, important historical trends in the study of electrochemical system by LSV and CV techniques are summarized in Table I.1. The systems of interest in this thesis are:

- Redox electrochemical reactions involving soluble species.
- Redox electrochemical reaction involving insoluble species.

**Table I.1.** Chronology of some important events in history of LSV and CV theories to study soluble-soluble and soluble-insoluble redox couples.

<i>soluble-soluble redox reactions</i>	
<b>1948</b>	<b>Randles</b> and <b>Ševčík</b> have developed the LSV theory in the case of reversible electron transfer reactions involving soluble species and published a well-known model relating the peak current in the reduction (oxidation) process to the scan rate, that is nowadays commonly used in estimation of the diffusion coefficient [40].
<b>1955</b>	<b>Matsuda</b> and <b>Ayab</b> have treated the case of quasi-reversible soluble-soluble redox reaction. subsequently, they have summarized the overall LSV responses as a function of kinetic rate constant and charge transfer coefficient into series diagrams. With these diagrams, one can estimate the standard rate constants regardless of the degree of reversibility and assess reversibility/irreversibility of the electrochemical reactions [22,41-42,44].
<b>1964</b>	<b>Nicholson</b> and <b>Shain</b> based on the two above theories, have simulated cyclic voltammetric behavior: First they solved PDEs for soluble-soluble redox couples, and tabulated their results in the form of dimensionless current-potential dependence. Next, they solved eight electrochemical mechanisms in which specific types of chemical reaction (preceding or following chemical reactions), that may occur in solution, were considered [22,43].
<i>soluble-insoluble redox reactions</i>	
<b>1953</b>	<b>Berzins</b> and <b>Delahay</b> were the first ones who established the LSV theory for studying the soluble-to-insoluble type of redox reaction by assuming fast electron transfer kinetics, and they derived an expression to describe the variation of peak current as a function of scan rate [45].
<b>1953</b>	<b>P.Delahay</b> was first who simulated LSV responses when the electron transfer is fully irreversible [45].
<b>1986</b>	<b>D.J. Schiffrin</b> developed the theoretical model for calculating cyclic voltammograms for reversible metal-metal ion couples under the hypothesis that there is no nucleation overpotential at the solid electrode and an instantaneous transition from bare electrode to an electrode with a monolayer of reduced species [46].

Since these works, there have been numerous studies investigating soluble-soluble process including a large class of models such as multiple charge transfer process, coupled chemical or adsorption-desorption processes, etc. [21,22]. On the contrary, only a few researchers have

been addressed to the simulation of voltammetric behavior in the case of solid product formation [47]. A visit to the Compton group website (<http://compton.chem.ox.ac.uk/>) is suggested if one wishes to get a feel for the remarkable breadth of voltammetric mechanisms that have been simulated in the last decade [43].

### I.5.3. Calculation of voltammograms for soluble-soluble redox reaction using semi analytical method

In what follows, we describe the simulation of potential sweep experiments (LSV and CV), case soluble-soluble redox reaction, through which a strategy, namely the Integral Equation (IE) method, also called Nicholson and Shain method which falls under the category of semi-analytical methods is used. For a full description of IE method, the reader is addressed to the following references: [21,48-50].

Let us consider an electroactive species “O” that is engaged in a single-step electrochemical reaction [26,51]:



O undergoes a n-electrons transfer at the electrode surface to give the product species R. Both species are soluble in the electrolytic solution for the so-called soluble-soluble redox reaction.

#### **Main assumption:**

- A one- step reaction is studied on planar electrode.
- All case, only diffusion is considered, so mass-transport of species O and R is expressed by Fick’s second law as:

$$\frac{\partial C_O(x,t)}{\partial t} = D_O \frac{\partial^2 C_O(x,t)}{\partial x^2} \quad (26)$$

$$\frac{\partial C_R(x,t)}{\partial t} = D_R \frac{\partial^2 C_R(x,t)}{\partial x^2} \quad (27)$$

To solve these differential partial equations, it is important to define the initial conditions and the boundary conditions [26]:

#### **a. Initial conditions**

- Initially, it considers that only one electroactive species is present in solution:

$$C_O(x,0) = C_O^* \quad (28)$$

$$C_R(x,0) = 0 \quad (29)$$

#### **b. Boundary conditions**

- Concentrations in a distant region from the electrode surface reach constant values ( $C_o^*$  for oxidized specie and zero for reduced one).

$$\lim_{x \rightarrow \infty} C_o(x, t) = C_o^* \quad (30)$$

$$\lim_{x \rightarrow \infty} C_R(x, t) = 0 \quad (31)$$

- By Considering the charge and mass balance at the working electrode, the other boundary condition results into the following equation:

$$J_o|_{x=0} = -J_R|_{x=0} = \frac{I}{nF} \quad (32)$$

- Concentrations of redox couple at the electrode surface vary as a function,  $f$ , of the electrode potential  $E$ :

$$C_o(0, t) = f(E) \quad (33)$$

$$C_R(0, t) = f(E) \quad (34)$$

Where  $f(E)$  depends on the kinetics of electron transfer.

In this context, it should be noted that the electrochemical reversibility, depends on the dimensionless electrode kinetic parameter  $\Lambda$ :  $\Lambda = k^0 \left( D \frac{nF}{RT} v \right)^{-1/2}$  as reported in references [22,50].

If  $\Lambda \geq 15$ , the electrochemical reaction is classified as reversible.

If  $15 \geq \Lambda \geq 10^{-2(1+\alpha)}$ , the reaction is classified as quasi-reversible.

If  $\Lambda \leq 10^{-2(1+\alpha)}$ , the reaction is termed irreversible.

### I.5.3.1. Reversible system

#### I.5.3.1.1. Theory and mathematical models

Since the reaction is reversible, the concentrations of the oxidized and reduced species at the interface are related via the Nernst equation, as [50]:

$$\frac{C_o(0, t)}{C_R(0, t)} = \exp\left(\frac{nF}{RT}(E(t) - E^0)\right) \quad (35)$$

following the Nicholson's procedure, in solving eqs (26) and (27) with the initial and boundary conditions, eqs. (28)-(35), case of linear and cyclic potential sweeps leads to the following integral equation [52]:

$$\int_0^t I(\tau)(t-\tau)^{-\frac{1}{2}} d\tau = \frac{nFA\pi^{1/2}D_o^{1/2}C_o^*}{\theta S(t)\xi + 1} \quad (36)$$

Recognizing that  $\tau$  is a dummy variable that disappears with integration,  $\xi = (D_o/D_R)^{1/2}$ ,

$\theta = \exp\left[nF/RT(E_i - E_{eq})\right]$ , specifically, for linear sweep excitation:  $S(t) = e^{-\sigma t}$ , while for

cyclic sweep excitation:  $S(t) = \begin{cases} e^{-\sigma t}, & t \leq t_\lambda \\ e^{\sigma t - 2\sigma t_\lambda}, & t \geq t_\lambda \end{cases}$ , and  $\sigma = nFv/RT$

Performing the change,  $I(t)$  to  $I(E)$  by a simple substitution and dividing by  $(D_o^{1/2}C_o^*)$ , one arrives at:

$$\int_0^{\sigma t} \frac{\Psi(z) dz}{(\sigma t - z)^{1/2}} = \frac{1}{1 + \xi\theta S(t)} \quad (37)$$

Defining further that  $\Psi = \frac{I}{nFAC_o^*(D_o\sigma)^{1/2}}$  is the so-called dimensionless current function.

The integral in eq (37) was solved numerically, and then rearranged to finally give the following voltammetry algorithm represented in the form of summation series (for a detailed analysis see [21-22, 49-52]).

$$2\sqrt{\delta} \left[ \Psi(1)\sqrt{k} + \sum_{j=1}^{k-1} \sqrt{k-j} [\Psi(k+1) - \Psi(k)] \right] = \frac{1}{1 + \xi\theta S(\delta k)} \quad (38)$$

So single scan or cyclic current-potential curves can be computed easily.

An example of voltammogram for reversible soluble-soluble system is illustrated in Fig I.10.

### I.5.3.1.2. Potential and current peaks in LSV and CV for reversible soluble-soluble redox reaction

The most prominent features that can be extracted from the red portion of the curve (i.e. curve corresponds to single scan) are [26,51]:

-The minimum value of the function is  $\Psi = -0.4463$ , therefore, the scan rate-dependent peak current can be expressed as:

$$(I_p)_{rev} = -0.4463nFAC_o^* \left(\frac{nF}{RT}\right)^{1/2} v^{1/2} D^{1/2} \quad (39)$$

The potential where the peak cathodic current is observed:

$$E_p - E^0 = -1.2RT/nF \quad (40)$$

The potential at half the peak current can be related to the peak potential as:

$$E_p - E_{p/2} = -2.20 \frac{RT}{nF} \quad (41)$$

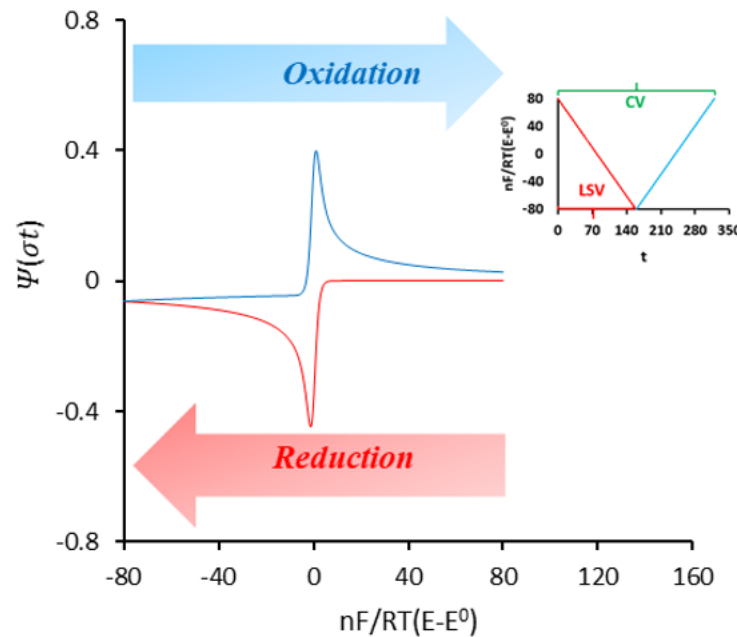


**Figure I.10.** Adimensional CV responses for reversible soluble-soluble system, for  $\Lambda=10^3$ . the cathodic portion of CV curve is the same for the LSV. Insert is a potential cycling profile.

In fact, on the return scan (backward CV component indicated in bleu in Fig I.10), the height and position of the anodic portion depend on the choice of the switching potential and the difference between the peak potential  $E_p$  and switching potential  $E_\lambda$ . For Nernstian charge transfer:

-Peak current ratio is unity:  $\left| I_{p_r} / I_{p_f} \right| = 1$ , (valid, when the product of the reaction is stable and  $(E_p - E) > 35 / nmV$ ).

-Peak to peak separation:  $\Delta E_p = 2.3RT / nF$ , which equal to  $58 / nmV$ , at exactly  $25^\circ\text{C}$ .

### I.5.3.2. Quasi-reversible system

#### I.5.3.2.1. Theory and mathematical models

The quasi-reversible redox system differs from the Nernstian case in that the relation between the redox couple concentrations at the electrode surface does not obey to Nernst equation. In such situation, the conditions at the electrode surface are dictated by the Butler-Volmer formalism [53]:

$$D_o \left( \frac{\partial C_o(x,t)}{\partial x} \right)_{x=0} = k^0 e^{-\alpha \frac{nF}{RT}(E(t)-E^0)} \times \left[ C_o(0,t) - C_R(0,t) e^{\frac{nF}{RT}(E(t)-E^0)} \right] \quad (42)$$

By similar way, numerical method was applied. Then, the formula representing the dimensionless current function of the quasi-reversible system is given by:

$$\Psi = I / \left[ nFAC_o^* D^{1/2} (vnF / RT)^{1/2} \right] \quad (43)$$

An example of CVs under quasi-reversible conditions by varying kinetic parameter are portrayed in Fig I.11.

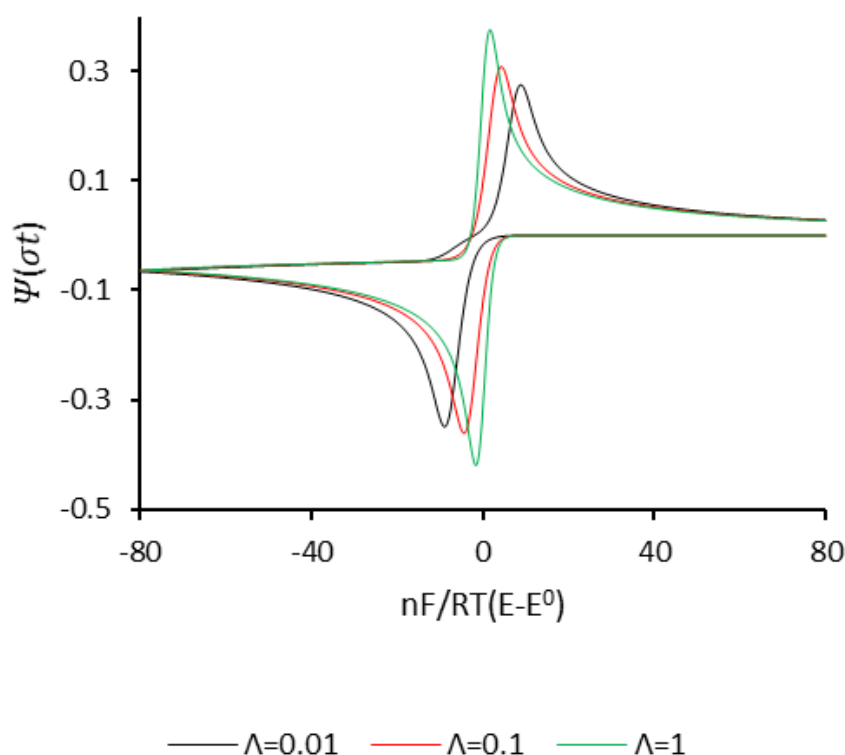


**Figure I.11.** Different CV responses for different  $\Lambda$  values in quasi-reversible region

### I.5.3.2.2. Potential and current peaks in LSV and CV for quasi-reversible soluble-soluble redox reaction

In quasi-reversible region might show qualitatively different voltametric responses depending on the kinetic parameter and the charge transfer coefficient. In such scenario, general

formulae describing peak current, peak potential, and half-peak potential were given by [22,42]:

$$I_p = (I_p)_{rev} K(\Lambda, \alpha) \quad (44)$$

$$E_p - E_{1/2} = -\Xi(\Lambda, \alpha) \frac{RT}{nF} \quad (45)$$

$$E_{p/2} - E_p = \Delta(\Lambda, \alpha) \frac{RT}{nF} \quad (46)$$

Where  $K(\Lambda, \alpha)$ ,  $\Xi(\Lambda, \alpha)$  and  $\Delta(\Lambda, \alpha)$  are dimensionless parameters defined by Matsuda and Ayabe, which account for the kinetic factor, and the charge transfer coefficient governing LSV responses.

When we deal with the cyclic voltammograms, other important criteria concerned the peak potential separation in cyclic voltammetry should be mentioned. Returning to the theory of Nicholson and Shain who demonstrated that the magnitude of the peak potential separation is function of a dimensionless kinetic parameter and unaffected by the variation in charge transfer coefficient, in the interval [0.3-0.7]. we have presented in Tab I.2 the theoretical values of  $\Delta E_p$  which is restricted in the range of 61-212/n mV for quasi reversible system [54].

**Table I.2.** Variation of the peak potential separation with dimensionless kinetic parameter at 25 °C for a One-Step Reaction, and for  $\alpha=0.5$ .

$\pi^{1/2}\Lambda$	20	7	6	5	4	3	2	1	0.75	0.50	0.35	0.25	0.10
$\Delta E_p \times n$ (mV)	61	63	64	65	66	68	72	84	92	105	121	141	212

These theoretical values can be used to estimate the standard rate constants for quasi-reversible systems.

### I.5.3.3. Totally irreversible system

#### I.5.3.3.1. Theory and mathematical models

In the case of totally irreversible redox reactions, it is necessary to take into account the boundary condition described the surface flux in eq (47) instead of eq (42) [50]:

$$D_o \left( \frac{\partial C_o(x,t)}{\partial x} \right)_{x=0} = C_o(0,t) k_i e^{bt} \quad (47)$$

Where:

$$k_i = k^0 \exp(-(\alpha n F / RT)(E_i - E^0)) \quad (48)$$

And

$$b = \alpha n F v / RT \quad (49)$$

In addition, it's important to pointing that only electro-reduction of O through reaction in eq (25) is considered [50].

Following the same sequence of steps as for reversible system, thus, the unknown current function can be determined by [51]:

$$\Psi = I / \left[ n F A C_o^* D^{1/2} v^{1/2} (\alpha n F / RT)^{1/2} \right] \quad (50)$$

An example of the obtained adimensional current-potential curve, for irreversible case is illustrated in Fig I.12.

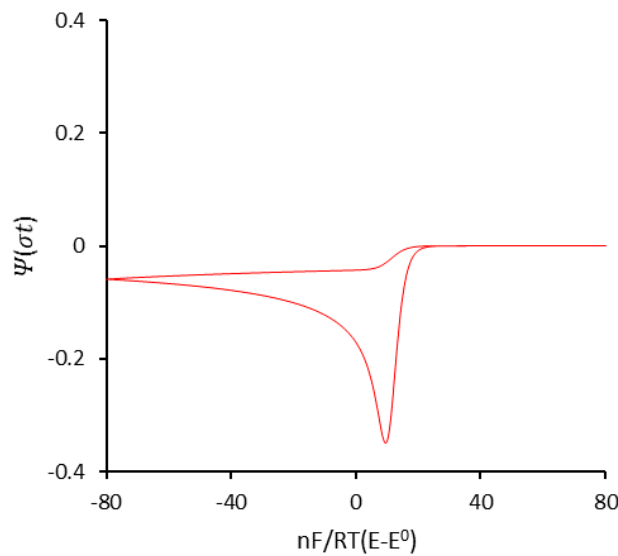


**Figure I.12.** Adimensional CV responses for irreversible soluble-soluble system, for  $\alpha=0.5$  and  $A=0.0001$ .

### I.5.3.3.2. Potential and current peaks for irreversible soluble-soluble redox reaction

Relationships for peak current, peak potential, and half peak potential are given by equations (51), (52) and (53) respectively [51]:

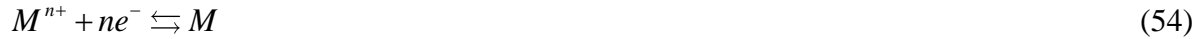
$$I_p = (2.99 \times 10^5) n (\alpha n)^{1/2} A C_o^* D_o^{1/2} v^{1/2} \quad (51)$$

$$E_p = E^0 - \frac{RT}{\alpha nF} \left[ 0.78 + \ln \left( \frac{D_o^{1/2}}{k^0} \right) + \ln \left( \frac{\alpha nF}{RT} \right)^{1/2} \right] \quad (52)$$

$$\left| E_p - E_{p/2} \right| = \frac{1.857RT}{\alpha nF} \quad (53)$$

#### 1.5.4. Calculation of voltammograms for soluble-insoluble redox reaction

A simple electrodeposition reaction,  $M^{n+}$  cations that react with electrons  $e^-$  at the surface of the electrode and are reduced to metal  $M$ , is theoretically described, and discussed elsewhere and can be in general presented as [45-48]:



This reaction was modeled under the following hypothesis [55]:

- The activity of the metal is unity,  $a_{M^{n+}} = 1$ .
- The starting potential is equal to the equilibrium potential of the metal/metal-ion electrode.
- Metal-ion transport is governed by Fick's Law as:

$$\frac{\partial C_{M^{n+}}(x,t)}{\partial t} = D_o \frac{\partial^2 C_{M^{n+}}(x,t)}{\partial x^2} \quad (55)$$

Eq (55) was integrated with initial and boundary conditions:

$$C_{M^{n+}}(x,0) = C_{M^{n+}}(x,0) = C_{M^{n+}}^* \quad (56)$$

$$x=0, t>0:$$

$$-\frac{I}{nFA} = D_{M^{n+}} \left( \frac{\partial C_{M^{n+}}(x,t)}{\partial x} \right) \quad (57)$$

- If the electron transfer is fast, Nernstian boundary condition is applied:

$$E_{Eq} = E^0 + \frac{RT}{nF} \ln(\gamma_{M^{n+}} C_{M^{n+}}^*) \quad (58)$$

- If the electron transfer follows Butler-Volmer kinetics, the following boundary condition is used:

$$D_{M^{n+}} \left( \frac{\partial C_{M^{n+}}(x,t)}{\partial x} \right)_{x=0} = k^0 e^{-\alpha \frac{nF}{RT}(E(t)-E^0)} \times \left[ C_{M^{n+}}(0,t) - e^{\frac{nF}{RT}(E(t)-E^0)} \right] \quad (59)$$

- When the electron transfer kinetics is fully irreversible, the boundary conditions given in eqs (58) and (59) should be simplified as:

$$D_{M^{n+}} \left( \frac{\partial C_{M^{n+}}(x,t)}{\partial x} \right)_{x=0} = C_{M^{n+}}(0,t) k_i e^{bt} \quad (60)$$

#### I.5.4.1. Reversible system

##### I.5.4.1.1. Theory and mathematical models

An analytical solution to the relevant PDE joined to its initial and boundary conditions was obtained by using Laplace transform and inverse Laplace transform techniques. The response current is expressed, in the following forms:

##### For a single voltammetric wave [45]:

$$I = -\frac{2}{\pi^{1/2}} \frac{(nF)^{3/2}}{(RT)^{1/2}} AD^{1/2} C_{M^{n+}} v^{1/2} \text{daw} \left[ \left( \frac{nF}{RT} vt \right)^{1/2} \right] \quad (61)$$

##### For cyclic voltammetric wave [46]:

$$I = \frac{1}{\pi^{1/2}} \frac{(nF)^{3/2}}{(RT)^{1/2}} AD^{1/2} C_{M^{n+}} v^{1/2} \left[ \begin{array}{l} 2 \left( \text{daw} \left[ (\sigma t)^{1/2} \right] - e^{-\sigma t_\lambda} \text{daw} \left[ (\sigma t - \sigma t_\lambda)^{1/2} \right] H_{(t-t_\lambda)} \right) \\ -1.772 \left( e^{-\sigma t_\lambda} e^{(\sigma t - \sigma t_\lambda)} \text{erf} \left( (\sigma t - \sigma t_\lambda)^{1/2} \right) H_{(t-t_\lambda)} \right) \end{array} \right] \quad (62)$$

where erf and daw are tabulated functions defined by [56]:

$$\left\{ \begin{array}{l} \text{daw}(z) = \exp(-z^2) \int_0^z \exp(\zeta^2) d\zeta \\ \text{erf}(z) = \frac{2}{\pi^{1/2}} \int_0^z \exp(-\zeta^2) d\zeta \end{array} \right. \quad (63)$$

Meanwhile, it is worth noting that  $H(t)$  is the Heaviside step-unit function that was used by D.J. Schiffrin to define the triangular potential-sweep [46].

##### I.5.4.1.2. Potential and current peaks in LSV and CV for reversible soluble-insoluble redox reaction

The Dawson function exhibits a maximum corresponding to  $\left( \frac{nF}{RT} vt \right)^{1/2} = 0.9241$ , thus the peak current  $I_p$  of the reduction wave is given by [44]:

$$I_p = -0.6104 \frac{(nF)^{3/2}}{(RT)^{1/2}} AC_{M^{n+}} D^{1/2} \nu^{1/2} \quad (64)$$

The peak potential can be calculated from that maximum value to give [55]:

$$E_p = E_{eq} - 0.854 \frac{RT}{nF} \quad (65)$$

likewise, the peak potential at the half height is expressed by [55]:

$$E_{p/2} = E_p + 0.77 \frac{RT}{nF} \quad (66)$$

It is important to mention that the certain features such as the peak potential separation cannot be used to diagnosis a soluble-insoluble system. Also, the peak current of stripping response is strongly dependent of the morphology of the deposit.

#### **I.5.4.2. quasi-reversible system**

The quasi-reversibility behavior of metal-ion/metal couple, exploiting the boundary condition in eq 58, will be studied in this thesis in details.

#### **I.5.4.3. Totally irreversible system**

##### **I.5.4.3.1. Theory and mathematical models**

Returning to the boundary condition eq (60), applying it at  $x = 0$ , and by proceeding again analogously to the steps leading to equation (50), one finds the relation for the current according to [45]:

$$I = nFAD^{1/2} C_{M^{n+}} \nu^{1/2} (\alpha nF / RT)^{1/2} \Psi \quad (67)$$

##### **I.5.4.3.2. Potential and current peaks for irreversible soluble-insoluble redox reaction**

The criteria for irreversibility are [57]:

##### **Peak current:**

$$I_p = -0.495nFAC_{M^{n+}} (\alpha nF\nu / RT)^{1/2} \quad (68)$$

##### **Peak potential:**

$$E_p = E^0 - \frac{0.78RT}{\alpha F} + \frac{RT}{\alpha F} \ln k^0 \left( \frac{RT}{\alpha F D_{M^{n+}} \nu} \right)^{1/2} \quad (69)$$

##### **Half peak potential:**

$$\left|E_p - E_{p/2}\right| = 1.857 \frac{RT}{\alpha nF} \quad (70)$$

### I.6. Scope of the present thesis

The research problem in this work is determined by the lack of sufficient criteria for investigating the soluble-insoluble type redox reactions via LSV or CV technique. This lack is caused by the absolute absence of theoretical models to predict current responses under quasi reversible conditions, incomplete theory to deal with full voltammograms, and the difficulty accessing to evaluate accurately the reversibility-irreversibility of that reactions.

Under this framework, the objective of this thesis is to make a contribution to the modeling of LSV/CV responses for reversible, quasi-reversible and irreversible soluble-insoluble systems. The developed models will be used to: determine what is not understood for such systems, to provide general relationships that can be used in the estimations of kinetic parameters whatever the degree of reversibility and at the end to determine the field that need to be investigated further.

### I.8. References

- [1] S. Petrovic, *Basic Electrochemistry Concepts, In Electrochemistry Crash Course for Engineers*, Springer, Cham, 2021.
- [2] G. J. Bauer, *A Coupled Finite Element Approach for Electrochemical Systems, Doctoral dissertation*, Technische Universität München, 2012.

- [3] J. H. Chang, Master thesis, *Modeling of an electrochemical cell*, University of Toronto, 2009.
- [4] J. Lück, A. Latz, *Modeling of the electrochemical double layer and its impact on intercalation reactions*, Phys. Chem. Chem. Phys., 20(44), 27804-27821, 2018.
- [5] P. K. Shen, C. Y. Wang, S. P. Jiang, X. Sun, J. Zhang, *Electrochemical Energy: Advanced Materials and Technologies*, CRC Press, Boca Raton, 2016.
- [6] L. F. Mao, *Electrical Double-Layer Modeling of Different Al-Content on the Performance of AlGaIn/GaN HEMTs*, ECS J. Solid State Sc, 7(9), 496-500, 2018.
- [7] A. Asthagiri, M. Janik, *Computational Catalysis*, Royal Society of Chemistry, London, 2013.
- [8] A. Rowe, *Ruthenium Oxide sol-gels and carbon-supported ruthenium oxide composites for use in supercapacitors*, Doctoral dissertation, Memorial University of Newfoundland, 2007.
- [9] R. Burt, G. Birkett, X. S. Zhao, *A review of molecular modelling of electric double layer capacitors*, Phys. Chem. Chem. Phys., 16(14), 6519-6538, 2014.
- [10] R. Burt, G. Birkett, X. S. Zhao, *A review of molecular modelling of electric double layer capacitors*, Phys. Chem. Chem. Phys., 16(14), 6519-6538, 2014.
- [11] A. Groß, S. Sakong, *Modelling the electric double layer at electrode/electrolyte interfaces*, Curr. Opin. Electrochem, 14, 1-6. 2019.
- [12] C. Dincer, *Electrochemical microfluidic multiplexed biosensor platform for point-of-care testing*, Doctoral dissertation, University of Freiburg, 2016.
- [13] D. Qu, G. Wang, J. Kafle, J. Harris, L. Crain, Z. Jin, D. Zheng, *Electrochemical impedance and its applications in energy-storage systems*, Small Methods, 2(8), 1-27, 2018.
- [14] S. Malkhandi, *Nonlinear phenomena during bulk CO electrooxidation on Pt electrodes*, Technische Universität München, Doctoral dissertation, 2008.
- [15] A. Jarlöv, *Corrosion studies on multicomponent TiZrNbTa thin films*, Doctoral dissertation, Uppsala universitet, 2020.
- [16] R. F. Savinell, K. I. Ota, G. Kreysa, *Encyclopedia of Applied Electrochemistry*, Springer, New York, 2014.
- [17] R. Smith, *Characterisation and Surface Modification of Graphitic Felts*, Doctoral dissertation, University of Liverpool, 2018.
- [18] R. Guidelli, R. G. Compton, J.M. Feliu, E. Gileadi, J. Lokowski, W. Schmickler, S. Trasatti, *Defining the transfer coefficient in electrochemistry: An assessment (IUPAC Technical Report)*, Pure Appl. Chem., 86(2), 245-258, 2014.

- [19] A. F. Khan, *The electrochemistry of 2d hexagonal boron nitride*, Doctoral dissertation, Manchester Metropolitan University, 2018.
- [20] B. T. Wang, C. P. Lee, M. C. Wu, T. L. Tsai, S. C. Tsai, K. C. Hsu, *Novel method for analyzing transport parameters in through-diffusion tests*, J. Environ. Radioact., 196, 125-132, 2019.
- [21] R. G. Compton, E. Laborda, K. R. Ward, *Understanding voltammetry: simulation of electrode processes*, Imperial College Press, London, 2013.
- [22] A. J. Bard, L. R. Faulkner, *Electrochemical Methods: Fundamentals and Applications*, 2nd ed., John Wiley & Sons, New York, 2001.
- [23] F. K. Ko, Y. Wan, *Introduction to nanofiber materials*, Cambridge University Press, Cambridge, 2014.
- [24] V. Colic, *The Impact of the Electrode/Electrolyte Interface Status on the Activity, Stability, and Selectivity of Electrocatalytic Centers*, Doctoral dissertation, Technische Universität München, 2016.
- [25] T. Kim, W. Choi, H. C. Shin, J. Y. Choi, J. M. Kim, M. S. Park, W. S. Yoon, *Applications of voltammetry in lithium ion battery research*, J. Electrochem. Sci. Technol., 11(1), 14-25, 2020.
- [26] N.G. Amado, *Design and fabrication of miniaturized electroanalytical systems*, Doctoral dissertation, Universitat Autònoma de Barcelona, 2010.
- [27] G. Bontempelli, R. Toniolo, *Measurement methods| Electrochemical: Linear sweep and cyclic voltammetry*, Elsevier, Amsterdam, 2009.
- [28] I. C. Emeji, O. M. Ama, U. O. Aigbe, K. Khoele, P. O. Osifo, S. S. Ray, *Electrochemical Cells, Nanostructured Metal-Oxide Electrode Materials for Water Purification*, Springer, Cham, 2020.
- [29] A. Felix, *Redox potential and metabolic stability. development of high throughput assays for early compound profiling*, Doctoral dissertation, University of Basel, 2009.
- [30] P. Khullar, J. Badilla, R. Kelly, *The Use of a Sintered Ag/AgCl Electrode as Both Reference and Counter Electrode for Electrochemical Measurements in Thin Film Electrolytes*, ECS Electrochem. Lett., 4(10), 2015.
- [31] A. M. Bond, *Broadening Electrochemical Horizons: Principles and illustration of voltammetric and related techniques*, Oxford University Press on Demand, Oxford, 2002.
- [32] K. Dutta, P. P. Kundu, *Progress and Recent Trends in Microbial Fuel Cells*, Elsevier, Amsterdam, 2018.

- [33] J. Tu, W. Cai, X. Shao, *Direct separation of faradaic and double layer charging current in potential step voltammetry*, *Talanta*, 116, 575–580, 2013.
- [34] A. M. Bond, *Modern polarographic methods in analytical chemistry*, CRC Press, New York, 2020.
- [35] R. Smith, *Characterisation and Surface Modification of Graphitic Felts*, Doctoral dissertation, University of Liverpool, 2018.
- [36] Z. Chen, *Understanding of the Modeling Method in Additive Manufacturing*, IOP Conf. Ser, Mater. Sci. Eng. C, 711(1), 2020.
- [37] A. Samin, E. Lahti, J. Zhang, *Analytical solutions of the planar cyclic voltammetry process for two soluble species with equal diffusivities and fast electron transfer using the method of eigenfunction expansions*, *AIP Adv.*, 5(8), 1-10, 2015.
- [38] G. Jia-yao, C. Duan, Z. Jie, Z. Dong-ping, *Cyclic Voltammetry Coupled with Faradic Adsorption/Desorption Processes: A Finite Element Simulation*, *Journal of Electrochemistry*, 26(2), 281-288, 2020.
- [39] C. Montella. *LSV modelling of electrochemical systems through numerical inversion of Laplace transforms. I - the GSLSV algorithm*, *J. Electroanal. Chem.*, 614(12), 121 - 130, 2008.
- [40] G.A. Mabbott, *Electroanalytical chemistry: principles, best practices, and case studies*, 1st ed, Wiley, Hoboken, 2020.
- [41] T. Tichter, *Theory of Cyclic Voltammetry at Macroporous Electrodes*, Doctoral dissertation, Freie Universität Berlin, 2020.
- [42] H. Matsuda, Y. Ayabe, *Zur Theorie der Randles-Sevcik'schen Zur Theorie der Randles-Sevcik'schen Für Elektrochemie*, *Berichte Der Bunsengesellschaft Für Phys. Chemie*, 59(6), 494–503, 1955.
- [43] A. M. Bond, *A perceived paucity of quantitative studies in the modern era of voltammetry: prospects for parameterisation of complex reactions in Bayesian and machine learning frameworks*, *J Solid State Electrochem*, 24, 2041-2050, 2020.
- [44] T. Berzins, P. Delahay, *Oscillographic polarographic waves for the reversible deposition of metals on solid electrodes*, *J. Am. Chem. Soc.*, 75, 555–559, 1953.
- [45] P. Delahay, *Theory of irreversible waves in Oscillographic polarography*, *J. Am. Chem. Soc.*, 75, 1190–1196, 1953.
- [46] D. J. Schiffrin, *Theory of cyclic voltammetry for reversible electrodeposition of insoluble products*, *J. Electroanal. Chem.*, 201(1), 199-203, 1986.
- [47] D. Krulic, N. Fatouros, D. Liu, *A complementary survey of staircase voltammetry with metal ion deposition on macroelectrodes*, *J. Electroanal. Chem.*, 754, 30–39, 2015.

- [48] D. Britz, J. Strutwolf, *Digital simulation in electrochemistry*, Springer, Berlin, 2005.
- [49] L. K. Bieniasz, *Modelling electroanalytical experiments by the integral equation method*, Springer, Berlin, 2015.
- [50] H. H. Girault, *Analytical and chemical electrochemistry*, 1st ed, EPFL Press, Lausanne, 2004.
- [51] A. Saila, *Etude des systèmes électrochimiques quasi-réversibles par voltamperométrie à balayage linéaire et semi-intégration, Applications aux comportements de rhenium et dysprosium en milieux de sels fondus*, Thèse de doctorat, Université de Badji Mokhtar, Annaba, 2010.
- [52] R.S. Nicholson, I. Shain, *Theory of stationary electrode polarography. Single scan and cyclic methods applied to reversible, irreversible, and kinetic systems*, J. Anal. Chem., 36, 706–723, 1964.
- [53] M. Lovric, D. Jadresko, *Theory of square-wave voltammetry of quasireversible electrode reactions using an inverse scan direction*, Electrochim. Acta, 55, 948–951, 2010
- [54] H. Wang, S. Y. Sayed, E. J. Luber, B. C. Olsen, S. M. Shirurkar, S. Venkatakrishnan, U. M. Tefashe, A. K. Farquhar, E. S. Smotkin, R. L. McCreery, J. M. Buriak, *Redox Flow Batteries: How to Determine Electrochemical Kinetic Parameters*, ACS Nano, 14, 2575–2584, 2020.
- [55] D. Liu, *Analyse Des Méthodes à Potentiel et à Courant Imposé Pour Des Réactions Avec Dépôt Métallique Rapides et Lentes - Dépôt d'argent Sur or Dans HNO<sub>3</sub> 1 M, KNO<sub>3</sub> 1M et Dans Le Liquide Ionique [EMIM][NTf<sub>2</sub>] Anhydre Ou Humide*, Thèse de doctorat, Université Pierre et Marie Curie, Paris, 2014.
- [56] L. K. Bieniasz, *Integral equation-based simulation of transient electroanalytical experiments at spherical electrodes, for the catalytic EC' mechanism with  $DO \neq DR$* , Electrochim. Acta, 317, 795-807, 2019.
- [57] M. Kergoat, L. Massot, M. Gibilaro and P. Chamelot, *Investigation on fluoroacidity of molten fluorides solutions in relation with mass transport*, Electrochim. Acta, 120, 258-263, 2014.

# **CHAPTER II**

## *Experiment and simulations details*

---

In order to validate the simulation prediction, the system Cu(I)/Cu(0) was investigated in organic medium. This chapter presents first, chemicals and describes the preparation process to carry out the copper deposition reaction under LSV conditions. Meanwhile, the rest of this chapter discusses simulation approaches and how it has been used to establish theoretical voltammograms in this thesis.

---

## II.1. Chemicals and supplies

Without further purification, all chemicals were used as received. The electroactive species: Tetrakis(acetonitrile) copper(I) tetrafluoroborate ( $\text{Cu}(\text{CH}_3\text{CN})_4\text{BF}_4$ ; 98% purity) was purchased from TCI, it's a white crystal powder that slowly decompose into a greenish solid in moist air. Supporting salt: Tetraethylammonium Tetrafluoroborate ( $\text{C}_8\text{H}_{20}\text{BF}_4\text{N}$ ; 99% purity) was obtained from ABCR, which it can be used in CV up to 3 V without any degradation. Solvent: Acetonitrile ( $\text{CH}_3\text{CN}$ ; 99.9% Extra Dry, over Molecular Sieves) was from Across Company. Electrodes were made with copper of 1 mm diameter, (99.99% purity), from GoodFellow. Ultrapure water is employed to clean electrodes and glassware,

## II.2. Apparatus and accessories

Linear sweep voltammetry (LSV) experiments were carried out by employing Autolab PGSTAT302N potentiostat equipped with the SCAN250 analog scan generator module, and the data for the Cu(I)/Cu(0) couple was processed using the Nova 1.9 software. All the experiments were executed in classical electrochemical cell setup with three electrodes immersed in a solution containing the analyte as well as an excess of the supporting electrolyte. Coils of copper wire, diameter 1 mm, were used as reference electrode and auxiliary electrode. In order to ensure a larger area compared to the WE, the auxiliary electrode was coiled. The WE was fabricated by heat sealing a length of 1 mm diameter copper wire in glass tube of suitable diameter, then polishing it with consecutively finer abrasive papers followed by different sizes of alumina, down to 0.05  $\mu\text{m}$  particles, on polishing cloths. the effects of solution resistance were corrected by Positive Feedback iR Compensation. Noted that, all experimental steps (solution preparation, LSV measurement) were carried out at ambient temperature (25 °C) under anaerobic conditions using a nitrogen filled glove box.

## II.3. Procedure

The linear sweep voltammetric (LSV) method was used to perform cathodic reduction of the Cu(I) to Cu(0). LSV scanning was carried out in the range of 0 V to -0.4 V, with an initial potential ( $E_i$ ) of 0 V, for which the scan rate was ranged from 25 to 200 mV/s . All potentials are expressed vs. the Cu wire in the solution of the given concentration of  $[\text{Cu}(\text{CH}_3\text{CN})_4\text{BF}_4]$ . the potential of the Cu reference in equilibrium with 10 mM  $\text{Cu}^+$  solution in acetonitrile on the “non-aqueous standard copper electrode” scale (SCuE), i.e. vs.  $\text{Cu}^+$  solution with the activity of 1 in equilibrium with Cu in acetonitrile is assumed to follow the Nernst equation considering the  $\gamma_{\text{Cu}^+} = 1$ , i.e. The potential of the reference is -0.118 V vs. SCuE in acetonitrile. To

establish the relation with the ferrocene (Fc) scale recommended by IUPAC, the potential of the Fc<sup>+</sup>/Fc couple vs. Cu/10 mM Cu<sup>+</sup> in ACN was measured as  $0.69 \pm 0.01$  V, i.e. the potential of our reference electrode is  $-0.69$  V vs. Fc<sup>+</sup>/Fc.

Electrolytic solutions were prepared by dissolving Tetrakis(acetonitrile) copper(I) tetrafluoroborate and Tetraethylammonium Tetrafluoroborate in acetonitrile. Concentrations for Cu(CH<sub>3</sub>CN)<sub>4</sub>BF<sub>4</sub> and TEABF<sub>4</sub> were 10 and 100 mM, respectively.

## II.4. Choice of Working Electrode material

The material of working electrode used was a metallic copper. This electrode was chosen in order to get an accurate estimation of the electrochemical kinetics of the Cu(I)/Cu(0) reduction process which is of utmost importance to better understand the limitations for the nonaqueous batteries utilizing Cu(I)/Cu(0) couple as the negative redox couple.

## II.5. Simulation and Analysis tools

In this thesis, the semi-analytical and numerical method were employed for simulating LSV and CV problem for soluble-insoluble redox reaction, with Butler-Volmer type kinetics. A semi-analytical solution is obtained under one-dimensional mass transport, using the Nicholson and Shain method [1], and subsequently, the models were coded in Fortran. Also, Finite element simulations with COMSOL Multiphysics was undertaken to compute theoretical voltammograms.

### II.5.1. Semi-analytical method

The solution methodology of voltammetry problem, case of soluble-insoluble system, by using semi-analytical method is summarized in flowchart in Fig II.1.

To define the system fully, the used inputs were the type of redox reaction: one step soluble-insoluble redox reaction, type of potential sweep: single- or cyclic- sweep, the type of reaction kinetics: Butler-Volmer (BV) and the type of mass transport process: Fickian diffusion transport process. the main outputs were the integral voltammetry equation (i.e. integral current function) and the infinite series summation formula for using to compute voltammetry responses.

As shown in Fig II.1, solution occurs in two stages:

In the first stage, the Partial Differential Equations (PDEs) involved in the mass transport models integrated with initial and boundary conditions were solved analytically using the

Laplace transform and numerical inversion, and by combining the obtained solution with the reaction kinetics, with some computation, we arrived at the voltammetry integral.

In the second stage, the numerical resolution was proceeded for solving the integral equation using the integral subdivision process and the integral by part method, and then an expression to calculate potential sweep curves was derived at the end.

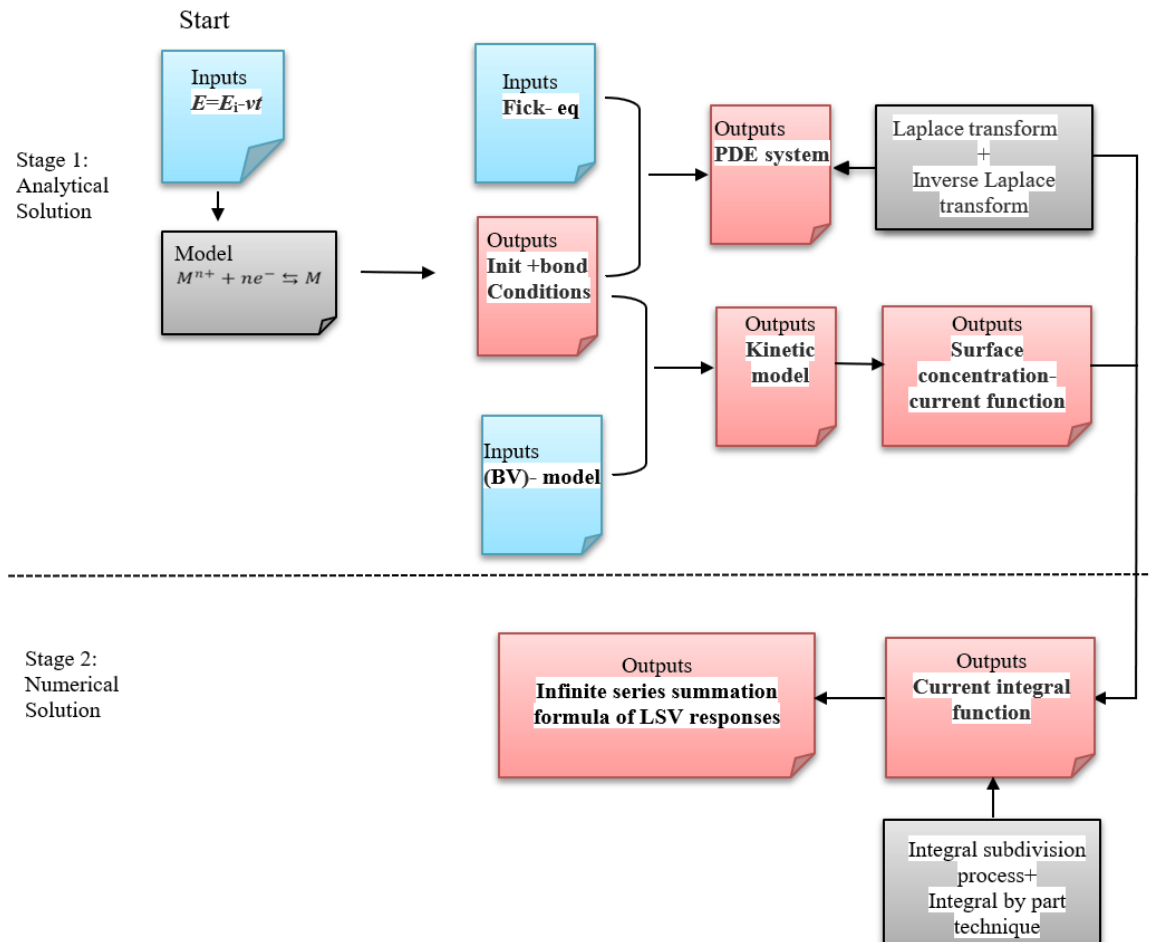


**Figure II.1.** Flowchart of semi-analytical simulation of LSV.

## II.5. 2. Finite element method software using COMSOL multiphysics

The software used to define and solve voltammetry models during this thesis was COMSOL Mutiphysics. COMSOL Multiphysics is a software package for simulating physical phenomena using partial differential equations (PDEs) and then solving it using finite element methods (FEM). The finite element method (FEM) is a numerical technique for finding approximate solutions to partial differential equations (PDE) and their systems, as well as (less often) integral equations that occur in a variety of engineering and applied sciences fields [2-3].

### **II.5. 2.1. Finite elements solution procedure**

The first step to solve the system of PDEs with FEM is to define the computational domain geometry, then this domain is partitioned into numerous subdomains, named finite element components [4]. An assembly of these elements called mesh which interconnected in points called nodes or vertices. the PDE problem thus can be converted into a discretized finite element with unknown nodal values. These unknowns combine to form a system of linear algebraic equations that can be numerically solved. There are several types of Finite Elements depending on their geometry [4]. In this thesis, we deal only with a simple, one-dimensional domain geometry (planar diffusion: macroelectrode).

### **II.5. 2.2. COMSOL Multiphysics calculation process**

Simulation of voltammetry for either single- or cyclic- sweep, under COMSOL Multiphysics, includes three stages: Pre-processing, processing and postprocessing [5].

The first stage (pre-processing) entailed the formulation of the voltammetry problem, case of metal deposition reaction. During this process. The system's governing equations were identified, notably the equation of mass transport, mass conservation equations, potential sweep equation, and the proposed kinetics equation. Then, to define the electrodeposition process, initial and boundary conditions were set, model geometry and meshing were done.

In the second stage (processing), the formulated problem was solved and plotting current vs. potential for soluble-insoluble redox reaction was made possible.

In the end-stage (post-processing), the results can be visualized, analyzed, and evaluated.

The above stages of model development are summarized in Fig II.2.

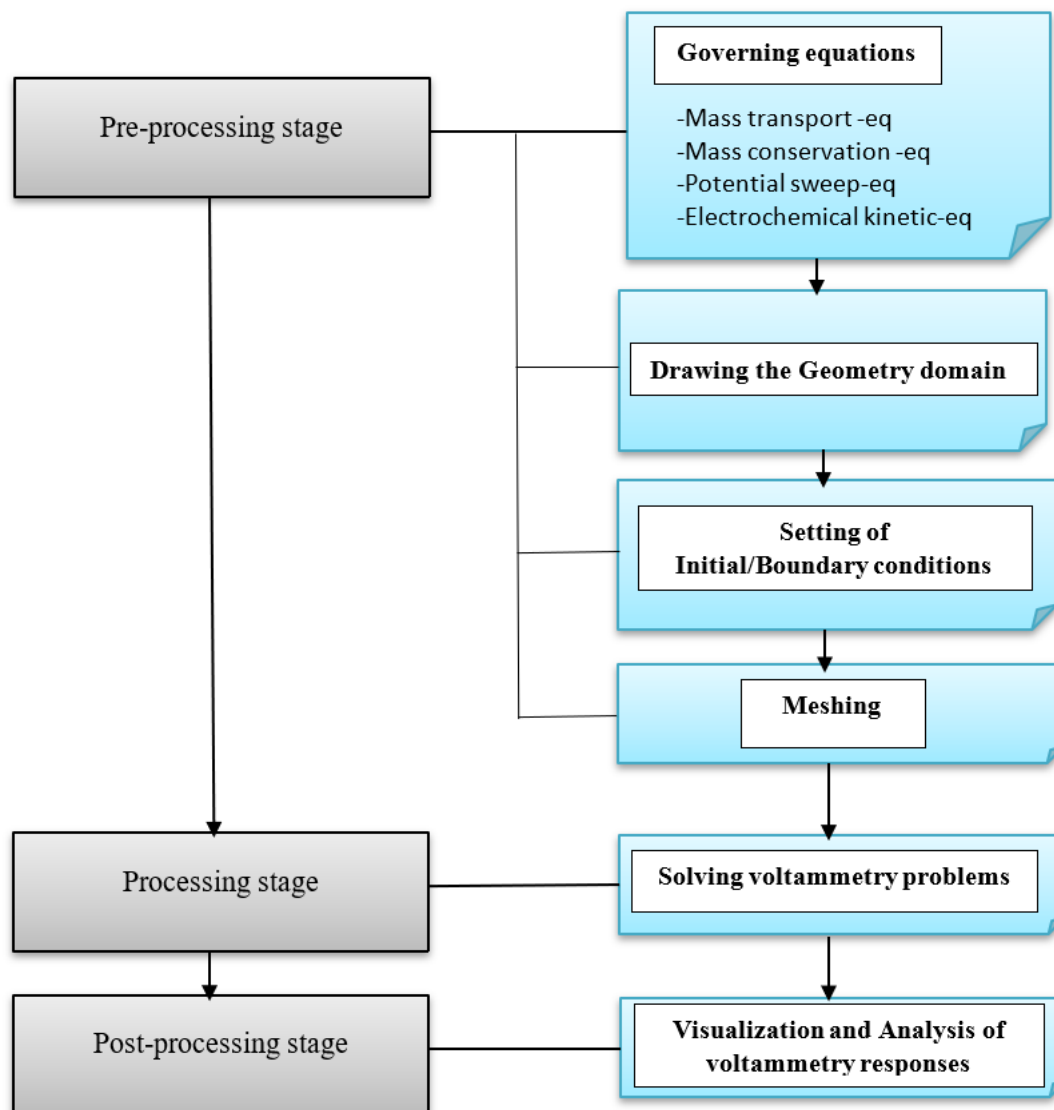


*Figure II.2. Flow chart of COMSOL Multiphysics model to simulate voltammetric responses.*

### II.5.3. Semi-integral method

To get information on the diffusion of Cu(I) ions in acetonitrile, experimental LSV data were first recorded and then convoluted into semi-integral current vs voltammetric potential, using the semi-integral method with Saila's algorithm [6].

**II.5. 4. Fortran**

Fortran 90 is the programming language used in this thesis. This type of tool is necessary and can be thought of as a supplement to the semi-analytical solution in order to calculate the infinite series summation and theoretical voltammograms.

**II.5.5. Origin software**

The origin software platform was used to analyze and process the data in order to plot various graphs in this thesis.

## II.6. References

- [1] R.S. Nicholson, I. Shain, *Theory of stationary electrode polarography. Single scan and cyclic methods applied to reversible, irreversible, and kinetic systems*, J. Anal. Chem., 36, 706–723, 1964.
- [2] P. Vyroubal, J. Maxa, T. Kazda, J. Vondrák, *The Finite Element Method in Electrochemistry—Modelling of the Lithium-Ion Battery*, ECS Trans, 48(1), 289-296, 2014.
- [3] H. Benguesmia, N. M'ziou, A. Boubakeur, *Simulation of the potential and electric field distribution on high voltage insulator using the finite element method*, Diagnostyka, 19(2), 41-52, 2018.
- [4] N.G. Amado, *Design and fabrication of miniaturized electroanalytical systems*, Doctoral dissertation, Universitat Autònoma de Barcelona, 2010.
- [5] R. Brendel, *Modeling solar cells with the dopant-diffused layers treated as conductive boundaries*, Prog Photovolt, 20(1), 31-43, 2012.
- [6] A. Saila, *Etude des systèmes électrochimiques quasi-réversibles par voltamperométrie à balayage linéaire et semi-intégration, Applications aux comportements de rhenium et dysprosium en milieux de sels fondus*, Thèse de doctorat, Université de Badji Mokhtar, Annaba, 2010.

# **CHAPTER III**

## *Simulation of Linear sweep voltammetric behaviour for soluble- insoluble redox reaction*

---

In this chapter, we use two methods: semi-analytical method and finite element method to construct the theory of linear sweep voltammetry for soluble-insoluble redox reaction with Butler-Volmer kinetics.

In the first part of this chapter, we present the details of the solution derivation for voltammetry in the case of one-step electrodeposition processes. Following that, we present a full analysis of the voltammetric responses following variation of both dimensionless rate constants and charge transfer coefficients in a broad range. In the second part, we propose numerical expressions for the peak parameters of the LSV curves and three limit regimes in terms of a global rate constant based on the nature of the electrode process. Finally, we conclude with the validation of the developed theoretical framework by studying the electrodeposition of Cu(I)/Cu(0) in acetonitrile.

---

### III.1. Mathematical formulation of the problem

#### III.1.1. Hypotheses to metal/metal-ion system

Five hypotheses are formulated to establish the LSV theory for soluble-insoluble redox reaction:

(1): In our model we suppose that a one-step reaction process occurs to form a metal deposit, as follows:



(2): All the calculations are based on the assumption that the metal's activity during the reaction is equal to 1.

(3): We suppose that at the initial state ( $t=0$ ), the equilibrium is achieved at the surface of electrode, so that the Nernst Equation applies:

$$E_i = E_{eq} = E^0 + \frac{RT}{nF} \ln(a_{M^{n+}}^*)$$

Where  $a_{M^{n+}}^* = \gamma_{M^{n+}} C_{M^{n+}}^* / C^0$  is the bulk activity of the metal cation ( $M^{n+}$ ),  $\gamma_{M^{n+}}$  is the activity coefficient and  $C^0$  is the standard concentration of 1 mol L<sup>-1</sup>.

(4): The Butler-Volmer type expression is employed to describe the reaction kinetics, in which the heterogeneous electron-transfer rate  $k^0$  is exponentially related to overpotential ( $E(t)-E^0$ ) as:

$$I(t) = nFAk^0 \left[ C_M(0,t) \exp\left(\frac{(1-\alpha)nF}{RT}(E(t)-E^0)\right) - C_{M^{n+}}(0,t) \exp\left(\frac{-\alpha nF}{RT}(E(t)-E^0)\right) \right] \quad (3)$$

Where  $\alpha$  and  $1-\alpha$  are the cathodic and anodic charge transfer coefficients, respectively.

(5): By using LSV technique, the electrode potential is swept linearly in one direction:

$$E(t) = E_i - vt \quad (4)$$

#### III.1.2. Governing equations of mass transport process

By considering the planar diffusion of metallic cation at the macroelectrode surface, and neglecting migration and convection contribution, the process of the mass transport can be quantified in accord with Fick's laws as:

$$\frac{\partial C_{M^{n+}}(x,t)}{\partial t} = D_{M^{n+}} \frac{\partial^2 C_{M^{n+}}(x,t)}{\partial x^2} \quad (5)$$

Eq (5) is subject to the following initial and boundary conditions:

**Chapter III: Simulation of linear sweep voltammetric behaviour for soluble-insoluble redox reaction**

$$t = 0; C_{M^{n+}}(x, 0) = C_{M^{n+}}^* \quad (6)$$

$$x \rightarrow \infty; C_{M^{n+}}(\infty, t) = C_{M^{n+}}^* \quad (7)$$

$$x \rightarrow 0; \frac{I(t)}{nFA} = -D_{M^{n+}} \left[ \frac{\partial C_{M^{n+}}(x, t)}{\partial x} \right]_{x=0} \quad (8)$$

## III.2. Solution methodology via use of semi analytical techniques

### IV.2.1. Stage I: Analytical solution

#### IV.2.1.1 Application of the Laplace transform and numerical inversion to diffusion equation.

The first step in proceeding to the solution of the equations system described by eqs (5) to (8), is to apply the Laplace transforming both sides of the equation (5) with respect to t, one arrives at:

$$s\bar{C}_{M^{n+}}(x, s) - C_{M^{n+}}(x, 0) = D_{M^{n+}} \frac{\partial^2 \bar{C}_{M^{n+}}(x, s)}{\partial x^2} \quad (9)$$

Where the over-bar denotes the Laplace transform and s is the Laplace variable.

Recalling the boundary condition in (6), one obtains:

$$\frac{s}{D_{M^{n+}}} \bar{C}_{M^{n+}}(x, s) - \frac{C_{M^{n+}}^*}{D_{M^{n+}}} = \frac{\partial^2 \bar{C}_{M^{n+}}(x, s)}{\partial x^2} \quad (10)$$

For our calculations it is convenient to rewrite the previous equation (10) in the following form:

$$\frac{\partial^2 \bar{C}_{M^{n+}}(x, s)}{\partial x^2} = \left[ \sqrt{\frac{s}{D_{M^{n+}}}} \right]^2 \bar{C}_{M^{n+}}(x, s) - \frac{C_{M^{n+}}^*}{D_{M^{n+}}} \quad (11)$$

Hence, the Laplace transform of eq (11) with the respect to the variable x is:

$$\bar{C}_{M^{n+}}(s) [s^2 - a^2] = sC_{M^{n+}}(0) + C_{M^{n+}}(0) - \frac{C_{M^{n+}}^*}{D_{M^{n+}}s} \quad (12)$$

With:  $a = \sqrt{\frac{s}{D_{M^{n+}}}}$

by rearrangement we have:

**Chapter III:** Simulation of linear sweep voltammetric behaviour for soluble-insoluble redox reaction

$$\bar{C}_{M^{n+}}(s) = \frac{s^2 C_{M^{n+}}(0) + s C_{M^{n+}}(0) - \frac{C_{M^{n+}}^*}{D_{M^{n+}}}}{s(s^2 - a^2)} \quad (13)$$

After converting (13) into fractional equations, one arrives:

$$\bar{C}_{M^{n+}}(s) = \frac{A'(s)}{s+a} + \frac{B'(s)}{s-a} + \frac{D'(s)}{s} \quad (14)$$

Where A'(s), B'(s), D(s)' are employed to describe the decomposition constants.

Multiplying equations (13) and (14) by s, and then setting s=0, one finds by comparison the value of the decomposition constant D'(s) which is equal to:  $C_{M^{n+}}^* / (a^2 D_{M^{n+}})$

Inverting eq (14), the general solution is obtained:

$$\bar{C}_{M^{n+}}(x,s) = \frac{C_{M^{n+}}^*}{s} + A'(s)e^{-\sqrt{\frac{s}{D_{M^{n+}}}}x} + B'(s)e^{\sqrt{\frac{s}{D_{M^{n+}}}}x} \quad (15)$$

Now let us determine the value of A'(s) and B'(s):

Taking the first boundary condition eq(7), where we have:

$$\lim_{x \rightarrow \infty} \bar{C}_{M^{n+}}(x,s) = \lim_{xc \rightarrow \infty} \left[ \frac{C_{M^{n+}}^*}{s} + A'(s)e^{-\sqrt{\frac{s}{D_{M^{n+}}}}x} + B'(s)e^{\sqrt{\frac{s}{D_{M^{n+}}}}x} \right] = C_{M^{n+}}^* \quad (16)$$

In this case, this term  $B'(s)e^{\sqrt{\frac{s}{D_{M^{n+}}}}x}$  should be tend to zero, which yields to: B'(s)=0

Hence, Eq (15) turn to be:

$$\bar{C}_{M^{n+}}(x,s) = \frac{C_{M^{n+}}^*}{s} + A'(s)e^{-\sqrt{\frac{s}{D_{M^{n+}}}}x} \quad (17)$$

After Laplace transforming eq (8), the second boundary condition takes the following form:

$$x \rightarrow 0, \left[ \frac{\partial C_{M^{n+}}(x,s)}{\partial x} \right]_{x=0} = -\frac{I(s)}{nFAD_{M^{n+}}} \quad (18)$$

when deriving Eq (17), we have:

$$\frac{\partial C_{M^{n+}}(x,s)}{\partial x} = -\sqrt{\frac{s}{D_{M^{n+}}}} A'(s) e^{-\sqrt{\frac{s}{D_{M^{n+}}}}x} \quad (19)$$

For  $x=0$ , eq (19) becomes:

$$\left[ \frac{\partial C_{M^{n+}}(x,s)}{\partial x} \right]_{x=0} = -\sqrt{\frac{s}{D_{M^{n+}}}} A'(s) \quad (20)$$

**Chapter III: Simulation of linear sweep voltammetric behaviour for soluble-insoluble redox reaction**

From the equality between equations (18) and (20),  $A'(s)$ , can be calculated:

$$A'(s) = \frac{I(s)}{nFD_{M^{n+}}} \sqrt{\frac{D_{M^{n+}}}{s}} \quad (21)$$

If we insert eq (21) into eq (17), and after inverse Laplace-transforming, we obtain the time evolution equation for the concentration:

$$C_{M^{n+}}(0,t) = C_{M^{n+}}^* + \frac{1}{nFA\sqrt{D_{M^{n+}}}} \frac{1}{\sqrt{\pi}} \int_0^t \frac{I(\tau)}{\sqrt{t-\tau}} d\tau \quad (22)$$

**IV.2.1.2. Derivation of the voltammetry integral equation**

Our starting point in this section is eq (3), we can introduce the expression describing the applied potential in LSV, eq (4):

$$I(t) = nFAk^0 C_M(0,t) \left[ e^{\frac{nF}{RT}(E_i - E^0)} e^{\frac{-nF}{RT}vt} \right]^{(1-\alpha)} - nFAk^0 C_{M^{n+}}(0,t) \left[ e^{\frac{nF}{RT}(E_i - E^0)} e^{\frac{-nF}{RT}vt} \right]^{(-\alpha)} \quad (23)$$

Where  $C_M$  denotes the metal concentration, and it can be expressed as:  $C_M = a_M C^0 = C^0$ .

On the other hand, for modelling purposes, it is more convenient to convert the dimensioned variables into a non-dimensional form. One then defines:

Dimensionless initial potential, INIT:

$$\text{INIT} = \frac{nF}{RT} (E_i - E^0) \quad (24)$$

Dimensionless end potential, LIMIT:

$$\text{LIMIT} = \frac{nF}{RT} (E_f - E^0) \quad (25)$$

Dimensionless applied potential,  $\Phi$ :

$$\Phi = \frac{nF}{RT} (E(t) - E^0) = \text{INIT} - \sigma t \quad (26)$$

Dimensionless scan rate,  $\sigma$ :

$$\sigma = \frac{nF}{RT} v \quad (27)$$

substituting eqs 22, 24, 25, and 27 into Eq (23) and after rearrangement, we get:

**Chapter III:** Simulation of linear sweep voltammetric behaviour for soluble-insoluble redox reaction

$$I(t) = nFAk^0 \left[ -\frac{1}{nFA\sqrt{\pi D_{M^{n+}}}} [\theta S(t)]^{-\alpha} \int_0^t \frac{I(\tau)}{\sqrt{t-\tau}} d\tau - C_{M^{n+}}^* / C^0 [\theta S(t)]^{-\alpha} + [\theta S(t)]^{(1-\alpha)} \right] \quad (28)$$

where we have defined:  $S(t) = \exp(-\sigma t)$ , and  $\theta = \exp\left(\frac{nF}{RT}\right) [E_i - E^0] = \frac{C_{M^{n+}}^*}{C^0}$

Now we divide by  $C_{M^{n+}}^* / C^0$  and rearrange equation (28), we arrive at:

$$\int_0^t \frac{I(\tau)}{\sqrt{t-\tau}} d\tau = -nFA \frac{C_{M^{n+}}^*}{C^0} \sqrt{\pi D_{M^{n+}}} \left[ 1 + \frac{I(t)}{nFA \frac{C_{M^{n+}}^*}{C^0} k^0} [\theta S(t)]^\alpha - \frac{[\theta S(t)]}{\frac{C_{M^{n+}}^*}{C^0}} \right] \quad (29)$$

Its solution is usually non-analytical and entails the numerical resolution of integral equations.

#### IV.2.2. Stage II: Numerical resolution

In order to adimensionalize Eq (29), we used the following redefinitions:  $Z = \sigma\tau$  and  $I(t) = g(z)$ .

Thus, eq (29) turn to be:

$$\int_0^{\sigma t} \frac{g(z)}{\sqrt{\sigma t - z} \sqrt{\sigma}} dz = -nFA \frac{C_{M^{n+}}^*}{C^0} \sqrt{\pi D_{M^{n+}}} \left[ 1 + \frac{I(t)}{nFA \frac{C_{M^{n+}}^*}{C^0} k^0} [\theta S(\sigma t)]^\alpha - [S(\sigma t)] \right] \quad (30)$$

And then dividing the resulting equation side by side by  $nFA \frac{C_{M^{n+}}^*}{C^0} \sqrt{\pi D_{M^{n+}}}$ , One then

defines the dimensionless current  $\Psi(\sigma t)$  as:

$$\Psi(\sigma t) = \frac{I(t)}{nFAC_{M^{n+}}^* (\pi D_{M^{n+}})^{1/2} \left(\frac{nFv}{RT}\right)^{1/2}} \quad (31)$$

Rewriting eq (30):

**Chapter III:** Simulation of linear sweep voltammetric behaviour for soluble-insoluble redox reaction

$$-\int_0^{\sigma t} \frac{\Psi(z)}{\sqrt{\sigma t - z}} dz = \left[ -1 - \frac{I(t)}{nFA \frac{C^*}{C^0} k^0} [\theta S(\sigma t)]^\alpha + [S(\sigma t)] \right] \quad (32)$$

Multiplying the second member on the right of Eq (32) by  $\frac{\sqrt{\pi D_{M^{n+}} \sigma}}{\sqrt{\pi D_{M^{n+}} \sigma}}$ , and putting that:

$$\omega = \frac{k^0}{\theta^\alpha \left( \pi D \frac{nF}{RT} v \right)^{1/2}} \quad (33)$$

Here  $\omega$  denotes the dimensionless heterogeneous rate constant. Hence, we obtain:

$$\int_0^{\sigma t} \frac{\Psi(z)}{\sqrt{\sigma t - z}} dz = - \left[ -1 - \Psi(\sigma t) \frac{1}{\omega} [S(\sigma t)]^\alpha + [S(\sigma t)] \right] \quad (34)$$

to solve Eq (34), it needs to divide the integration interval into equidistant sub-intervals, each of distance  $\delta$ .

Thus, assuming that:  $z = \delta k$  and  $\sigma t = \delta N$

By using the above definitions, Eq (34), takes the form:

$$\sqrt{\delta} \int_0^{\delta N} \Psi(z)(\delta k) \frac{1}{\sqrt{N - k}} dk = - \left[ -1 - \Psi(z)(\delta N) \frac{1}{\omega} [S(\delta N)]^\alpha + [S(\sigma t)] \right] \quad (35)$$

Performing the integration by part of the left-hand side of Eq (35), yields

$$2\sqrt{\delta} \Psi(0) \sqrt{N} + 2\sqrt{\delta} \int_0^{\delta N} \sqrt{N - k} d(\Psi(\delta k)) = - \left[ -1 - \Psi(\delta N) \frac{1}{\omega} [\theta S(\delta N)]^\alpha + [S(\sigma t)] \right] \quad (36)$$

the left-hand side of eq(36), can be expressed as a summation:

$$\Psi(1) \sqrt{N} + \sum_{i=1}^{N-1} \sqrt{N - i} [\Psi(i+1) - \Psi(i)] = - \frac{1}{2\sqrt{\delta}} \left[ -1 - \Psi(\delta N) \frac{1}{\omega} [\theta S(\delta N)]^\alpha + [S(\sigma t)] \right] \quad (37)$$

Where:  $\Psi(i) = \Psi(\delta i)$

The development of the summation formula of eq (37) leads to:

$$\Psi(1) \sqrt{N} + \sqrt{N-1} [\Psi(2) - \Psi(1)] + \sqrt{N-2} [\Psi(3) - \Psi(2)] + \sqrt{N-3} [\Psi(4) - \Psi(3)] + \dots + \sqrt{N-(N-2)}$$

**Chapter III: Simulation of linear sweep voltammetric behaviour for soluble-insoluble redox reaction**

$$+\left[\Psi(N-1)-\Psi(N-2)\right]+\sqrt{N-(N-1)}+\left[\Psi(N)-\Psi(N-1)\right]=-A(N)+B(N)\Psi(N)+C \quad (38)$$

Where:

$$A(N)=\frac{1}{2\sqrt{\delta}}\left[\left[S(\delta N)\right]\right] \quad (39)$$

$$B(N)=\frac{1}{2\sqrt{\delta}}\left[\frac{1}{\omega}\left[\theta S(\delta N)\right]^\alpha\right] \quad (40)$$

And

$$C=\frac{1}{2\sqrt{\delta}} \quad (41)$$

Noting that there are N equations of  $\Psi(i)$ .

$$\Psi(N)+\sum_{i=1}^{n-1}\left[\sqrt{N-(i-1)}-\sqrt{N-i}\right]\Psi(i)=-A(N)+B(N)\Psi(N)+C \quad (42)$$

Finally, we can deduce the following expressions required to establish adimensional curves of current  $\Psi(K)$  versus potential  $\Phi(k)$  as:

**Dimensionless current expression:**

$$\Psi(k)=-A(k)-\sum_{i=1}^{k-1}\frac{\left[\sqrt{k-(i-1)}-\sqrt{k-i}\right]\Psi(i)}{1-B(k)}+C \quad (43)$$

**Dimensionless applied potential expression:**

$$\Phi=\frac{nF}{RT}(E-E^0)=\text{init}-\delta k \quad (44)$$

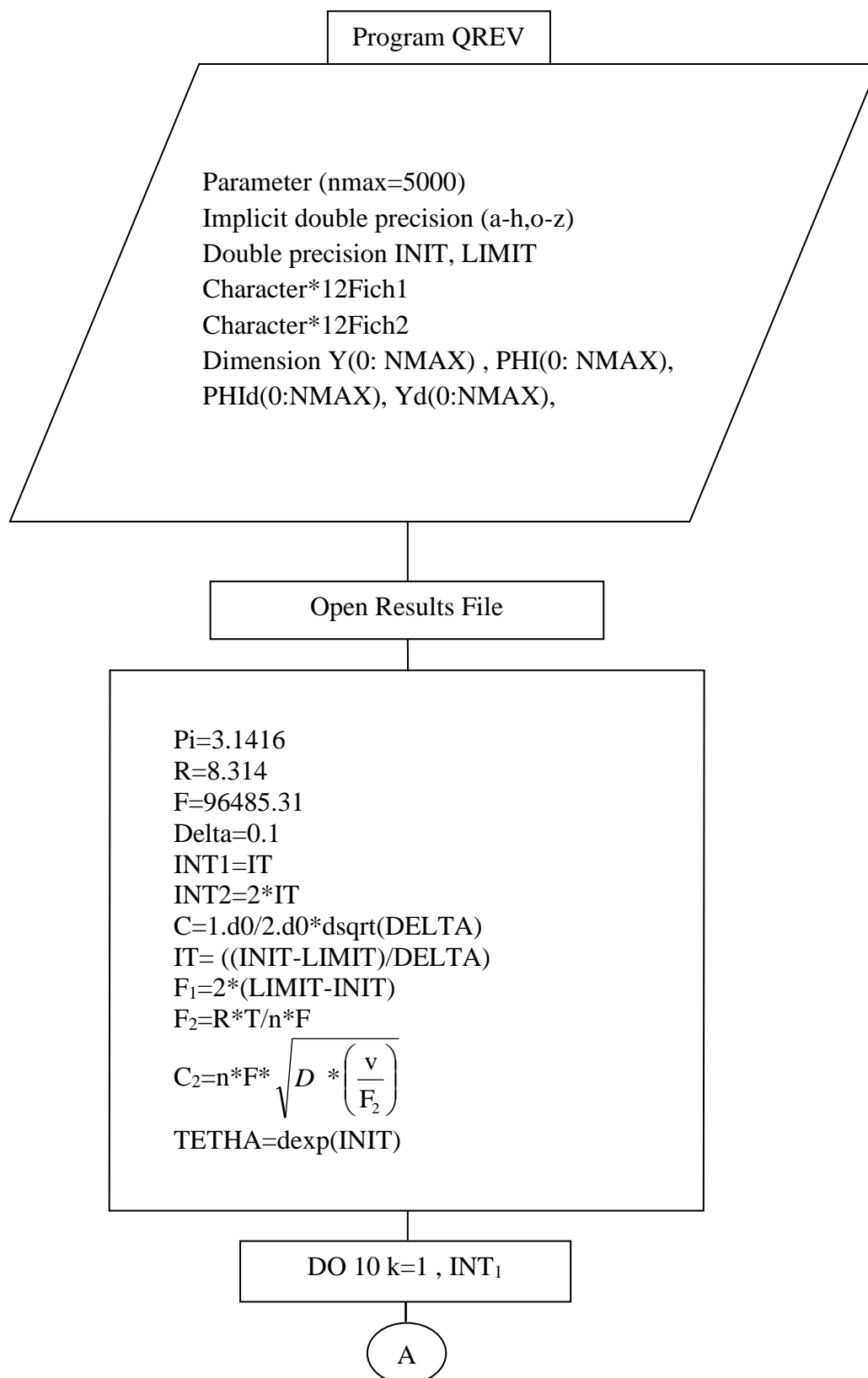
With:

$$A(k)=\frac{1}{2\sqrt{\delta}}\left[\left[S(\delta k)\right]\right] \quad (45)$$

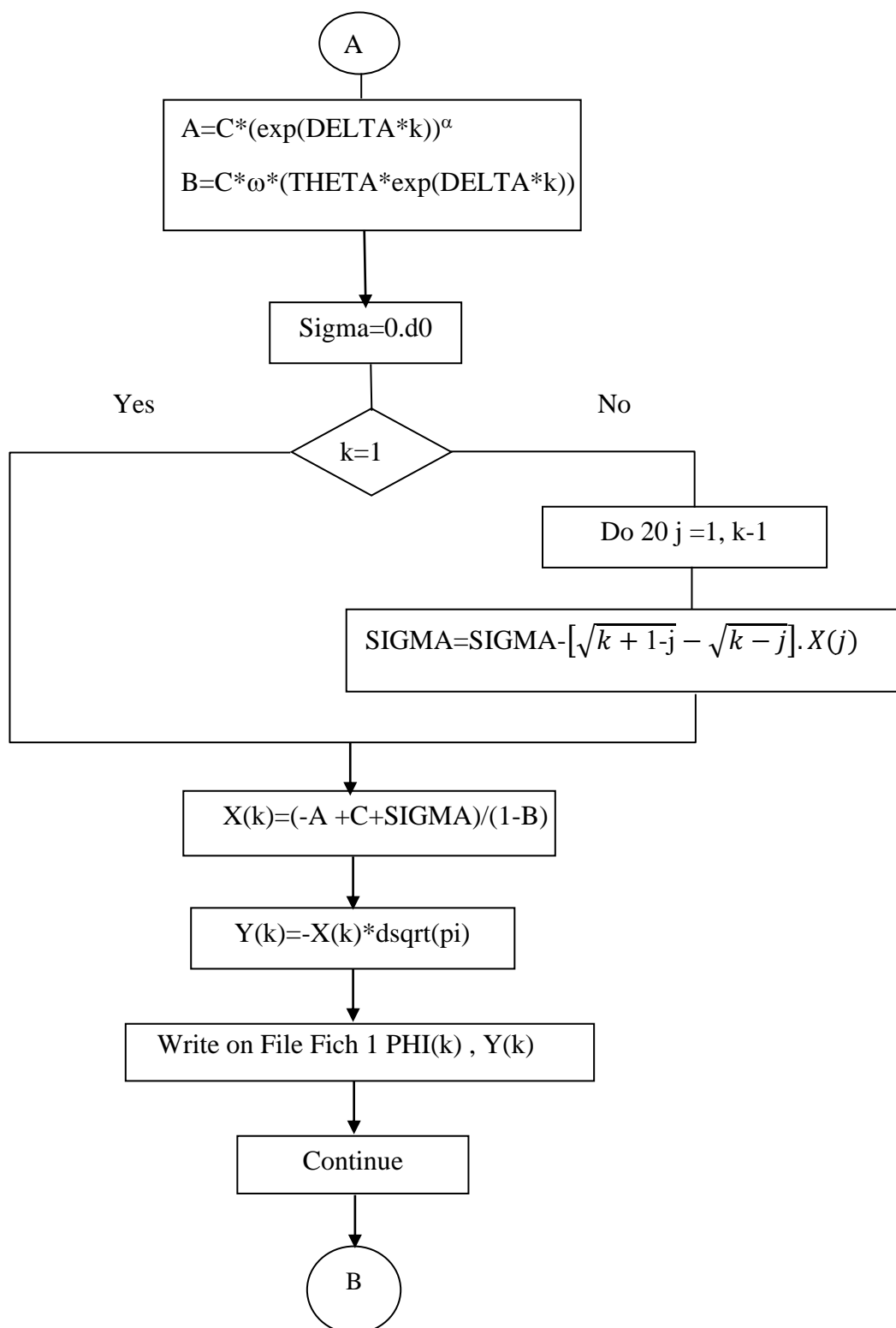
$$B(k)=\frac{1}{2\sqrt{\delta}}\left[\frac{1}{\omega}\left[\theta S(\delta K)\right]^\alpha\right] \quad (46)$$

### IV.2.3. Implementation of developed models in Fortran

In Fig III.1 there is a flowchart of our implementation based on the above LSV models, with a step-by-step calculation. These models are implemented using a Fortran code.



**Chapter III:** Simulation of linear sweep voltammetric behaviour for soluble-insoluble redox reaction



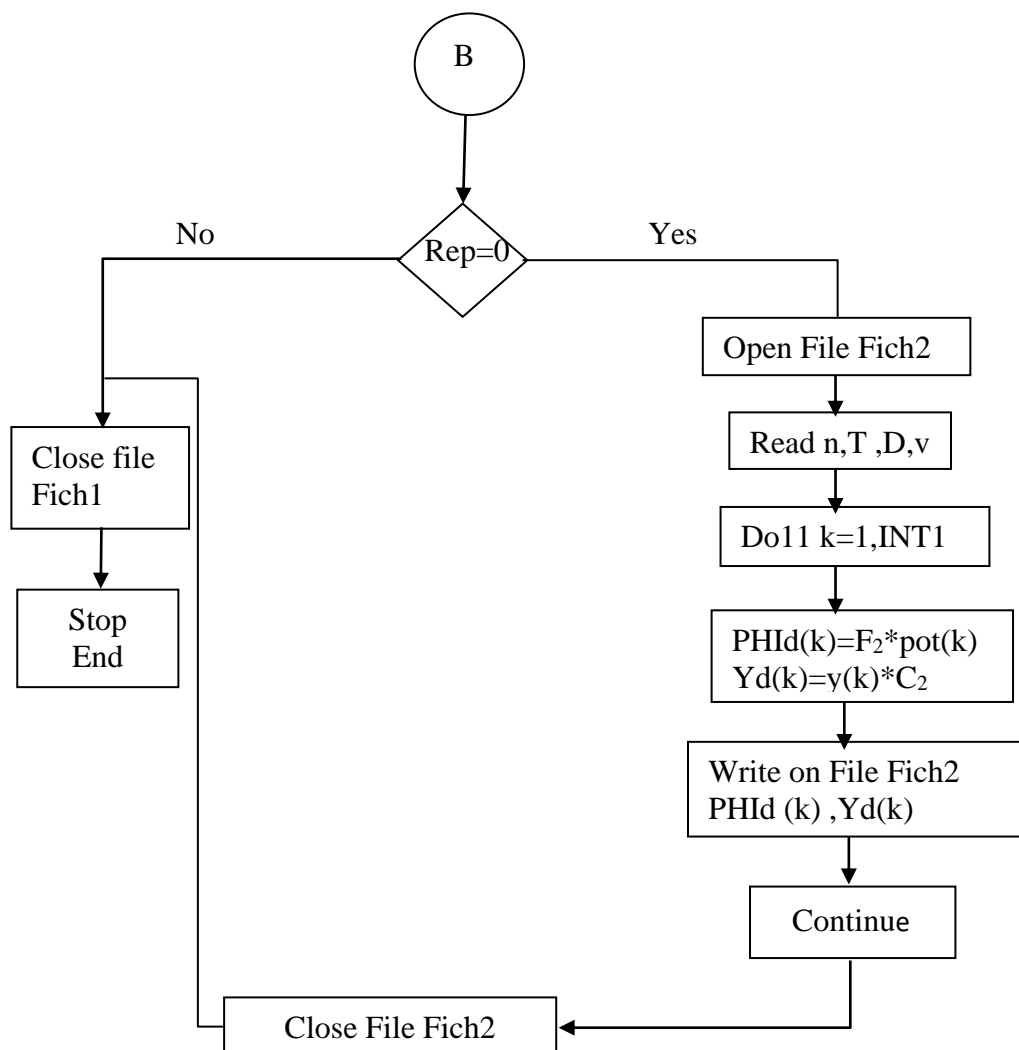


**Figure III.1.** Flowchart of the implemented LSV models

Thus, the algorithm under the name “QREV” enables the dimensionless voltammograms to be calculated, provided that the values of INIT, LIMIT,  $\omega$  and  $\alpha$  are known.

### III.3. Solution methodology via use of the finite element COMSOL Multiphysics software

We also numerically solved the Butler-Volmer LSV problem described in section III.1.1 by using the finite element commercial software package, COMSOL Multiphysics 5.2a.

To carried out the simulation of theoretical voltammograms, we go through the following stages:

### **III.3.1. Stage I: Pre-processing Stage**

The pre-processing stage includes 5 steps:

#### **III.3.1.1. Definition of governing equations**

Three governing equations were required to define the linear sweep voltammetry problem for the case soluble-insoluble system in COMSOL:

##### **III.3.1.1.1. Mass transport and mass conservation equations**

To describe the transport of ionic species  $i$  to and away from the electrode surface, Nernst-Planck equation was used:

$$J_i = -D_i \nabla C_i - z_i u_i F C_i \nabla V + u C_i \quad (47)$$

In COMSOL Multiphysics, this equation is embedded in the dilute species transport node.

Mass conservation equation for ionic species was expressed as:

$$\frac{\partial C_i}{\partial t} + \nabla J_i = R_i \quad (48)$$

Note that it is assumed that there are no homogeneous reactions in the electrolyte, and no migration or convection contribution will be considered. In this case, eq (48) is reduced to the Fick's law of diffusion.

##### **III.3.1.1.2. Potential sweep equation**

In our model, through the use of a triangular waveform, the LSV experiment's potential was forward swept.

##### **III.3.1.1.3. Electrochemical reaction kinetics**

Quasi-reversible kinetics is assumed and the Butler-Volmer type expression was used to determine the current density at the electrode-electrolyte interface.

##### **III.3.1.2. Drawing the Geometry domain**

In our model, the one-dimensional transport was assumed and represented by a single line on the domain  $0 \leq x \leq L$  (see Fig III.2), where  $L = \sqrt{2Dt}$ , is the diffusion distance traveled by an electroactive species over the duration of the voltammetry experiment [1].

### Chapter III: Simulation of linear sweep voltammetric behaviour for soluble-insoluble redox reaction

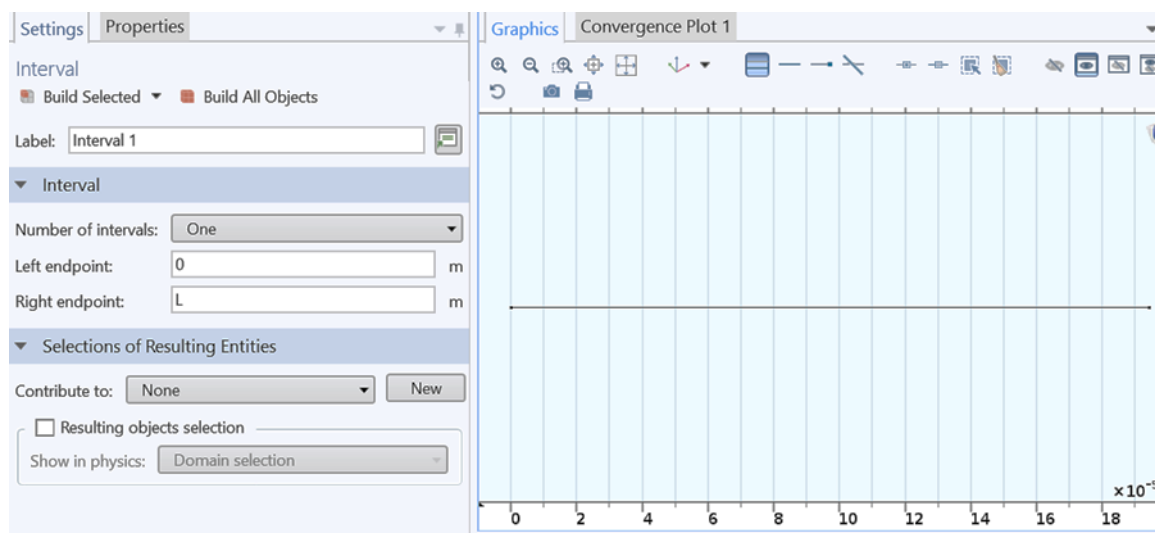


Figure III.2. 1D geometry model used for simulating the diffusion of metal ion.

#### III.3.1.3. Setting of initial and boundary conditions

Initially, the concentration of metal ions is equal to the concentration in the bulk. As shown in Fig III.2, the 1 D model consists of two boundaries, where the following conditions are imposed as follows:

- Boundary 1 is at the electrode surface  $x=0$ , that is, where the Butler-Volmer expression was used to define the flux boundary condition as follows:

$$J|_{x=0} = -k_f * C_{M^{n+}} + k_b * a_M \quad (49)$$

Where  $k_f$  and  $k_b$  are the forward and backward rate constants, respectively with:

$$k_f = k^0 e^{-\alpha \frac{nF}{RT} (E(t) - E^0)} \quad (50)$$

and

$$k_b = k^0 e^{(1-\alpha) \frac{nF}{RT} (E(t) - E^0)} \quad (51)$$

- Boundary 2 is at the domain's right-hand edge  $x=L$ , where we assume that a uniform concentration of metal ion equal to that in the bulk.

Furthermore, it should note that a zero-flux condition was applied at the outer boundaries of the geometry:

$$-nJ_i = 0 \quad (52)$$

### **III.3.1.4. Meshing**

To solve the voltammetry equation in the domain geometry defined above we need to create an element mesh. For this purpose, our computational domain is discretized into segments. During the meshing process, the properties shown in Table III.1 were used.

*Table III.1. Mesh properties*

<b>Mesh property</b>	<b>value</b>
Maximum element size	0.02
Minimum element size	$6 \times 10^{-4}$
Element ratio	100000
Number of elements	1000
Resolution of narrow regions	1
Maximum element growth	1.1

### **III.3.2. Stage II: Processing stage**

The governing equations under the defined boundary conditions described above are solved employing the time-dependent solver with a backward differentiation formula (BDF) time-stepping method (maximum BDF order: 2). the relative error tolerance used was  $10^{-9}$ .

### **III.3.3. Stage III: Post-processing stage**

The graphical representations of the current-potential responses as well as the listing of their values, were made at this stage.

## **III.4. Results and discussion**

### **III.4.1. Theoretical results**

#### **III.4.1.1. Calculation of linear scan voltammograms using semi analytical method and finite element method (COMSOL Multiphysics)**

As examples, in Fig III.3 we plot the non-dimensional current-potential response curves calculated using the algorithm “QREV” (solid curves) and COMSOL software (dashed curves) with the set parameters of  $\alpha=0,5$ ,  $INIT=0$ ,  $LIMIT=-30$ , a)  $\omega=10^3$  and b)  $\omega=10^{-1}$ .

### Chapter III: Simulation of linear sweep voltammetric behaviour for soluble-insoluble redox reaction

As it seen, we find agreement when testing the derived semi-analytical solutions against simulations using finite element method (COMSOL Multiphysics) to calculate voltammograms for soluble-insoluble system.

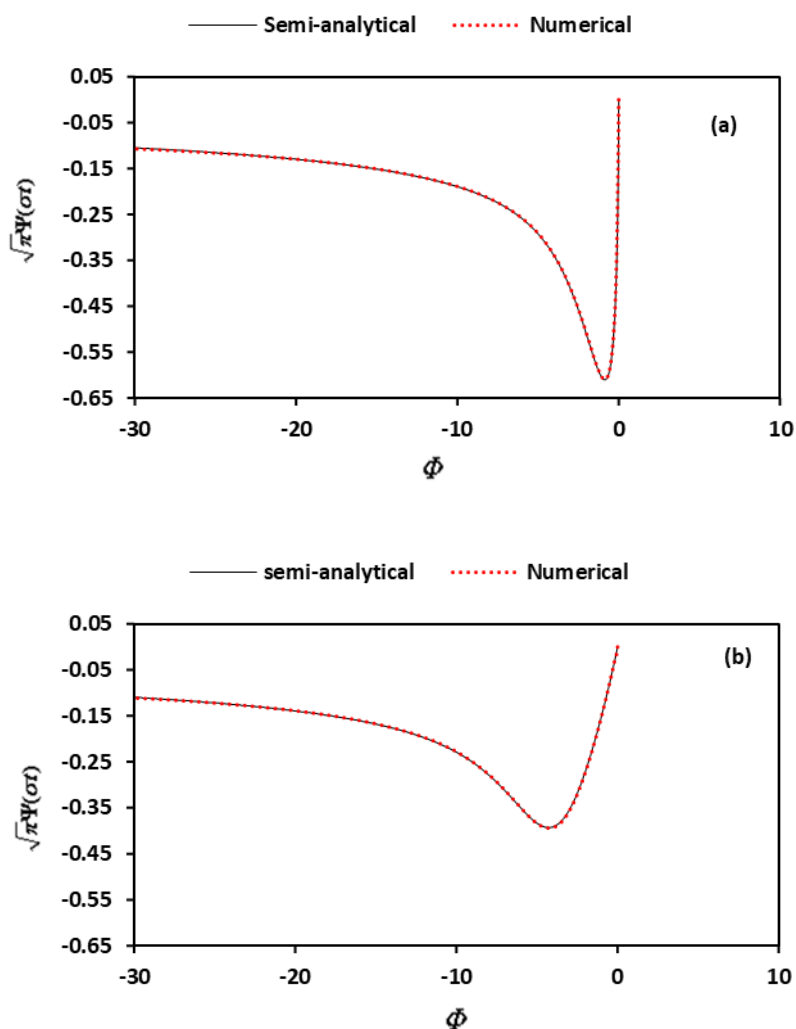


**Figure III.3.** Simulated LSV with the Butler-Volmer equation through use of the derived semi-analytical solutions (solid curve) and by the finite element method.  $\alpha=0,5$ ,  $INIT=0$ ,  $LIMIT=-30$  and  $\omega=10^3$   $LIMIT=-30$ , a)  $\omega=10^3$  and b)  $\omega=10^{-1}$ .

#### III.4.1.2. Effect of the kinetic rate

Generally, the critical parameters used for the diagnosis of electron transfer reactions via linear sweep voltammograms are the magnitudes of the peak current, the peak potential, and the half peak width. These LSV responses may depend on multiple variables including the

### ***Chapter III: Simulation of linear sweep voltammetric behaviour for soluble-insoluble redox reaction***

charge transfer coefficient  $\alpha$ , the potential sweep rate  $\nu$ , and the heterogeneous standard rate constant  $k^0$ . In the present paper, the mutual influence of  $k^0$  and  $\nu$  is expressed through the magnitude of the dimensionless parameter,  $\omega$ , defined by Eq (33). The effects of varying  $\omega$  for a constant value of  $\alpha$  on the position, high and width of peak are examined and shown in Fig III. 4, in which three distinct regions can be seen:

#### **1) $\omega > 10^3$**

For which, the dimensionless current-potential curves become insensitive to the dimensionless rate constant (curves a, b, c in the inset of Fig III.4). The dimensionless peak current,  $\pi^{1/2}\Psi_p$ , takes a constant value of -0.6105, as reported by Berzin and Delahay [2] for reversible system.

#### **2) $\omega \leq 10^{-3}$**

In this region, the calculated linear sweep voltammograms retain their shape (curves i-k in Fig III.4). The dimensionless peak current ( $\pi^{1/2}\Psi_p$ ) keeps stable in value of -0.350, which is in good agreement with literature values for irreversible systems [3]. Contrary to the peak shape, the peak position is shifted towards more negative potentials as  $\omega$  decreases.

#### **3) $10^{-3} < \omega < 10^3$**

Within these two kinetic regions (curves d–h in Fig III.4), a decrease in  $\omega$  leads to a diminution in the peak height, an increase in peak half width, and a shift of the dimensionless peak potential ( $\Phi_p$ ) towards more negative values. These observations refer to characteristics of quasi-reversible waves.

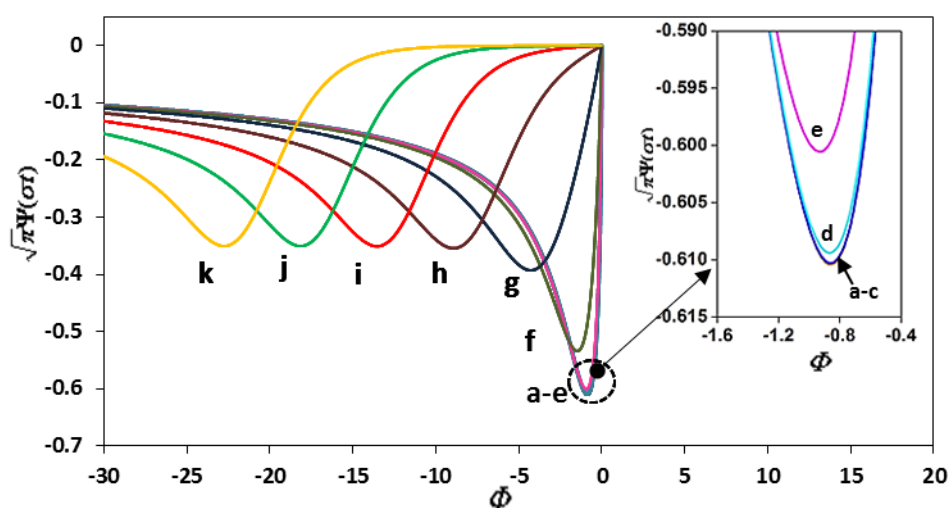


**Figure III.4.** Calculated linear sweep voltammograms for various value of  $\omega$  with  $\alpha=0.5$ ; **a:**  $\omega=10^5$ , **b:**  $\omega=10^4$ , **c:**  $\omega=10^3$ , **d:**  $\omega=10^2$ , **e:**  $\omega=10^1$ , **f:**  $\omega=1$ , **g:**  $\omega=10^{-1}$ , **h:**  $\omega=10^{-2}$ , **i:**  $\omega=10^{-3}$ , **j:**  $\omega=10^{-4}$ , **k:**  $\omega=10^{-5}$

### III.4.1.3. Effect of the charge transfer coefficient

A series of theoretical voltammograms in which the charge transfer coefficient  $\alpha$  is varied, are displayed in Fig III.5. Note that the impact of  $\alpha$  on the peak parameters depends upon the magnitude of the dimensionless kinetic rate  $\omega$ .

- For  $\omega=10^3$ , no change occurs in current and potential values with  $\alpha$  varying from 0.2 to 0.8. This observation agrees reasonably with previous studies for reversible system [2].
- For  $\omega=1$ , an increase in  $\alpha$  value from 0.2 to 0.8 is followed by a slightly increase in the dimensionless peak current (in absolute value), while the peak potential remains almost constant.
- For  $\omega=10^{-3}$ , the effect of the electron transfer coefficient has an appreciable influence on the height, position, and the shape of the peak.

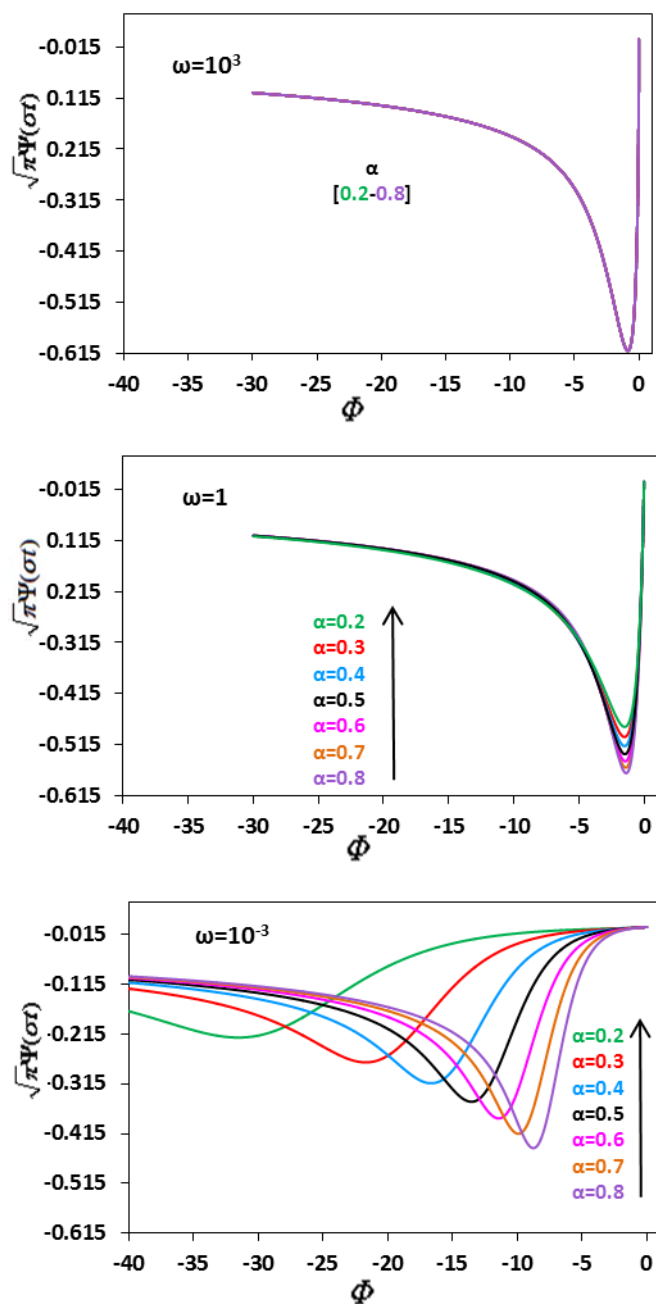


**Figure III.5.** The effect of transfer coefficient  $\alpha$  on theoretical voltammograms

#### III.4.1.4. Kinetics curves: coupling effects of kinetic rate and charge transfer coefficient

It is clear from the above results that the voltammograms in the intermediate region,  $10^{-3} < \omega < 10^3$ , are qualitatively different. Furthermore, until now, as no characteristic equations or practical tools for analysis of experimental voltammograms for soluble-insoluble quasi-reversible systems has been reported, our goal in this section is to provide a general, simple,

**Chapter III: Simulation of linear sweep voltammetric behaviour for soluble-insoluble redox reaction**

and direct model capable to solve the problem of the determination of the kinetic parameters in the case of these systems.

In the next set of figures, we have constructed three kinetic curves (i.e. the so-called working curves) for single electron transfer process, in which we show quantitatively the coupling effects of the dimensionless kinetic rate  $\omega$  and the electron transfer coefficient  $\alpha$  on LSV responses. The values of  $\omega$  in these calculations was varied from  $10^6$  to  $10^{-6}$  while the values of  $\alpha$  was varied from 0.2 to 0.8. Indeed, the original 'working curves', the first curves relating a system's responses to the LSV excitations with kinetic parameters originated from Matsuda and Ayab models [4] which were utilized later for the calculation of rate constant for quasi-reversible soluble-soluble redox reactions.

Fig III.6 shows the plot of the peak current ratio  $\Psi_p / (\Psi_p)_{rev}$  vs.  $\log(\omega)$ , where  $(\Psi_p)_{rev}$  is the reversible dimensionless peak current. Fig III.7 shows quantitatively the variation of the peak shape through the half peak width changes,  $\Delta\Phi_{p/2} = \frac{nF}{RT}(E_p - E_{p/2})$  as a function of  $\log(\omega)$

and  $\alpha$  and Fig III.8 describes how the cathodic peak position  $\eta_p$ ,  $\eta_p = \frac{nF}{RT}(E_p - E_{eq})$ , changes as a function of  $\log(\omega)$  and  $\alpha$ . It is apparent from Fig III.6 and Fig III.7, that the plots of the LSV responses as a function of both, the dimensionless heterogeneous rate constant  $\omega$  and the charge transfer coefficient  $\alpha$ , exhibit sigmoidal shapes. Data were then fitted perfectly by the sigmoidal Boltzmann functions:

$$\frac{\Psi_p}{(\Psi_p)_{rev}} = 1 + \frac{(0.811\alpha^{0.5} - 1)}{1 + \exp\left[\frac{X - (-0.528\alpha - 0.099)}{0.477\alpha^{0.248}}\right]} \quad (53)$$

$$-\Delta\Phi_{p/2} = 0.770 + \frac{(1.857\alpha^{-1} - 0.770)}{1 + \exp\left[\frac{X + (0.557\alpha^{-0.216})}{0.445\alpha^{0.316}}\right]} \quad (54)$$

Where:  $X = \log(\omega)$ .

**Chapter III:** Simulation of linear sweep voltammetric behaviour for soluble-insoluble redox reaction

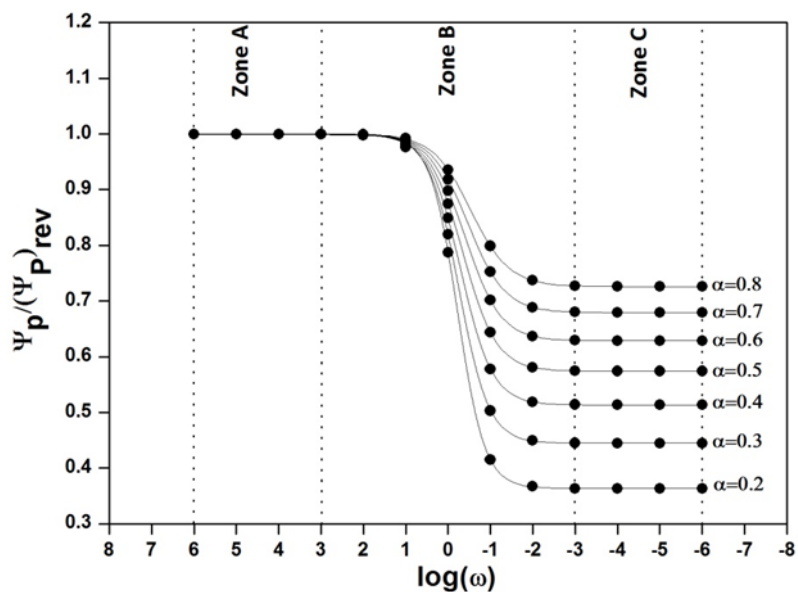


**Figure III.6.** Variation of the peak current ratio,  $\Psi_p / (\Psi_p)_{\text{rev}}$ , as the function of the dimensionless rate constant for several values of  $\alpha$ . Solid lines are best fits to the sigmoidal Boltzmann functions with a correlation coefficient of 0.99. Zones A, B, C denote the reversible, quasi-reversible and totally irreversible zones, respectively.

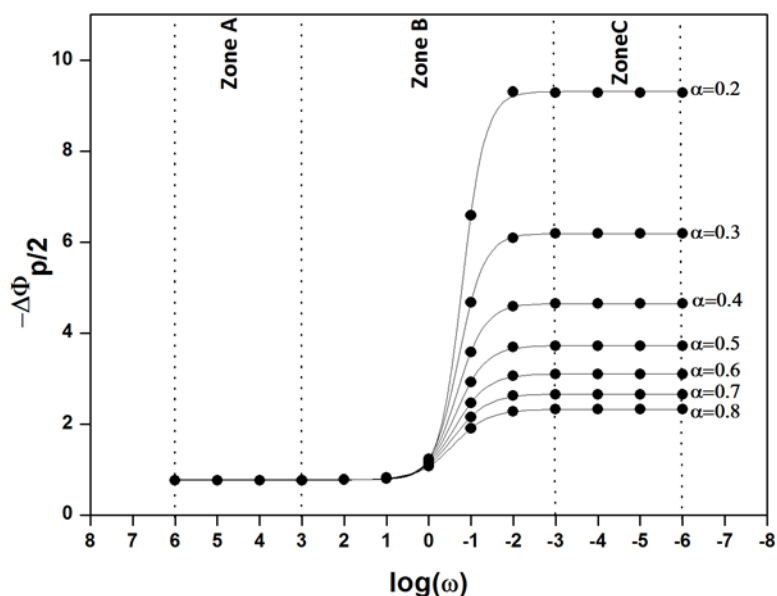


**Figure III.7.** Dependence of the half peak width of linear sweep voltammograms ( $\Phi_{p/2}$ ) on the logarithm of the kinetic parameter  $\omega$  for various  $\alpha$  values. Solid lines are best fits to the sigmoidal Boltzmann functions with a correlation coefficient of 0.98.

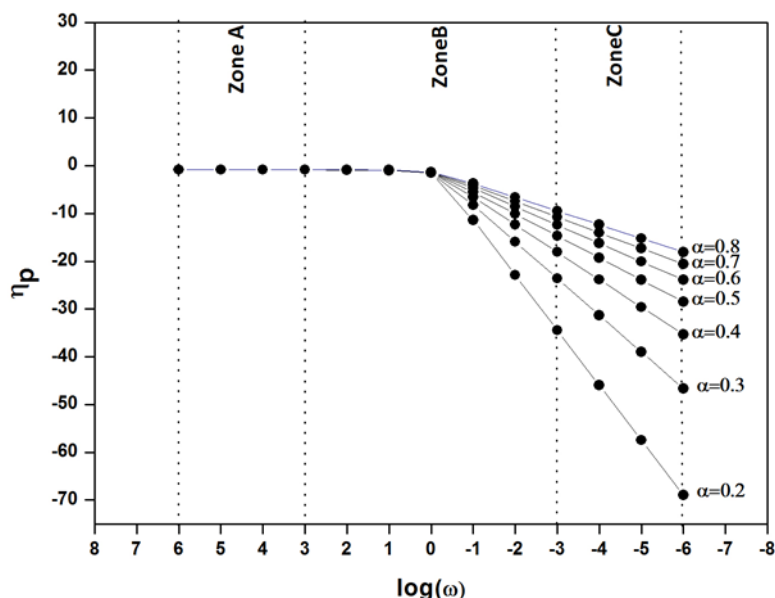


**Figure III.8.** Plots of the reduction peak position ( $\eta_p$ ) against  $\log(\omega)$  for various  $\alpha$  values

Each of these fit models enables voltammetric quantification of the electrode kinetics from simple peak current and peak potential measurements of the experimental linear sweep voltammograms for either reversible, quasi reversible or totally irreversible electron transfer process, provided that the value of  $\alpha$  is known or can be estimated accurately.

Also, from Figs III.6–III.8, the following kinetic zones properties can be concluded:

In the zone A ( $\omega \geq 10^3$ ) both the current and the peak potentials are independent of the values of  $\alpha$  and the dimensionless kinetic rate  $\omega$ . All peak parameters  $\eta_p$ ,  $\Psi_p$ , and  $\Delta\Phi_{p/2}$ , reach their reversible values, yielding to the following reversible criteria:

**$\omega \geq 10^3$**

$$I_p = -0.6105nFAC_{M^{n+}}^* (D_{M^{n+}})^{1/2} \left( \frac{nFv}{RT} \right)^{1/2} \pm \quad (55)$$

$$E_p = E_{eq} - 0.854 \frac{RT}{nF} \quad (56)$$

$$E_p - E_{p/2} = -0.77 \frac{RT}{nF} \quad (57)$$

These criteria for kinetically reversible system are in excellent agreement with those of previous theoretical investigations [2,5-7, 8].

**Chapter III: Simulation of linear sweep voltammetric behaviour for soluble-insoluble redox reaction**

Quasi-reversible features are observed in the zone B ( $-3 < \log \omega < 3$ ), where marked changes in the various peak parameters as a function of both  $\log \omega$  and  $\alpha$  are evident. As shown in Figs III.6–7, the peak height ratio increases while the half peak width decreases for increasing values of  $\alpha$ . Both values decrease with decreasing values of  $\log \omega$ . This effect of the charge transfer coefficient can be interpreted by the change in the symmetry of the energy barrier.

Irreversible behaviour is evident in the zone C  $\omega \leq 10^{-3}$ , where the peak current and half peak width remain constant with decreasing  $\log \omega$  for specific values of  $\alpha$  while the peak potential continues to decrease linearly as the function of decreasing  $\log \omega$ . As for the quasi-reversible case, the peak height ratio and peak potential increase and the half peak width decreases for increasing values of  $\alpha$ . Therefore, the following conclusions can be drawn:

**$\omega \leq 10^{-3}$**

$$I_p = -0.4951nFAC_{M^{n+}}^* (D_{M^{n+}})^{1/2} \left( \frac{nFV}{RT} \right)^{1/2} \alpha^{1/2} \quad (58)$$

$$E_p - E_{p/2} = 1.857 \frac{nF}{\alpha RT} \quad (59)$$

These equations show a very good agreement with those obtained by Delahay for irreversible soluble–insoluble redox system [3].

A further key point to consider in Fig. III.8, which was also observed and demonstrated by Krulic et al [9], is that in the region when  $\log \omega \leq -1$ , the magnitude of  $\eta_p$  depends linearly on the logarithm of the kinetic parameter  $\omega$ . Therefore, by using linear regression approximations, the dependency of  $\eta_p$  on  $\omega$  and  $\alpha$  could be expressed as follows:

$$\alpha \eta_p = 2.303X - [0.115 \log(\alpha) + 0.78] \quad (60)$$

This equation coincides with that established by Krulic for  $\alpha=0.5$  [9], it can be used for estimation of the kinetic rate constant, in particularly for quasi-reversible and irreversible electrodeposition processes if the value of  $\alpha$  is known or can be estimated.

### *Chapter III: Simulation of linear sweep voltammetric behaviour for soluble-insoluble redox reaction*

On the other hand, when we move to compare the profiles of the working curves for peak current to reversible peak current ratio and the difference between the peak and half peak potentials against decimal logarithm of kinetic rate constant (Figs III.6 and III.7) with as presented by Matsuda and Ayab for soluble-soluble redox couple [4], we note that they have qualitatively the same shape, but they have completely different quantitative behavior. Meanwhile, It is worth to mention that it's not possible to compare the last working curve plotted in Fig III.8 with that down by Matsuda and Ayab, because the manipulated variable

are not identical (a y-axis variable for soluble-insoluble system was  $\eta_p = \frac{nF}{RT}(E_p - E_{eq})$ ,

while for soluble-soluble system was  $\Xi(\Lambda, \alpha) = -\frac{nF}{RT}(E_p - E_{1/2})$ ).

#### **III.4.2. Experiment–theory comparison**

In order to test the validity of our numerical approach to extract kinetic and mass transport parameters from LSV data, an example of Cu electrodeposition reaction in organic solution is presented. The Cu system includes a simple one-electron transfer reaction according to [10]:



although, the removal of the complexing solvent should also be considered [11-12].

Fig III.9a depicts typical LSV profiles collected at different scan rates for reduction reaction, Cu(I)/Cu(0), in acetonitrile. Regarding to the peak heights, an increasing trend was observed on increasing the scan rates. Furthermore, the peak potential was seen to shift gradually towards more negative potential values over 25–200 mV/s scan rate suggesting a quasi-reversible character. To deduce the mass-transport and kinetic proprieties of the Cu(I)/Cu(0) system, the unknown parameters values:  $D_{\text{Cu}(I)}$ ,  $\alpha$  and  $k^0$  need to be derived. There are two ways for the calculation of  $D_{\text{Cu}(I)}$ ,  $\alpha$  and  $k^0$ : by either computationally (**Utilization of working curves**) or by adjustment to linear sweep voltammograms (**Fit and simulation**) based only on QREV algorithm and different combinations of  $D_{\text{Cu}(I)}$ ,  $\alpha$  and  $k^0$ .

### Chapter III: Simulation of linear sweep voltammetric behaviour for soluble-insoluble redox reaction

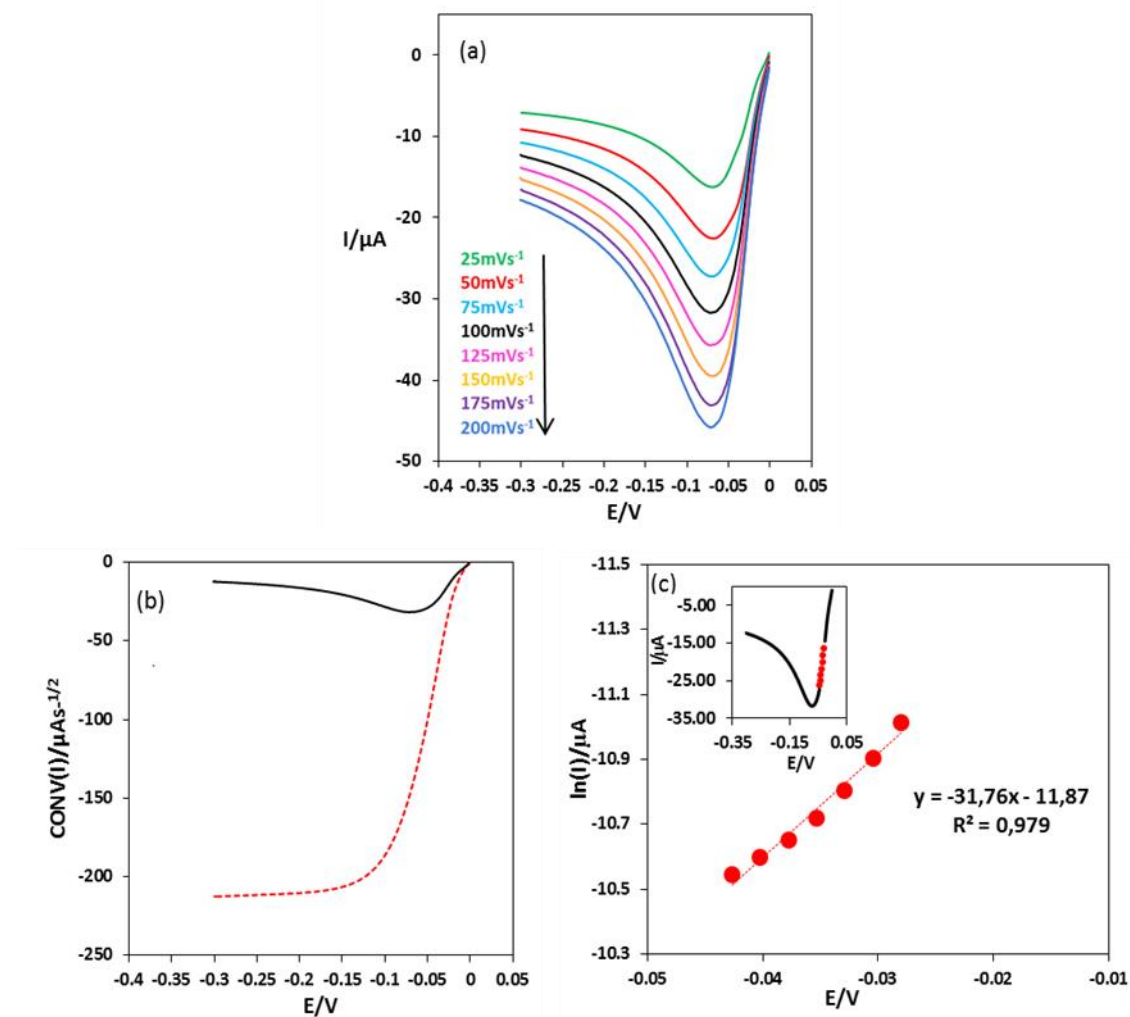


**Figure III.9.** (a) LSV curves of electrodeposition of Cu(I) on Cu disc electrode from 10.25 mM of tetrakis(acetonitrile)copper(I) tetrafluoroborate in acetonitrile at various scan rates. (b) LSV curve of reduction reaction of Cu(I) recorded scan rate of 100 mV/s. The dotted line indicates semi-integrated current for forward scan (c) Tafel curve derived from the rising part of the LSV curve at scan rate of 100 mV/s. The inset shows the LSV data used for drawing the Tafel curve. The potential is expressed vs. the Cu reference in equilibrium with 10.25 mM  $\text{Cu}^+$  in solution, i.e.  $-0.118$  V vs. standard copper electrode in acetonitrile.

#### III.4.2.1. Utilization of working curves

First, we used the common employed procedure, the semi-integrative voltammetry, for the calculation of Cu(I) diffusion coefficient and a direct Tafel analysis for the measurement of the transfer coefficient  $\alpha$ . Fig III.9b shows a sigmoidal curve (dotted line) obtained from semi-integration of typical voltammetric current recorded at 100 mV/s. It should be noted that we

**Chapter III: Simulation of linear sweep voltammetric behaviour for soluble-insoluble redox reaction**

have employed the Saila methodology [13] for establishing semi-integrated plots. As shown in Fig III.9b and as per principle of semi-integration technique, the semi-integration of the voltammetric current responses with respect to time yields to the sigmoidal-type curve with a plateau. This plateau level represents the limiting semi-integral current, of height  $m^*$  :

$$m^* = nFAC_{M^{n+}}^* D_{M^{n+}}^{1/2} \quad (62)$$

and the diffusion coefficient of Cu(I) in acetonitrile at 25 °C was computed utilizing this equation (as shown in Table 1) by considering the following experimental values:  $n = 1$ ,  $C_{Cu^+}^* = 10.25mM$ . Fig III.9c depicts the representation of the Tafel plot obtained from experimental LSV data, at a scan rate of 100 mV/s. Using the slope calculated from Fig III.9c and the Tafel equation, the value of  $\alpha$  was calculated and the result is reported in Table 1. In the next step, a more detailed examination of the voltammetric peaks allowed us to quantify the standard rate constant ( $k^0$  in  $cm^2/s$ ) for the Cu(I)/Cu(0) redox couple according to the models presented in Section III.4.1.4 .The results are listed in Table 1. With these values, Eqs (53), (54) and (60) were used to obtain the final value for the  $k^0$ .

**Table III.2.** Kinetic-mass transport parameters extracted from the LSV curve at 100 mV/s, for Cu(I)/Cu(0) redox couple

	Diffusion coefficient		Charge transfer coefficient		Rate constant			
Cu(I)/Cu(0) System	$D_{Cu(I)}[10^{-9}m^2s^{-1}]$		$\alpha$		$k^0[10^{-5}cms^{-1}]$			
	Semi integration	Fit	Tafel	Fit	Working curves			Fit
					Eq (53)	Eq (54)	Eq (60)	
	1.75	1.70	0.82	0.80	3.835	4.99	7.73	5.12

### III.4.2.2. Fit and simulation

The parameters,  $D_{Cu(I)}$ ,  $\alpha$  and  $k^0$  were also obtained by comparison of theoretical and the experimental linear scan voltammograms (in 100 mM TEABF<sub>4</sub> and 10 mM Cu(CH<sub>3</sub>CN)<sub>4</sub>BF<sub>4</sub>), using the LSV model algorithm with a series of adjustments in the input values. For this purpose, theoretical voltammograms were obtained by utilizing the diffusion coefficient of Cu ions within the range reported in the literature [14], and varying the values

### **Chapter III: Simulation of linear sweep voltammetric behaviour for soluble-insoluble redox reaction**

for  $k^0$  and  $\alpha$  for the Cu(I)/Cu(0) system as these values have not been reported previously in the literature. In our work,  $\alpha$  was varied from 0.1 to 0.9 while the dimensionless kinetic rate was varied from  $10^{-3}$  to  $10^3$ .

In the purpose to compare the two approaches: i) theoretical fitting and ii) working curves, and to illustrate the LSVs are obtained with the parameters from Eqs (53), (54) and (60), an analysis study was performed first with the voltammetric data collected at 100 mV/s. To achieve best fit to experimental LSV data obtained at 100 mV/s, we tested various values of  $D_{\text{Cu}(I)}, \alpha$  and  $k^0$ . With the following parameters:  $D_{\text{Cu}(I)} = 1.7 \times 10^{-9} \text{ m}^2 \text{ s}^{-1}$ ,  $\alpha = 0.8$  and  $k^0 = 5.12 \times 10^{-5} \text{ cm s}^{-1}$ , the resultant theoretical voltammogram is in very good agreement with the experimental LSV curve (see Fig III.10a).

To demonstrate the applicability of the working curves, theoretical voltammograms were calculated with Eq (53) with the parameters shown in Table III.2 and the results are presented in Fig III.10b. Better agreement was obtained by using Eqs (53) and (54) than by Eq (60). The small discrepancy in kinetic prediction using Eq (60) could be attributed to the dimensionless kinetic rate constant  $\omega$  of copper reduction which was just out of range of applicability of Eq (60). We have found above that Eq (60) is valid for  $\omega \leq 0.1$ ; however the  $\omega$  value calculated for Cu reaction is 0.15.

Table III.2 shows the obtained parameters for the reduction of Cu(I) to Cu(0) in acetonitrile at 100 mVs<sup>-1</sup>. The obtained  $D_{\text{Cu}(I)}$  values are similar with the values previously reported in reference [14], i.e,  $1.64 \times 10^{-5} \text{ m}^2 \text{ s}^{-1}$ , although slightly higher diffusion coefficient was obtained from semi-integration analysis. Furthermore, the calculated values of  $k^0$  indicated that the Cu deposition process in acetonitrile is quasi-reversible. Likewise, the kinetics of the Cu(I)/Cu(0) system were analyzed at all scan rates. The use of Eqs. (53), (54) and (60), yielding average values of the standard rate constant  $k^0$ :  $4.86 (\pm 0.68) \times 10^{-5}$ ,  $4.63 (\pm 0.22) \times 10^{-5}$  and  $7.76 (\pm 0.76) \times 10^{-5} \text{ cm/s}$ , respectively. Excellent fits were reproduced between the experimental LSVs and simulated ones under various scan rates (see Fig III.10) and the average fitted  $k^0$  value was found:  $5.43 (\pm 0.52) \times 10^{-5} \text{ cm/s}$ .

**Chapter III: Simulation of linear sweep voltammetric behaviour for soluble-insoluble redox reaction**

These results confirm the above conclusions and reveal that the working curves provided in this work can be used to accurately analyze the linear scan voltammetric current responses for quasi-reversible soluble/insoluble system. The high transfer coefficient value of 0.8 obtained in this work is in line of the values obtained for Cu deposition on amalgams from nitrile solvents, indicating that the reaction site is located in the inner part of the electric double layer [11,12]. However, the apparent rate constants measured in this work for Cu deposition are three orders of magnitude smaller than the standard rate constants obtained for copper deposition on mercury [11,12], indicating that ion transfer into mercury is easier than nucleation on copper surface.

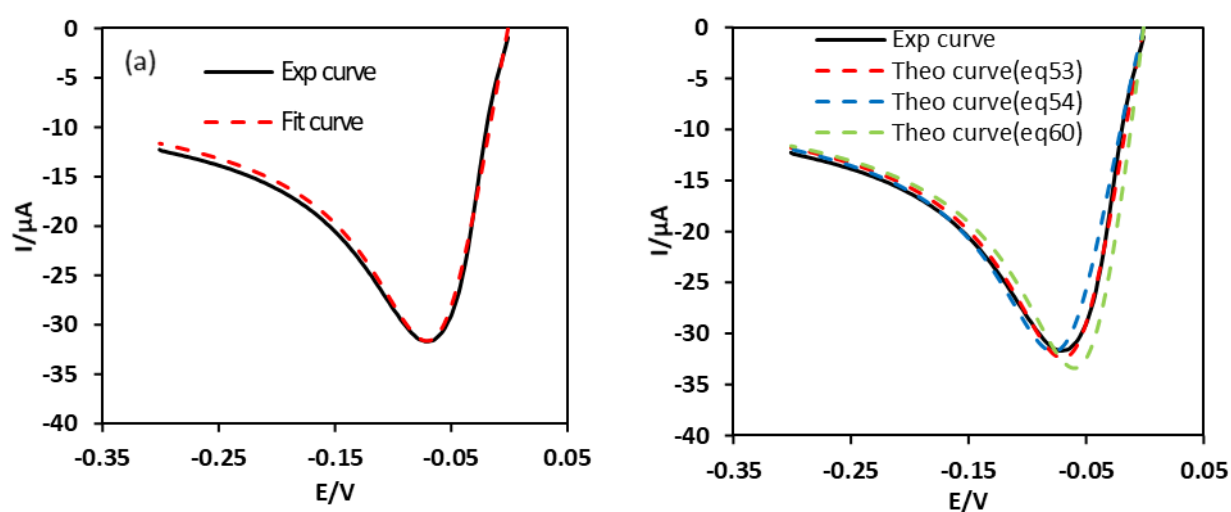


**Figure III.10.** (a) Comparison between theoretical linear scan voltammogram and experimental voltammogram obtained and recorded at  $100\text{mV s}^{-1}$  scan rate. The parameters used for theoretical prediction are:  $D_{\text{Cu}(I)} = 1.70 \times 10^{-9} \text{m}^2 \text{s}^{-1}$ ,  $\alpha = 0.8$  and  $k^0 = 5.12 \times 10^{-5} \text{cm s}^{-1}$  (b) Comparison of theoretical LSV responses with experimental data using Fit models presented by Eq (53), Eq (54) and Eq (60). Parameters used for LSV modelling:  $D_{\text{Cu}(I)} = 1.75 \times 10^{-9} \text{m}^2 \text{s}^{-1}$ ,  $\alpha = 0.82$  and  $k^0 = 3.83 \times 10^{-5} \text{cm s}^{-1}$  calculated from Eq (53),  $k^0 = 3.83 \times 10^{-5} \text{cm s}^{-1}$  calculated from Eq (54) and  $k^0 = 5.88 \times 10^{-5} \text{cm s}^{-1}$  calculated from Eq (60) The potential is expressed vs. the Cu reference in equilibrium with  $10.25 \text{mM Cu}^+$  in solution, i.e.  $-0.118 \text{V}$  vs. standard copper electrode in acetonitrile.

### **III.5. Conclusion**

In summary, using a semi analytical method, a new LSV algorithm has been proposed for use in the computing of voltammograms in the case of soluble-insoluble system where the electron transfer takes place in a single step. A numerical method based on finite element method (COMSOL) has been also used in simulating LSV responses.

The experimental verification of the theoretical framework is carried out by studying the electrodeposition of Cu(I) / Cu (0) in acetonitrile.

In this chapter, the presentation, and the analysis of the results are divided into three parts:

- In the first part, a comparison was made between the semi-analytical (using QREV algorithm) and numerical solution (using COMSOL software) which shows a good agreement between them.
- The second part is dedicated to the theoretical analysis of simulated LSV responses. The effect of the kinetic parameters on the LSV responses has been examined. Through the variation of the peak parameters with dimensionless kinetic rate ( $\omega$ ) and the transfer coefficient ( $\alpha$ ), series of kinetic curves have been established. The obtained results showed that according to the magnitude of the dimensionless rate constant the various LSV responses limitation could be divided into three zones: Zone A:  $\omega \geq 10^3$ , reversible process. Zone B:  $10^{-3} < \omega < 10^3$ , quasi-reversible process. Zone C:  $\omega \leq 10^{-3}$ , irreversible process. Moreover, we offer here three working curves to extract kinetic details with high accuracy and simplicity to use, as only the experimental values corresponding to the peak high, peak position and peak width are required.
- In the third part, the voltammetry comparison of simulation and experiment was performed. Kinetic and diffusive parameters of Cu(I) ions were determined. The calculated  $k_0$  indicated that the Cu(I)/Cu(0) was quasi-reversible. The LSV theory developed in this study showed an accurate prediction to the current responses for Cu(I)/Cu(0) couple in acetonitrile medium and a very good agreement between experiment-theory was obtained.

### III.6. References

- [1] N.G. Amado, *Design and fabrication of miniaturized electroanalytical systems*, Doctoral dissertation, Universitat Autònoma de Barcelona, 2010.
- [2] T. Berzins, P. Delahay, *Oscillographic polarographic waves for the reversible deposition of metals on solid electrodes*, J. Am. Chem. Soc., 75, 555–559, 1953.
- [3] P. Delahay, *Theory of irreversible waves in Oscillographic polarography*, J. Am. Chem. Soc., 75 1190–1196, 1953.
- [4] H. Matsuda, Y. Ayabe, *Zur Theorie der Randles-Sevcikschen Zur Theorie der Randles-Sevcikschen Für Elektrochemie*, Berichte Der Bunsengesellschaft Für Phys. Chemie, 59(6), 494–503, 1955.
- [5] D.J. Schiffrin, *Theory of cyclic voltammetry for reversible electrodeposition of insoluble products*, J. Electroanal. Chem., 201, 199–203, 1986.
- [6] G. Mamantov, D.L. Manning, J. M. Dale, *Reversible deposition of metals on solid electrodes by voltammetry with linearly varying potential*, J. Electroanal. Chem., 253–259, 1965.
- [7] N. White, F. Lawson, *Potential sweep voltammetry of metal deposition and dissolution: part I. Theoretical analysis*, J. Electroanal. Chem., 25, 409–419, 1970.
- [8] N. Fatouros, D. Krulic, H. Groult, *Linear sweep and staircase voltammetries for reversible deposition of metal ions on the same metal and on foreign substrates*, J. Electroanal. Chem., 625 1–6, 2009.
- [9] D. Krulic, N. Fatouros, D. Liu, *A complementary survey of staircase voltammetry with metal ion deposition on macroelectrodes*, J. Electroanal. Chem., 754 30–39, 2015.
- [10] P. Peljo, D. Lloyd, N. Doan, M. Majaneva, K. Kontturi, *Towards a thermally regenerative all-copper redox flow battery*, Phys. Chem. Chem. Phys., 16, 2831–2835, 2014.
- [11] W.R. Fawcett, C. A. Foss, *Role of the solvent in the kinetics of heterogeneous electron and ion transfer reactions*, Electrochim. Acta ,36,1767–1774, 1991.
- [12] W.R. Fawcett, C.A. Foss, *On the nature of the transfer coefficient for ion transfer reactions*, J. Electroanal. Chem., 250, 225–230, 1988.
- [13] A. Saila, *Etude des systemes electrochimiques quasi-reversibles par voltamperometrie a balayage lineaire et semi-integration. Applications aux comportements de rhenium et dysprosium en milieux de sels fondus*, Université de Badji Mokhtar, Annaba, 2010.

**Chapter III:** *Simulation of linear sweep voltammetric behaviour for soluble-insoluble redox reaction*

[14] R. R. Bessette, J. W. Olver, *Measurement of diffusion coefficients for the reduction of copper(I) and (II) in acetonitrile*, J. Electroanal. Chem., 21, 525–529, 1969.

# **CHAPTER IV**

## *Simulation of cyclic voltammograms for soluble-insoluble redox reaction*

---

In this chapter, first we build based on the Butler-Volmer type rate expression, a cyclic voltammogram simulation model for one-step electrodeposition reactions using the semi-analytical method and the finite element COMSOL software. Second, we show how the soluble-insoluble redox system behaves under cyclic voltammetry condition through the variation of the following parameters: dimensionless rate constants, charge transfer coefficients and switching potential. At the end of this chapter the theoretical concentration profiles for reversible, quasi-reversible and irreversible electron transfer are established and analysed.

---

## **IV.1. Modelling cyclic voltammetry profile for metal/metal-ion system**

For simulation of cyclic voltammograms for the metal/metal ion system, we have used the same assumptions as in the previous chapter, except we now consider the forward-backward potential sweep. The CV curve is then modelled using the bipartite function [1]:

$$E = \begin{cases} E_i - vt, & t \leq t_\lambda \\ E_i + 2vt_\lambda - vt, & t > t_\lambda \end{cases} \quad (1)$$

Where  $t_\lambda$  is the switching time.

## **IV.2. Resolution**

### **IV.2.1. Semi-analytical approach**

We have followed step-by-step procedures used in chapter III, to develop the current–potential profile, to arrive at:

**Dimensionless current expression:**

$$\Psi(k) = -A(k) - \sum_{i=1}^{k-1} \frac{[\sqrt{k-(i-1)} - \sqrt{k-i}] \Psi(i)}{1-B(k)} + C \quad (2)$$

**Dimensionless applied potential expression**

For the forward sweep:

$$\Phi = \frac{nF}{RT} (E - E^0) = \text{init} - \delta k \quad (3)$$

With:

$$A(k) = \frac{1}{2\sqrt{\delta}} [\exp(-\delta k)] \quad (4)$$

$$B(k) = \frac{1}{2\sqrt{\delta}} \left[ \frac{1}{\omega} [\theta \exp(-\delta k)]^\alpha \right] \quad (5)$$

For the backward sweep

$$\Phi = -\text{INIT} + 2\text{LIMIT} + \delta k \quad (6)$$

With:

$$A(k) = \frac{1}{2\sqrt{\delta}} \left[ \frac{1}{1 + [\theta \exp(2(\text{LIMIT} - \text{INIT}) + \delta k)]} \right] \quad (7)$$

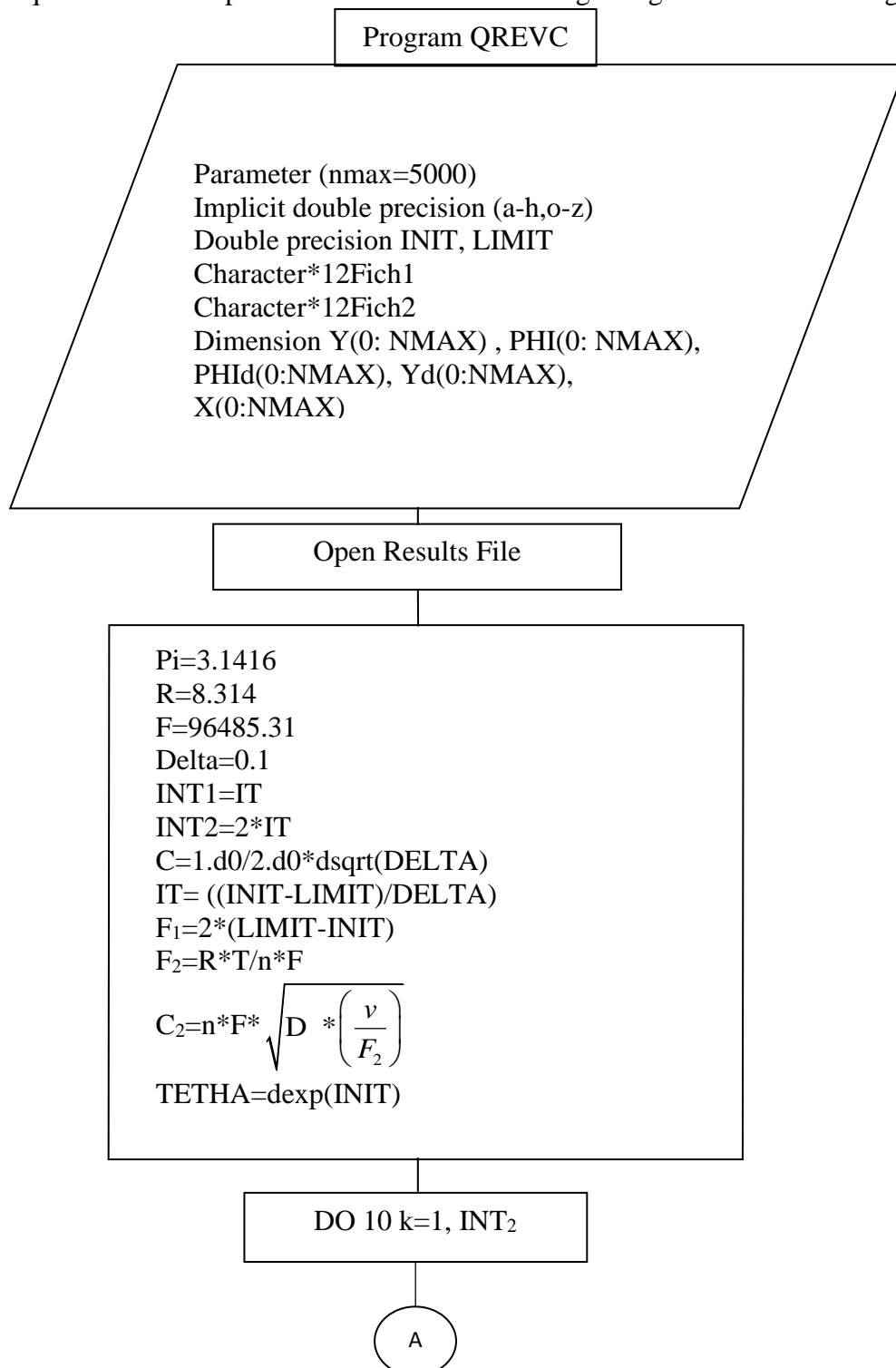
**Chapter IV: Simulation of cyclic voltammograms for soluble-insoluble redox reaction**

$$B(k) = \frac{1}{2\sqrt{\delta}} \left[ \frac{1}{\omega} \left[ \theta \exp(2(\text{LIMIT} - \text{INIT}) + \delta k) \right] \right]^\alpha \quad (8)$$

Noted that the dimensionless switching potential is expressed as follows:

$$\text{LIMIT} = \frac{nF}{RT} (E_\lambda - E^0) \quad (9)$$

The above equations were implemented in Fortran according to algorithm shown in Fig IV.1.



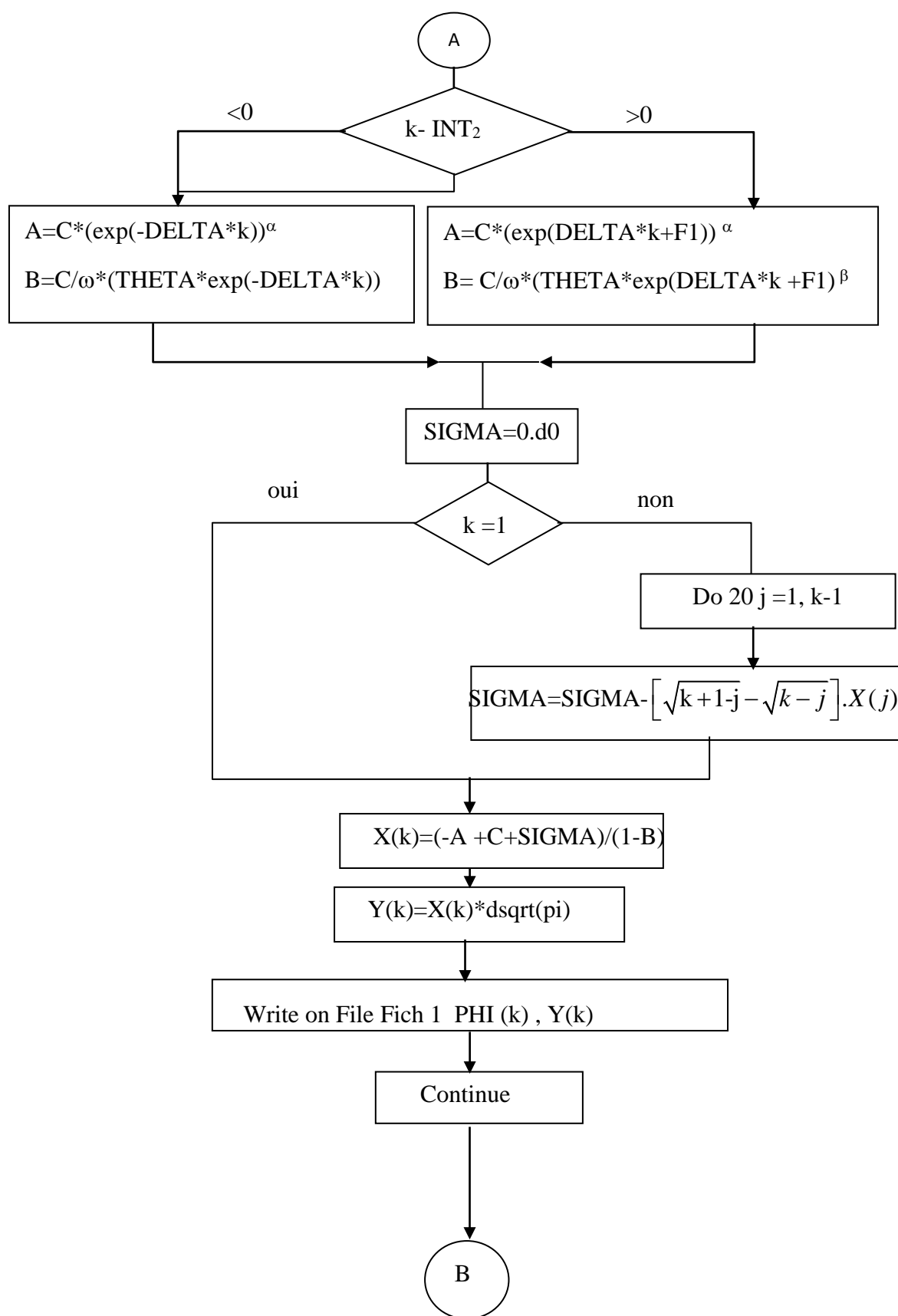
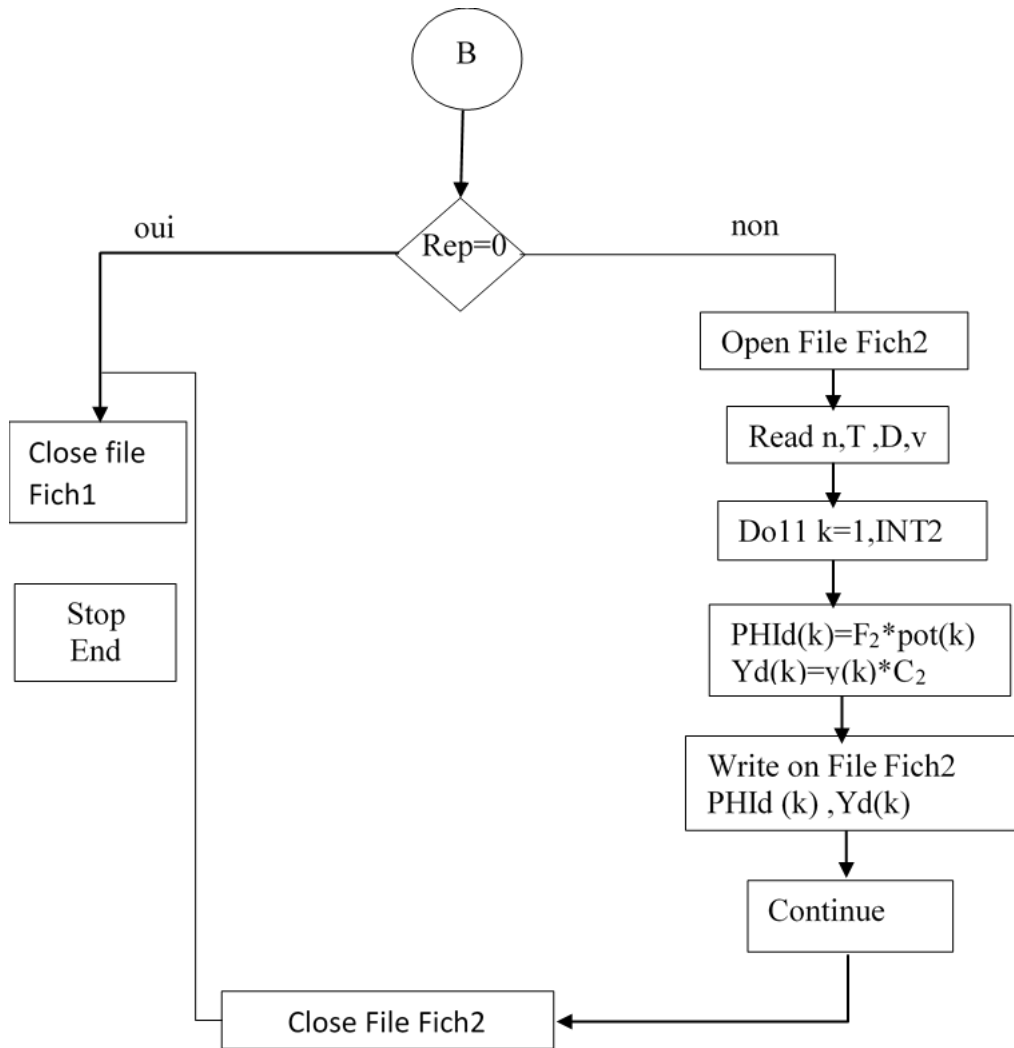


Figure IV.1. Flowchart of the implemented CV models



As a result, the “QREVC” algorithm can calculate cyclic voltammograms if the values of INIT, LIMIT,  $\omega$  and  $\alpha$  values are put.

#### **IV.2.2. Finite element approach (COMSOL Multiphysics)**

Essentially, same steps involved in LSV model development are also followed for finite elements simulation of cyclic voltammograms, except for the point of type of potential sweep, which was swept linearly forward and backward, using a triangular waveform.

## IV.4. Results and discussion

### IV.4.1. Calculation theoretical cyclic voltammograms using semi analytical method and finite element method (COMSOL Multiphysics)

Figure IV.2 shows an example of dimensionless cyclic voltammograms calculated by using the algorithm “QREV (black dashed curve) as well as that calculated by COMSOL software (red-dashed curve), the agreement between the two curves is remarkably good.

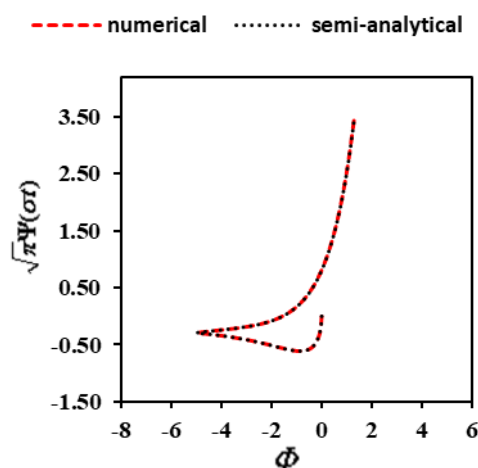


**Figure IV.2.** Simulated cyclic voltammograms obtained with the Butler-Volmer equation through use of the derived semi-analytical solutions (black curve) and by the finite element method (red-curve).  $\alpha=0.5$ ,  $INIT=0$ ,  $LIMIT=-5$  and  $\omega=10^3$

### IV.4.2. Effect of the kinetic rate

To illustrate the transition from reversible to irreversible behaviour, in Fig IV.3 we showed a set of simulated CVs in which the dimensionless kinetic parameter took the following values:  $10^3$ ,  $10^{-1}$  and  $10^{-3}$  for reversible, quasi-reversible and irreversible cases, respectively. Several key differences in the effect of  $\omega$  on the theoretical CVs can be identified. Peak currents decrease in intensity when the behaviour of the soluble-insoluble system changed from reversible to quasi-reversible or irreversible. The forward and backward potential peaks are very close to each other for reversible case ( $\omega=10^3$ ) and they become well separated for irreversible case ( $\omega=10^{-3}$ ). This is the consequence of the shift of the anodic branch to more anodic values and the shift of the cathodic peak to more cathodic values when the dimensionless rate constant goes towards quasi reversible or irreversible zone. The same observation was found with the soluble-soluble redox system [2].

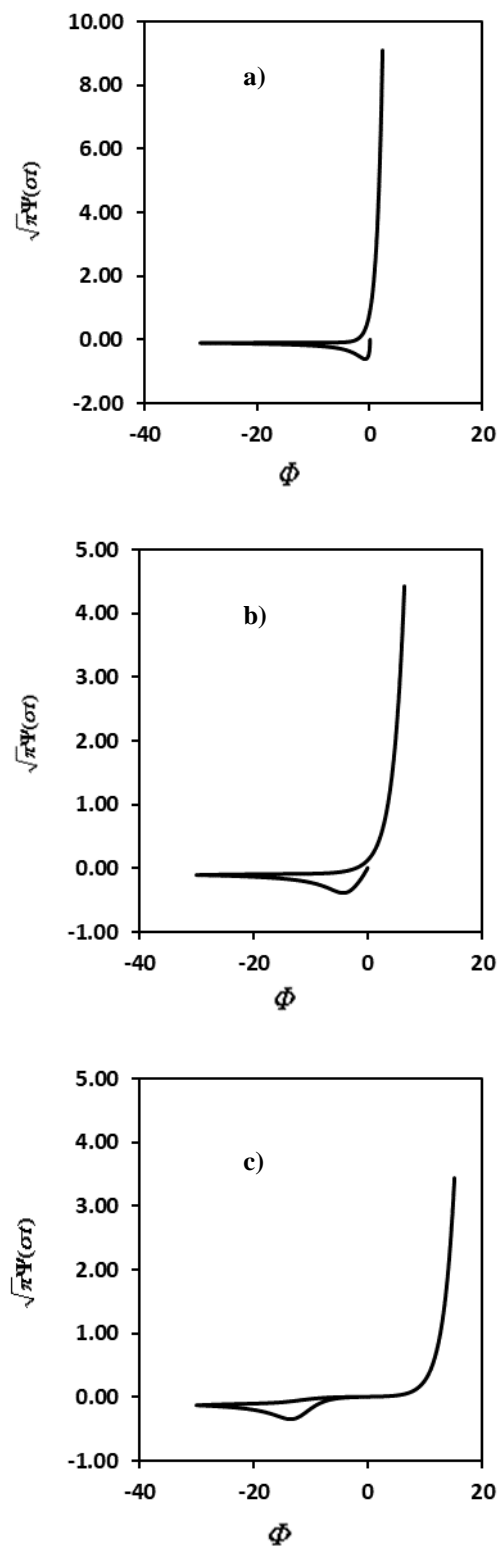


**Figure IV.3.** Calculated cyclic voltammograms for various value of  $\omega$  with  $\alpha=0.5$ ,  $INIT=0$ ,  $LIMIT=-30$ . (a) reversible case ( $\omega=10^3$ ), (b) quasi-reversible case ( $\omega=10^1$ ), (c) irreversible case ( $\omega=10^{-3}$ ).

### IV.4.3. Effect of the charge transfer coefficient

Fig IV.4a and IV.4b showed the dependence of the CV responses on the transfer coefficient for the quasi-reversible and irreversible cases, respectively. As the cathodic transfer coefficient  $\alpha$  increases, the cathodic peak potential shifts to more anodic values. In addition, we must mention that the reversible systems are not infected by the variation of the charge transfer coefficient.

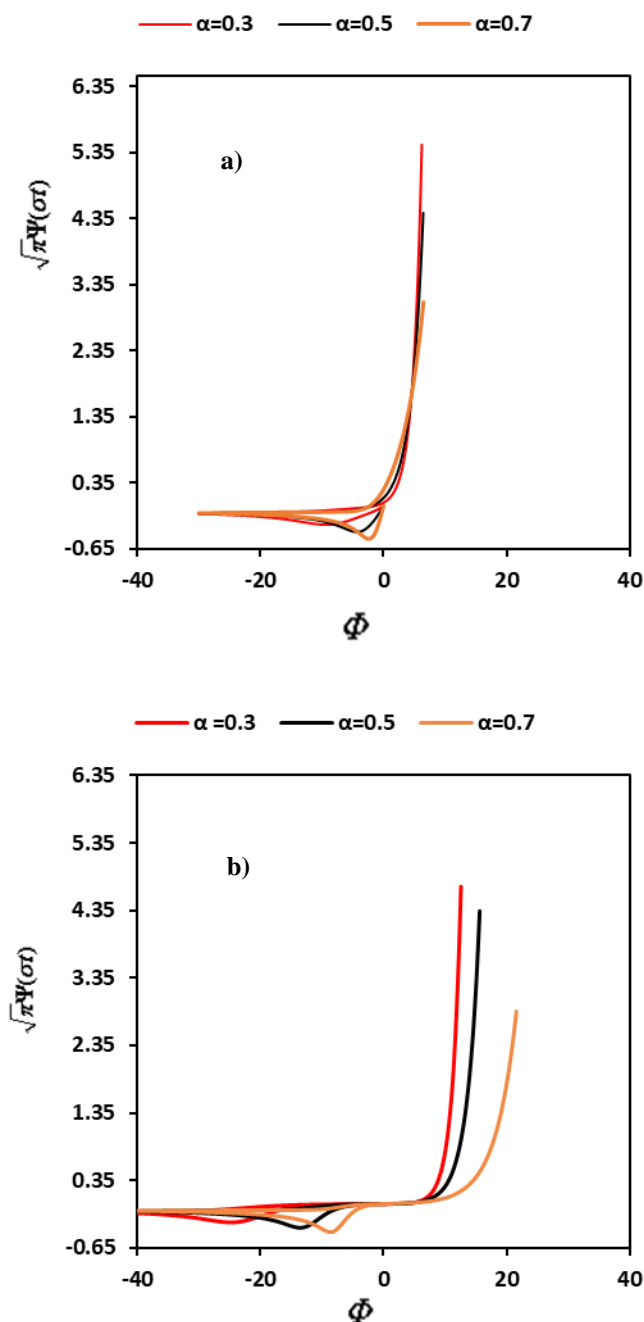


**Figure IV.4.** Effect of the transfer charge coefficient on the cyclic voltammetry responses for soluble-insoluble system. (a) quasi-reversible case ( $\omega=10^{-1}$ ), (b) irreversible case ( $\omega=10^{-3}$ ).

#### IV.4.4. Effect of the switching potential

In Figs. IV.5a, IV.5b and IV.5c the variations of the CV responses with the switching potential are shown for the three general cases of reversible, quasi-reversibile and irreversible systems. It seems that increasing the value of the dimensionless switching potential increases the magnitude of the peak current. In contrast, no effect was observed on the cathodic branch of the CVs.

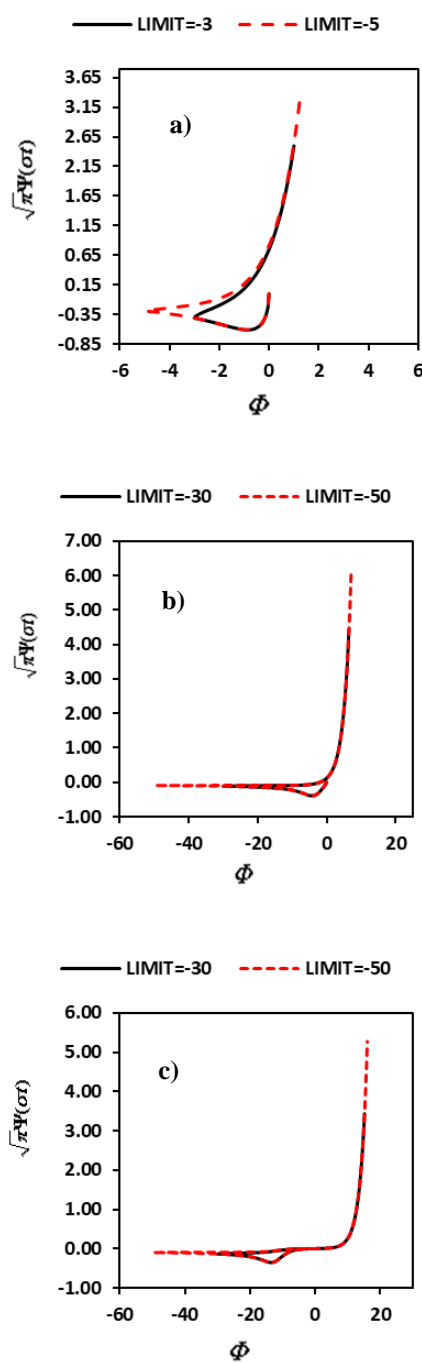


**Figure IV.5.** The effect of switching potential on theoretical CVs. (a) reversible case ( $\omega=10^3$ ), (b) quasi-reversible case ( $\omega=10^{-1}$ ), (c) irreversible case ( $\omega=10^{-3}$ ).

#### **IV.4.5. Theoretical visualization of concentration profiles**

Contrary to the soluble-insoluble redox system, the concentration profile for soluble-soluble system have been theoretical investigated in several studies [3]. In the Fig IV.6 the theoretical concentration–distance plots at different times of the cyclic voltammogram were shown. We can observe that the time at which the concentration of the metal ion dropped to zero at the electrode surface increases with the degree of reversibility. This is due to the rate of consumption of reduced species at solution-electrode interface. For reversible system, the kinetic rate constant is high resulting in rapid consumption of the electroactive species.

In addition, it's worth noting that the variation in concentration during metal cation reduction is less than that during metal oxidation. This is explained by the fact that the reduction reaction of the metal ion is under diffusional control, but the metal oxidation reaction is under pure activation.

#### **IV.5. Conclusion**

Theory of cyclic voltammetry for soluble-insoluble redox reaction was established by using two different methods, semi analytical and finite element method. This theory is applicable to planar electrode. It was found that Both methods yield the same results.

Different theoretical CVs responses under variation of kinetic rate constant, charge transfer coefficient and switching potential have been presented.

Using the developed CV models in this chapter, it's possible to visualize the theoretical concentration profiles whatever the degree of the reversibility.

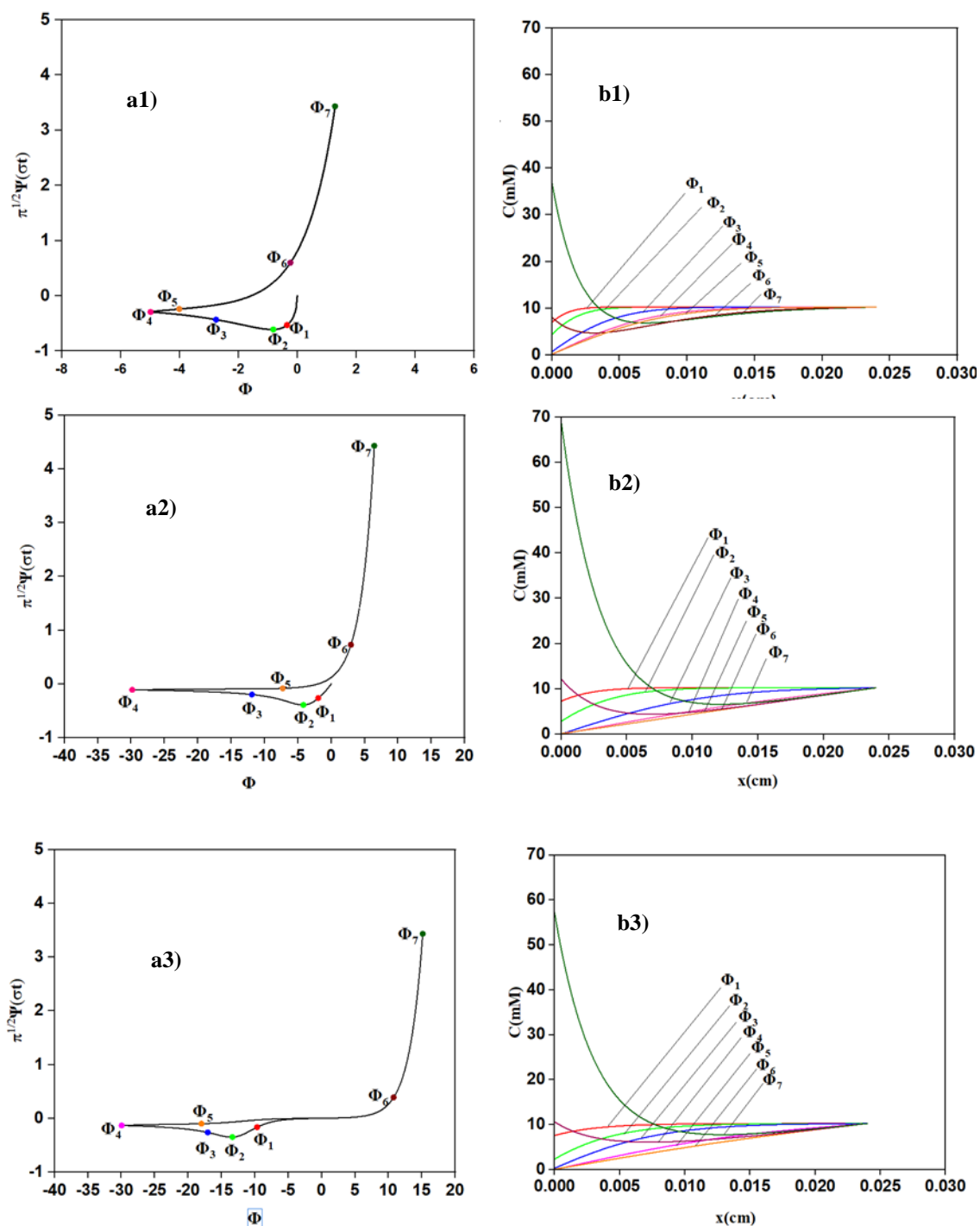


**Figure IV.6.** Simulated CVs (a1, a2 and a3) and theoretical concentration profiles (b1, b2 and b3) of the soluble-insoluble redox system. a1-b1: reversible case ( $\omega=10^3$ ), a2-b2: quasi-reversible case ( $\omega=10^{-1}$ ) and a3-b3: irreversible case ( $\omega=10^{-3}$ ).

## **IV.6. References**

- [1] C. Montella, V. Tezyk, E. Effori, J. Laurencin, E. Siebert, *Linear sweep and cyclic voltammetry of porous mixed conducting oxygen electrode: Formal study of insertion, diffusion and chemical reaction model*, Solid State Ion., 359, 115485. 2021
- [2] R.S. Nicholson, I. Shain, *Theory of stationary electrode polarography. Single scan and cyclic methods applied to reversible, irreversible, and kinetic systems*, J. Anal. Chem., 36, 706–723, 1964.
- [3] N. Elgrishi, K. J. Rountree, B. D. McCarthy, E. S. Rountree, T. T. Eisenhart, J. L. Dempsey, *A practical beginner's guide to cyclic voltammetry*, J. Chem. Educ., 95(2), 197-206, (2018).

# ***General Conclusion***

## General conclusion

We are interested in the theoretical and numerical study of electrochemical systems that include an insoluble product formation using voltammetry-sweep techniques.

In this regard, to have theoretical tools to approach the diagnosis and the theoretical prediction of experimental voltammograms corresponding to the soluble-insoluble redox reactions, we have first built mathematical models based on the Butler-Volmer type kinetics and then we have solved them by using two different methods: a semi-analytical method that incorporates Laplace transform and inverse Laplace transform, and the finite-element method included in COMSOL Multiphysics software, and finally, the proposed mathematical models have been tested by experiment where the system Cu (I)/Cu (0) in acetonitrile medium was investigated.

The following conclusions are reached:

-Two algorithms based on the semi analytical method were proposed to simulate the LSV and CV responses where the electron transfer takes place in a single step. The results of the simulation were compared to those produced using finite element method and excellent agreement was confirmed.

The influence of kinetic factors on LSV and CV responses was investigated. series of kinetic curves have been produced by varying the peak parameters with the dimensionless kinetic rate ( $\omega$ ) and the transfer coefficient ( $\alpha$ ). The obtained simulation results showed that according to the magnitude of the dimensionless rate constant the various voltammetric responses limitation could be divided into three zones: Zone 1:  $\omega \geq 10^3$  , reversible process. Zone 2:  $10^{-3} < \omega < 10^3$  , quasi-reversible process. Zone 3:  $\omega \leq 10^{-3}$  , irreversible process. Moreover, we have offered three working curves to extract kinetic details with high accuracy and simplicity to use, as only the experimental values corresponding to the peak high, peak position and peak width are required. Moreover, our developed CV model can be used for establishing theoretical concentration profile for soluble-insoluble redox couples whatever the degree of the reversibility.

-The kinetic and mass transport properties of the Cu deposition that required to understand better the limitations for the nonaqueous batteries utilizing Cu(I)/Cu(0) couple as the negative redox, were successively computed using models suggested in this work calculated value of the

kinetic rate  $k^0$  was found to be equal to  $5.12 \times 10^{-5} \text{ cm s}^{-1}$  which indicated that the Cu deposition process in acetonitrile is quasi-reversible, the diffusion coefficient was  $1.7 \times 10^{-9} \text{ m}^2\text{s}^{-1}$  and the cathodic transfer coefficient was 0.8.

-LSV or CV models proposed in this work are applicable only to a situation where instantaneous nucleation takes place, such as metal deposition on same metal, or for example silver deposition on gold in some specific conditions. If nucleation overpotential is required to induce the nucleation, followed by for example progressive 3D nucleation, the shape of the voltammogram will change, LSV and CV models should be thoroughly studied. In perspective, it will be necessary to modify the LSV or CV theory developed in this study in the case where the activity of the metal as the function of surface coverage would be required.